VEINS Synthesis

Large scale modeling results

By R. Gerdes, M.Karcher, F.Kauker, C.Köberle, J.Brauch, and M.Prange

Alfred-Wegener-Institut, Bremerhaven

Introduction

This paper was compiled using results from two hindcast experiments (prescribed history of atmospheric forcing data). Both were performed with coupled ocean-sea ice models. Details of the model and the experimental design can be found in the literature (Gerdes and C Köberle, 2000; Karcher et al., 1999) and in the VEINS reports. One experiment was performed with a high-resolution model (**HRM**) of the Nordic Seas, the Arctic Ocean, and large parts of the subpolar North Atlantic (Fig. 1). This experiment covers 20 years and uses atmospheric data from the ECMWF re-analysis (1979-1993) and analysis for the years 1994 through 1998. The other hindcast experiment was performed with a lower resolution model (**LRM**) that covers the whole Atlantic north of approximately 20^{o}S (Fig. 2). Here, the reanalysis data from NCEP/NCAR (Kalnay et al., 1996) for the period 1958 through 1997 were employed.

In addition to the hindcast experiments a number of response experiments were performed to elucidate certain aspects of the atmospheric forcing and the response of the ocean-sea ice subsystem. These experiments are described in the section ”Findings from response experiments”.

The mean surface circulation of the HRM (Fig. 3) shows an intense subpolar gyre with several branches of the North Atlantic Current (NAC). The Atlantic water enters the Nordic Seas in a branch immediately east of Iceland and two branches between Faeroe and Scotland. The former feeds into the outer branch of the Norwegian Atlantic Current (NwAC). One of the latter enters the North Sea and then combines with the Norwegian Coastal current. Different branches of the NwAC are still visible north of the Iceland-Scotland Ridge. These branches only join north of 68^{o}N to form a rather

broad northward current. Part of the Atlantic water enters the Barents Sea while the major part continues in a cyclonic fashion around the Greenland Sea. There is little or no inflow into the Arctic Ocean with the West Spitzbergen Current (WSC) at the surface. The East Greenland Current (EGC) appears as a continuation of the transpolar drift in the Arctic Ocean. The transpolar drift also feeds a westward current north of Greenland and the Canadian Archipelago, apparently a boundary current of the Beaufort gyre in the model. The EGC branches into the Jan Mayen Current that separates the quiescent Greenland and Iceland seas. The water carried by the Jan Mayen Current is a mixture of Polar Water with the recirculating Atlantic Water and is thus a relatively warm and saline contribution in this area. The average picture shows no pronounced branching of the EGC into the East Icelandic Current (EIC) which, however, is clearly present in individual years. The fluctuations in the EIC are a source of strong variability in the area of the western Atlantic inflow. The EGC flows parallel to the recirculating Irminger Current south of Denmark Strait. The currents lose their individual properties at the southern tip of Greenland.

The HRM produces a highly detailed current structure in the Nordic Seas and the passages that connect the Nordic Seas with the Atlantic proper and the Arctic Ocean. The transport pathways reappear throughout this paper because an important part of the oceanic variability in the area consists of propagating signals that follow these pathways. The LRM can not reproduce all the details that are present in the HRM. Because of the width of individual currents, it becomes difficult to distinguish the interiors of e.g. the Greenland Sea and the Labrador Sea from the boundary current regimes. However, this model does reproduce the major currents and the variability that can be described with such a resolution is indeed rather similar to that in the HRM. While rather subtle shifts in frontal position can for instance not be reproduced with the LRM, the propagating modes of temperature and salinity anomalies are well captured. This encourages us to present a number of results from the LRM, especially because the simulated period is twice as long as for the HRM. We thus also capture a period of predominantly low NAO forcing (before 1970) where the HRM is limited to a period with high NAO forcing throughout.

Transport time series

This is a preliminary account of volume, heat, and salt transports through the different passages in the HRM (see Fig. 1 for the location of the sections through the passages). A comprehensive analysis of the heat and fresh water balance of the Nordic Seas is forthcoming. We distinguish northward and southward fluxes. Northward (southward) volume fluxes are computed as positive (negative) velocity component times the area of a grid box. Northward (southward) heat fluxes are computed as temperature above -2^{o}C times positive (negative) velocity component times grid box area times the specific heat of sea water. Salt fluxes are calculated relative to 34.9 using the same convention for the direction of the flux as for the heat fluxes.

Following the cyclonic circulation in the Nordic Seas we begin with the Atlantic inflows between Iceland and Norway / Scotland, continue with the Svinøy section, the Barents Sea inflow, Fram Strait and then return to the Greenland-Scotland-Ridge in Denmark Strait (Fig. 4).

The two inflows of Atlantic water are well distinguished. Between Iceland and Faeroe, we find around 6 Sv of northward transport. This transport has a weak seasonal cycle and is also rather constant at lower frequencies. The same is true for the transports of heat (around 200 TW) and salt. The eastern branch between Faeroe and Norway is weaker (around 3.5 Sv) but features much higher variability from seasonal to interannual time scales. The inflow here is enhanced from 1989 to 1995, followed by a sharp reduction in 1996. The enhanced volume flux in 1989-1995 is associated with higher heat (typical value 150 TW) and salt transports.

The volume transport time series for the Svinøy section shows strong similarities with the Atlantic inflow between Faeroe and Norway. The total northward transport is consistent with the Atlantic inflow further south. Superimposed on the interannual variability, however, is a decadal scale fluctuation that imprints a downward trend (from around 10 Sv down to 7.5 Sv) before 1988 and an upward trend (11.5 Sv in 1995) afterwards. A drop in transport interrupts the upward trend during 1996 and 1997.

The northward heat flux (around 300 TW) increases since 1989 except for a short decline in 1997. The salt flux behaves similarly; however, it is rather constant before 1988.

The western entrance to the Barents Sea shows large interannual fluctuations (between 2 and 4 Sv) and a large seasonal cycle in eastward volume flux. The Barents Sea inflow increases at the end of the 1980s and in the early 1990s (with largest influx between 1988 and 1992) as do the Svinoy and Faeroe-Scotland sections further upstream. However, overall the correlation with Svinøy and the Faeroe-Norway section is rather small. The heat flux (around 70 TW) behaves similarly to the volume flux. The maximum in the early 1980s is associated with a warm temperature anomaly over much of the water column. The upward trend in salt flux on the other hand differs remarkably from the volume and heat fluxes.

The second inflow into the Arctic Ocean through Fram Strait decreases (from 2 to 1 Sv) early in the simulation. An inflow event (2.5 Sv) marks the period 1992-1995. The northward heat flux is similar to the volume flux, dominated by the event around 1993 (30 TW). The salt flux on the other hand is rather constant, except for a dramatic drop in 1998 that is caused by low salinity in the northward flowing water. The 1993 event has no obvious relation with transport variability at the other sections. The southward transport is also at a maximum (4.5 Sv) in 1993. It is associated with an increased southward fresh water transport.

At Denmark Strait, we find a slightly increasing southward volume transport (5 to 6 Sv) over the integration period. This is the total southward transport, including the shallow EGC and the deep overflow. Maximum transports (7 Sv) occur in 1989 and 1990 as well as 1993 and 1995. The southward fresh water flux is decreasing; a small increase in 1994 and 1995 could be due to the increased southward fresh water transport in Fram Strait. An anomalously high sea ice transport in 1992, 1993 and 1995 also contributes to this increase.

Summary:

The variability of the Atlantic inflow occurs mainly in the eastern branch although

the main inflow is with the western branch situated near Iceland over the Iceland-Faeroe-Ridge. All sections show an intensification of the transports in the late 1980s and early 1990s. This coincides with the most recent continuous period of strong NAO forcing. A correlation analysis for stream function (for the vertically integrated flow) anomalies and NAO (Fig. 5) exhibits an intensification of the cyclonic circulation in a cell that covers the eastern subpolar North Atlantic, the whole Nordic Seas and the Eurasian Arctic (Zhang et al. 1998; Gerdes, 2000). The sudden breakdown in the NAO in 1995/1996 leaves a signature in most transport time series, as does the recovery of the NAO during the last two years of the simulation period. However, there is generally no good correlation with the NAO on a year to year basis. While some of the transport fluctuations seem to be imposed by (or at least coincident with fluctuations in) the Atlantic inflow, there are also longer-term fluctuations that are apparently local to the Nordic Seas. The long term transport variability at the Svinøy section for instance is partly due to processes internal to the Nordic Seas and is not completely determined by the Atlantic water inflow.

The branching of the Atlantic inflow into the Arctic through the Barents Sea and Fram Strait shows a different behavior from the upstream sections. However, the high inflow into the Barents Sea coincides with the high northward transports upstream in the late 1980s while strong northward flow in Fram Strait coincides with the upstream transports in the early to mid 1990s. It thus appears that the Barents Sea and Fram Strait filter out different signals that propagate from the southern entrances of the Nordic Seas. Heat transport analysis for individual passages (see below "Heat flux modes in individual passages") shows that strong northward flow in Fram Strait is associated with strong meridional flow east of Iceland. Barents Sea inflow is associated with a zonal flow along the Iceland-Scotland Ridge with inflow on the eastern boundary of the Nordic Seas. It is conceivable that, through topographic steering, the different inflows and the different pathways northward result in preferred inflows at one or the other northern passage.

Temperature and salinity variability

Surface

The hydrographic properties in the Nordic Seas exhibit strong interanual variability. As an example we show temperature anomalies in 100 m depth for four different winters (Fig. 6). In winter 82/83 a large anomalously warm structure dominates the southern part of the Nordic Seas stretching from the Greenwich meridian in north-eastern direction to the Barents Sea, following the baseline of the Norwegian continental slope. It marks the meandering front between the Atlantic Water and the interior water of the Nordic Seas gyre. In the Barents Sea remnants of a previous cold anomaly advected with the NwAC still cover large areas. A warm anomaly in the inner branch of the NwAC is visible close to the Norwegian coastline from southern Norway to the Lofoten Islands. One year later this warm anomaly has moved into the southern Barents Sea and slightly intensified in amplitude. A new cold anomaly is approaching through the Faeroe-Scotland gap along the path of the NwAC. Its peak will reach the Barents Sea in about 1987. Both cold anomalies and the warm anomaly along the Norwegian coast are depth intensified and can be identified already south of the Iceland-Scotland gap before being advected into the Nordic Seas proper. A second warm anomaly of the NwAC and the coastal waters in the late 1980s and early 1990s exhibits very different charcteristics. This anomaly instantaneously covers large parts of the eastern Nordic Seas and the North Sea. The large-scale warming commences in 1987/88 and has its maximum amplitude and areal coverage in 1989/90. In contrast to the Atlantic Water anomalies described before, this warm anomaly is surface intensified. In the following winter it has diminished in the southern areas but intensified south of Spitsbergen. The instantaneous widespread occurrence and the surface and downstream intensification are the results of reduced heat losses to the atmosphere in the North Sea and the eastern Nordic Seas in the late 1980s/early 1990s. There are no indications for this anomaly being advected from south of the Iceland-Scotland gap.

The first two EOFs for SST (using annual averages, each from May through April)

provide a summary of the variability in the Nordic Seas in the HRM (Fig. 7). The EOFs describe 43% and 23%, respectively, of the variance. Both EOFs describe long term developments in SST, EOF #1 shows a time scale of roughly 20 years and EOF #2 has a period of around 10 years. The next two EOFs (14% and 9% of the variance, not shown) also behave rather periodic with periods close to 10 years. Largest amplitudes (EOF #1) are found near the fronts associated with the NwAC, over the western edge of the Voring Plateau, and along the path of the WSC. The frontal system of the EIC stands out with amplitudes of clearly above 1^{o}C. Furthermore, we find high amplitudes near the ice edge position in the Greenland Sea. The permanently ice covered part of the EGC itself has practically no SST variability. A broad seam of high amplitudes extends from the North Sea along the Norwegian coast into the Barents Sea. Here, large positive temperature anomalies occurred during the late 1980s and the early 1990s, coincident with the maximum transport values shown above and the prolonged positive phase of the NAO. Outside the Nordic Seas, EOF #1 features large amplitudes in the central subpolar North Atlantic and in the Irminger Sea as well as in the Labrador Current. Generally, the major branches of the North Atlantic Current System and the cold western boundary currents are places of the high long-term SST variability captured by EOF #1.

The higher frequency EOF #2 describes variability in similar areas as EOF #1 although the details of the spatial structure are different. This mode describes the temperature variability associated with relocations of the ice edge in the southern parts of the EGC and north of Iceland. High positive temperature anomalies occurred in the EGC, West Greenland Current, and Labrador Current system during the mid 1980s and near the end of the simulation. Both EOFs describe an out of phase relationship between the Labrador Sea and the Barents Sea that is typical for the response to NAO-like forcing.

Much of the variability in SST and other variables is apparently related to the NAO. To quantitatively assess the importance of the NAO we calculated correlations with the NAO index. For both, the index and the data, we use winter means that were further treated with a three-year running mean and then detrended. Fig. 8a shows the

fraction of low-frequency variability of the SST in the HRM that can be accounted for by a linear relationship with the NAO index. The associated standard deviation is shown in Fig. 8b. This can be interpreted as the response to an NAO index of one standard deviation from the mean. The standard deviation again highlights the regions with high SST variability that were discussed above using EOF analysis. High correlations are also present in large parts of the Arctic where, however, the amplitude is vanishingly small. Negative correlation (low SST at high NAO phase) can be found along a band from the Barents Sea and the western rim of the Norwegian Sea (roughly following Mohns Ridge) into Denmark Strait and around the southern tip of Greenland into the Labrador Sea. Highest positive correlation (approaching 1, i.e. identical normalized time series with the NAO index) are present in the North Sea, along the Norwegian coast, and in the southern Barents Sea. These signals can be regarded as the instantaneous, local response to the NAO forcing. The large scale, elongated spatial structure hints at a simultaneous response along a semi-permanent oceanic front or the ice edge.

The correlation analysis for SSS and NAO index (Fig. 9a and 9b) corroborates this relationship. SSS shows a similar elongated structure from the Iceland Basin into the Labrador Sea. Phases of positive NAO are associated with low temperatures and salinity, consistent with increased flux of sea ice into the area, leading to melting and a corresponding reduction in SSS. On the other hand, there is very little surface salinity variability depicted on the eastern side of the Nordic Seas, where NAO related temperature variability is large. In the Arctic Ocean we also find a pronounced difference in temperature and salinity variability. The sea ice cover constrains the winter SST to be close to the freezing point. Differences in melting and freezing on the other hand lead to large fluctuations in surface salinity. Fig. 9b reveals positive salinity anomalies in the Laptev Sea, the East Siberian Sea, and eastern Eurasian Basin during positive NAO phases. Many features of the salinity anomaly pattern are reflected in the surface fresh water flux associated with NAO (Fig. 10). A horizontal shift in the ice production sites manifests itself in the dipole of positive and negative anomalies in the interior Arctic, roughly aligned along the position of the mean transpolar drift. High

NAO is associated with increased sea ice production and brine release in the Laptev Sea and north of it. Sustained salinification during long periods of high NAO appears as another candidate for the retreat of the Arctic halocline in the Eurasian Basin (Steele and Boyd, 1998) Increased ice export from the Arctic leads to melting and negative salinity anomalies in the EGC, especially in the narrow region from the Iceland Sea into the Irminger Sea pointed out above. This is consistent with the results from the response experiments where the wind forcing is switched from high NAO to low NAO (see below ”Findings from response experiments”). Enhanced evaporation from the anomalously warm water during positive NAO overcompensates the high precipitation off Norway. However, the effect of these fluxes on surface salinity variability is rather minor.

Contrary to temperature, the NAO index is not everywhere a good predictor for salinity anomalies in the Nordic Seas and the subpolar Atlantic. Sea ice transport through Fram Strait is not very well correlated with the NAO for the whole simulation period (although there is a good correlation for recent years). Because melting of sea ice dominates the surface fresh water fluxes in the EGC, the Jan Mayen Current, the EIC, and the Labrador Sea, we can not expect the SSS variability to be well described by the NAO index.

Deeper layers

The correlation with NAO for potential temperature on a (quasi-zonal) section through the Nordic Seas (Fig. 11a) shows that the anomalies (described above for the surface) reach deep into the water column. On the eastern side, the signal is found down to 1000 m depth with amplitudes up to 0.1^{o}C. The interior of the Greenland Sea shows no NAO related temperature anomalies. On the western side, the temperature signal is present down to 300 m depth. The origin of the signal apparently lies on the eastern side from where it propagates cyclonically around the Nordic Seas. It reaches the eastern side of the basin, just outside of the EGC, first in the upper parts of the water column. From Fig. 10 we can also infer that during the propagation the signal has been damped at the surface as the maximum anomaly is situated at around 100 m

depth (Fig. 11b).

Horizontal correlation maps of NAO and potential temperature for 200 m and 500 m depth (Fig. 12) no longer contain the continuous band of negative correlation extending from the NwAC and WSC to the Labrador Sea. Largest NAO related signals are organized as a chain of rather small-scale areas with alternating sign of the correlation along the western front of the NwAC. The LRM provides a clearer picture of high positive correlation with NAO at 500 m depth (Fig. 13) all along the cyclonic circulation path of the Atlantic water from the Iceland-Scotland-Ridge to the recirculating branch off-shore the EGC. We suggest that this very deep reaching signal is a combination of a signal originating northwest of Iceland, part of which circulates in the Nordic Seas, and local heat flux forcing. A tongue of positive correlation also extends into the Arctic Ocean at this depth, along the pathway of the Fram Strait branch of the Atlantic inflow. It is possible that the larger amount of meandering of the main currents in the HRM obscures the picture for the relationship between NAO and temperature signal at depth. Salinity in the Nordic Seas behaves very much like temperature at these depths because salinity is no longer affected by the strong surface fluxes due to melting in the EGC and its eastward branches. The standard deviation of the NAO related salinity signal at 500 m is very weak. At 200 m depth we still find very strong signals in the Arctic Ocean, especially the Beaufort gyre region. These strong fluctuations are very well correlated with fluctuations of the barotropic streamfunction and are due to variations in the depth of the halocline. It is not conceivable that these fluctuations could affect the Nordic Seas.

Summary:

SST variability is strongest on the decadal time scale. The major branches of the North Atlantic Current System and the cold western boundary currents are the places of high long-term SST variability. SST variability is imposed by the Atlantic inflow, by local heat fluxes, and by ice edge related processes. We find opposite phases of SST variability on the eastern and western sides of the Nordic Seas. This is only partly due to the local surface air temperatures as the Atlantic inflow and the ice import from the

Arctic are important components; high Atlantic heat transport and high ice transport occur for positive NAO. Variability on the eastern side is mostly density compensated as Atlantic inflow of warm and saline water as well as local evaporation dominate the precipitation. This is not the case for the western boundary where temperature variability is curtailed by freezing. Variability associated with the Atlantic Water in the Nordic Seas reaches down to 1000 m depth.

Propagating signals

Propagation of temperature and salinity anomalies in the Nordic Seas has been described by Kauker et al. (1999a) based on LRM results. They use lagged linear regression to identify anomalies related to the NAO, the Arctic Oscillation (AO), ice transport through Fram Strait, and the SFR (storm formation region) index. The latter is defined as the SST anomaly in a region off Florida and has been used by Sutton and Allen (1997) to identify propagating SST signals in the North Atlantic. The indices are mutually very different (except for the NAO and the AO) and propagating signals in different areas of the Nordic Seas could be detected, related to different indices. For the long integration period of the LRM hindcast it was found that long-term SST fluctuations had the highest correlation and amplitudes with the SFR index. These signals in SST were detectable for the longest propagation times. The lag zero pattern contains correlations of up to 0.9 north of Iceland and negative correlations of up to 0.8 in the Labrador Sea. Five years later, the anomaly north of Iceland is advected into the Labrador Sea. Here, the anomaly merges with a positive anomaly created in the SFR that was described by Sutton and Allen (1997). Kauker et al. (1999b) point out that the anomaly created north of Iceland is stronger than the anomaly created in the ”storm formation region” itself.

NAO related surface signals

SFR index variability dropped to small values after 1980 and the NAO index yields a better description for the HRM simulation period that starts in 1979. We therefore

present NAO related signals in the following discussion of HRM results. To identify propagating signals we perform correlation analysis as above for different time lags between the time series for the variable of interest and the NAO index (Fig. 14). The lag zero correlation pattern has been discussed above (Fig. 8). At a lag of one year the highest positive correlations that could be found in the North Sea and along the Norwegian coast for zero lag have moved out of the North Sea, into the Barents Sea, and north-westward along the WSC. After two years the positive correlation occupies most of the Barents Sea and has propagated into the Kara Sea. Positive correlation develops east of the EGC (the high correlation at the Greenland coast is not associated with considerable SST variance) and travels within one year (Fig. 14g) into the area north of Iceland. In the mean time a negative correlation intensifies in the North Sea (Fig. 14f-g) and spreads along the Norwegian coast, initiating the negative phase of the NAO related variability in this area.

The temporal development of the SST anomalies suggests propagation along the major branches of the Atlantic water in the system. The time scale is two years for propagation from the Norwegian Sea through the Barents Sea and into the Kara Sea. The signal needs three years to reach the Iceland Sea. Without inspecting the local heat fluxes, however, a local response to atmospheric forcing anomalies can not be ruled out. For zero lag (Fig. 15) we find positive correlation of the local heat flux with the NAO in the North Sea, indicating that the temperature anomaly there is at least partly locally forced. Along the Norwegian coast, however, the heat flux correlation is negative, the atmosphere is cooling the anomalously warm ocean. This is a clear indication of a propagating signal that originates elsewhere. Similarly, surface heat flux anomalies at greater lags damp SST anomalies in the Barents Sea and in the recirculating Atlantic water. Similar anti-phase relationships between heat flux and SST anomaly are present in the EIC area, the Irminger Current recirculation and in the Labrador Sea.

The filament of negative correlation at zero lag (Fig. 14d and Fig. 8) extending through the Nordic Seas and Denmark Strait, along the boundary currents into the Labrador Sea splits into two major parts during the following development. One part

intensifies south of Denmark Strait and in the Labrador Sea. At 3 years lag the anomaly leaves the Labrador Sea through the southern boundary of the model. The surface heat flux indicates damping of the anomaly. The other part propagates eastward along the axis of the EIC. The anomaly grows to more than 1^{o}C, the largest amplitude in the whole domain. The sign of the surface heat flux shows damping of the SST anomaly that propagates into the area. The EIC extends far east during maximum NAO phase and the following years. The EIC seems to interact with the Atlantic inflow east of Iceland that occupies a more southerly position and is diverted eastward during strong EIC periods. For minimum NAO index and the following years, the Atlantic inflow occupies the position of the EIC during opposite phase and provides for a warm and saline anomaly there.

One peculiar feature of the correlation patterns is the occurrence of high correlations for negative lags with the NAO index. This is most pronounced in the Irminger Sea and the Labrador Basin where we find correlations larger than 0.8 for negative lags of 2 and 3 years (Fig. 14b and 14a), i.e. the SST signal leads the NAO index. This is not just the consequence of a nearly periodic NAO forcing because the autocorrelation for the NAO at 3 years or longer lag is only 0.3 (the maximum that one could expect for periodic signals correlated with NAO). The surface heat flux for these lags is negatively correlated with NAO (Fig. 15); i.e. the anomalously warm ocean heats the atmosphere. Together this could indicate an active role of the ocean in the climate cycle that establishes the quasi-periodic nature of the NAO during the last 30 years.

Propagating signals at greater depths

Temperature maps at 500 m depth (Fig. 16) exhibit stationary and propagating signals. A stationary, anticyclonic loop enclosing positive anomalies intensifies in the northern Norwegian Sea over the shown period from September 1990 through March 1992. Downstream, near Fram Strait, single boluses of warm water are shed from the recirculating Atlantic water. Apparently, no signal enters the Arctic Ocean through Fram Strait. The boluses reach Denmark Strait after 1.5 years. Diversion along the Greenland fracture zone, the Jan Mayen fracture zone, and into the Iceland Sea slow

the progress and diminish the amplitude of these signals. The Iceland Sea acts a reservoir that smoothes variability that appears at Denmark Strait.

For a more systematic account of these deep propagating signals we again turn to lag correlation analysis where the NAO index can describe a large part of the variance during the HRM hindcast. At 200 m (Fig. 17) the propagation of the positive correlations is similar to the surface signals. The propagation pathways along the branches of the Atlantic water in the Nordic Seas are even more pronounced than at the surface, where atmospheric variability plays a large role. Propagation of negatively correlated temperature anomalies from Denmark Strait into the western subpolar North Atlantic is also well established. The signals are spatially confined to the strong currents that are rather stable in the model. We find no correlation between the boundary currents and the interior of the Labrador Sea. A signal that is present in the northern part of Denmark Strait at zero lag covers the distance to the southern model boundary in one year. The highest correlations, however, need more time to develop. This indicates two phases of adjustment. Conceivably, changes in the density field at Denmark Strait first propagate as coastal waves along the western boundary. This phase is then followed by the advective propagation of the signal with the mean currents. At 500 m (not shown), we find the propagation of individual lenses of anomalous temperature that was discussed above using an example from the 1990-1992 period (Fig. 16). Another feature is the eastward spreading of anomalies north of Iceland and into the Faeroe-Shetland-Channel. This is already visible at 200 m depth (Fig. 17). It seems that the anomaly propagates through the channel and enters the eastern subpolar gyre. However, the amplitude is strongly reduced south of the ridge, probably due to strong entrainment in the overflow.

Ice export related signals

Ice export through Fram Strait is one of the major components of the Arctic fresh water balance and also affects the properties of the East Greenland Current and perhaps the conditions in the deep water formation regions of the Greenland and Labrador seas. Transport and melting of sea ice is more important for the oceanic surface

variability than the oceanic fresh water transport through Fram Strait. As shown above, SSS variability has largest amplitudes not in Fram Strait but much further downstream in the EGC – where the ice is melting. Recent direct measurements suggest that ice transport is well correlated with the NAO and that an especially large ice export occurred during the high NAO+ winter of 1994/95 (Vinje et al. 1998; Kwok and Rothrock, 1999). Our model results reproduce this large ice export in very good agreement with the observational estimates (Köberle et al., 2000a). Our simulation revealed the exceptional nature of the 1994/95 ice export event that combined extremely high ice velocities and an under average ice thickness. This event, contrary to previous events in the late 1960s and early 1980s and 1990s, was not preceded by a build-up of ice volume in the Arctic Ocean. The earlier events usually lasted for more than one winter and the total ice export was considerably larger than during the 1994/95 event. Correspondingly, the effect of the latter event on surface salinity and deep water formation was not especially pronounced (Fig. 18).

Only the ice velocity is well correlated with the NAO. Large ice thickness in Fram Strait, as it is related to the ice volume in the interior Arctic, requires several years of favorable conditions for ice accumulation in the Arctic (Köberle et al., 2000b). Thickness is not necessarily correlated with NAO. Over longer time scales, a correlation of ice export with NAO is thus not to be expected and is not found in the simulations.

Lagged linear regression is used to track sea surface salinity anomalies related to Fram Strait ice export. At one year lag negative SSS anomalies north of Greenland, in Fram Strait, and south of Greenland are associated with anomalously high southward ice transport. Positive correlations up to 0.7 and amplitudes up to 0.4 occur in the East Siberian and Laptev seas. These anomalies are connected to propagating signals in sea ice thickness in the Arctic Ocean (cf. Gerdes et al., 2000; Köberle et al., 2000b). Three years later, the area of negative correlation has shifted into the Labrador Sea where amplitudes of around 0.3 are achieved. The positive correlated areas in the East Siberian and Laptev seas have propagated towards the Barents Sea. One year lagged correlations up to 0.7 can be found in the overturning in the Atlantic. The overturning is weakened by 2 Sv five years after maximum ice transport through Fram Strait.

Summary:

Propagating signals constitute a large part of the variability in the Nordic Seas. Using different index variables we could identify propagating signals in different areas of the Nordic Seas. Propagation along the major branches of the Atlantic Water is very prominentely displayed with the NAO index. SST signals that start in the North Sea and along the Norwegian coast propagate within two years into the Barents and Kara seas. The recirculating signal needs three years to reach the Iceland Sea. Negative temperature signals associated with high NAO in the western parts of the Nordic Seas split in one part that continues into the Labrador Sea and beyond in the subpolar North Atlantic and one part that propagates eastward along the axis of the EIC. This signal is connected with a locally very strong temperature and salinity anomaly because of a switch between EIC waters and the Atlantic inflow east of Iceland. Ice export related signals occur not only south of Fram Strait and enter the large scale cyclonic circulation there. Signals also appear in the Arctic - and could affect the Nordic Seas through changing hydrographic properties in Fram Strait - as ice export events are connected with large changes in ice thickness and ice concentration. These lead to chagnes in thermodynamic growth of sea ice. At deeper levels we could identify boluses of warm water shed from the recirculating Atlantic water near Fram Strait and propagating within 1.5 years to Denmark Strait.The diversions of these signals along the way and especially into the Iceland Sea diminish the amplitude that reaches the overflow considerably.

Heat flux modes in individual passages

In this section we attempt to relate the variability in volume, heat, and salt transports through individual passages to the large scale oceanic transport patterns and the atmospheric forcing, namely the sea level pressure (SLP) field. We use the vertical area mean (over the upper 250 m) of the product of velocity and temperature relative to T_o=-2^{o}C as a proxy for heat transport. Salt transport is similarly defined with 34.90 as reference salinity. It should be noted that due to the nonlinear nature of the transports this analysis contains a part that is independent of temperature or salinity fluctuations:

$$HT^{x}_{proxy} = \int_{-250\,m}^{0m} u(T - T_o)\,\Delta y\,dz$$ or for an averaged quantity

$$\overline{HT^{x}_{proxy}} = \Delta y \int_{-250m}^{0m} dz \left\{ \bar{u}\bar{T} - \bar{u}T_o + \overline{u'T'} \right\}$$

where Δy is the meridional grid distance. The contribution due to uT_o can be relatively large, depending on the velocity field and the absolute magnitude of T. When we use absolute temperatures (relative to -273^{o}C) the contribution from the velocity field alone dominates the transport variability, i.e. this is a measure of the volume transport. For a reference temperature of -2^{o}C, the temperature fluctuations become relatively more important.

To identify different modes of heat transport within the passages we perform an EOF analysis of the transport vectors in a subarea just containing the passage (see Fig. 21). The principal component of the EOFs is then used as an index in a linear regression analysis for the large scale transport field and SLP.

The two first EOFs for (heat) transport in the Iceland-Scotland area describe 53% and 15%, respectively (Fig. 20). The first EOF contains meridionally oriented transport vectors with largest transports immediately east of Iceland, where the main Atlantic inflow is situated. The second EOF contains more zonally oriented transport vectors in the area. The correlation of the transport vectors with the PC of EOF #1 (Fig. 21) shows that enhanced transport east of Iceland is associated with a somewhat weakened inner branch and an enhanced outer branch of the NwAC. The outer branch is directly fed by the NAC. The dominating pattern in the subpolar North Atlantic is a shift in the NAC position. For negative phases of the heat flux EOF #1, the NAC assumes a zonal and southern position; its eastward extent is curtailed as it sharply turns northward at around 30^{o}W. In this phase, the exchanges between Nordic Seas and the Atlantic and the Arctic Oceans are weak. During positive phases, the NAC flows in a northeastward direction and extends far east. A strong inflow near Iceland continues in a broad NwAC. There is a strong inflow into the Barents Sea. The second heat transport EOF in the Iceland-Scotland area is associated with the cyclonic

circulation in the Nordic Seas, there is no apparent correlation with NAC variability. This EOF involves the North Sea and the exchange with the Barents Sea (Fig. 22). Positive amplitudes for EOF #1 are associated with a stronger cyclonic circulation in the subpolar gyre of the North Atlantic, a stronger cyclonic circulation in the Nordic Seas (except for the Norwegian Sea) and the Eurasian Arctic (Fig. 23). For EOF #2 we find different signs for the barotropic circulation north and south of the Greenland-Scotland-Ridge, an enhancement of the subpolar gyre that occupies a larger area and an anticyclonic anomaly over the whole area north of 60^{o}N for positive amplitudes of EOF #2.

We can use correlation of the PCs of the transport modes with SLP anomalies to pinpoint the relationship with the large scale atmospheric conditions. This is not to imply that all the oceanic variability is wind induced (circulation changes could also be due to changes in deep convection as some response experiments suggest). Certain SLP patterns might nevertheless be indicative of the overall atmospheric forcing. For positive amplitudes of EOF #1 we find positive SLP anomalies over Greenland and northern Canada, and a negative anomaly over the eastern North Atlantic, south-east Europe, and northern Africa (Fig. 24). This implies stronger NE winds in Denmark Strait and the Labrador Sea that could explain the enhanced outflow in Denmark Strait and the strengthening of the Labrador Current. An obvious connection with the enhanced inflow east of Iceland, however, is not apparent. The associate SLP pattern for EOF #2 is very similar to the negative NAO pattern (Fig.24), consistent with the enhanced cyclonic circulation in the Nordic Seas for positive phases.

The two leading (heat) transport EOFs for the Denmark Strait area both describe fluctuations in the outflow strength. Positive amplitude of EOF #1 (with 49% of the variance) implies weakened outflow, positive amplitude of EOF #2 (25%) means strengthened outflow. The second mode also describes variability in the source region of the EIC, with positive amplitude implying a weak branching into the EIC (Fig. 25). The associated SLP anomalies are a NAO-like pattern (sign inverted) for EOF #1 and a somewhat similar pattern for EOF #2 that contains, however, a westward wind anomaly at the latitude of Iceland (Fig. 25). Positive EOF #2 is associated with a strong

inflow of Atlantic water east of Iceland and a strong outer branch of the NwAC, establishing a shortcut of the heat transport through the Nordic Seas (Fig. 26). The large scale pattern associated with EOF #2 is similar to EOF #1 for the Iceland-Scotland area, implying that there is a dynamic link between Iceland inflow and the Denmark Strait outflow.

An extreme case of negative amplitude phase of EOF #1 (Fig. 26) is characterized by a meridional course of the NAC, a strong inflow into the Barents Sea, a strong outflow from the Barents Sea into the Arctic Ocean through the St. Anna Trough, and a weak and spatially reduced Beaufort gyre. The positive amplitude phase contains a strong Labrador Current and a strong Beaufort Gyre that involves the East Siberian Sea. Contrary to EOF #1, EOF #2 combines a strong inflow into the Arctic (high positive amplitude) with a strong Beaufort Gyre.

The two leading modes for the western Barents Sea entrance are associated with SLP modes that project strongly on the NAO pattern. The information provided by these modes is somewhat redundant with that from the other areas as strong inflows into the Arctic via the Barents Sea are correlated with high transport through the Iceland-Scotland gap.

For Fram Strait we present results from the HRM. The two leading modes of heat transport (relative to -2^{o}C) describe 60% and 20% of the variance (Fig. 27). Mode #1 represents a decadal variability in the recirculation of Atlantic Water inside the passage. The amplitude of the mode is small except for a strong recirculation (negative sign of the PC) in the early 1990s. This mode is associated with a shift in the position of the WSC. Negative amplitude implies a strong WSC that reaches far north inside Fram Strait before it recirculates (Fig. 28). There is apparently no large scale heat transport connected with this mode that describes a large part of the high local variability in Fram Strait. While EOF #2 thus describes less variability in Fram Strait itself, it is associated with large scale transport pattern changes (Fig. 28). Among these changes are enhanced heat transport in the Fram Strait branch of the Atlantic Water in the Arctic Ocean and a strong Eurasian Basin recirculation of this heat. We also notice stronger inflow from the Atlantic and in the NwAC. This EOF is associated with a

NAO-like SLP pattern (the negative sign of the PC in the early 1990s associated with the high NAO during that time). However, the maxima and minima of the SLP anomalies (Fig. 29) are shifted westward compared to the classical NAO pattern.

Summary:

All passages to the Nordic Seas respond to changes in the Atlantic inflow. Changes in the NAC are connected with changes in the NwAC and the inflow into the Arctic Ocean. Although the overall variability in the cyclonic circulation encompassing the subpolar North Atlantic, the Nordic Seas and the Eurasian Basin seems to be overwhelming signal, there are more subtle changes that are at least regionally important. It was for instance shown at the beginning ("Transport time series") that strong northward flow in Fram Strait is associated with strong meridional flow east of Iceland. Barents Sea inflow is associated with a zonal flow along the Iceland-Scotland Ridge with inflow on the eastern boundary of the Nordic Seas. It was suggested that, through topographic steering, the different inflows and the different pathways northward result in preferred inflows at one or the other northern passage. The analysis here supports this view as it confirms the different pathways inside the Nordic Seas for different modes.

Findings from response experiments

We have now results from a number of response experiments available. Some of the results are published (Gerdes and Köberle, 2000; Brauch et al. 1999) and others have been documented in earlier VEINS reports. Therefore, we here provide only a short account of the major results.

Driving the LRM with daily winds produces a large amount of current variability on all timescales (Fig. 30). When the daily variability is retained only over the high northern latitudes of the domain, the high frequency variability in the northward flow (the NwAC) ceases while variability in the EGC stays on a high level. High frequency signals that are generated in the Arctic are able to propagate along the EGC. A similar

Hovmöller diagram south of Iceland (not shown) exhibits no high frequency variability. This documents that the signals are strongly guided by topography and are not able to cross the Greenland-Scotland-Ridge into the North Atlantic. The signals follow the ridge eastward into the North Sea (Kauker 1998).

Topographic barriers do not restrict low frequency signals that involve advective changes to such a degree. It is known that convective activity in different deep water mass formation areas varies considerably (Lazier, 1980; Dickson et al., 1988) and have ceased occasionaly or even for decades (Rhein 1991). To test the influence of these changes on the large scale circulation, experiments were conducted where the surface density was increased in different areas. Examples for deep convection induced that way in the Labrador Sea were shown in Gerdes and Köberle (1995). The response consists of two stages, the first, fast response is determined by topographic waves that travel southward along the western boundary (Fig. 31). The signal reaches the equator within a few months. The second stage encompasses an advective response where dense water propagates either with pre-existing boundary currents or with self-induced currents in a quasi-westward (given by the topographic vorticiy gradient) direction. Both stages lead to large scale adjustments of the thermohaline circulation. This is similar for other convection sites in the North Atlantic, south of the Greenland-Scotland-Ridge. On the other hand, the response to enhanced convection in the Greenland Sea has almost no effect on the North Atlantic circulation (Fig. 32). While the stages are similar, the response is not on as large a scale as for sites south of the ridge. The ridge imposes a barrier for the topographic waves as seen above. The advective response differs from that south of the ridge, because there is no pre-existing deep boundary current that could carry the dense water across the ridge. The self-induced velocities are either barotropic and thus strongly topography dependant or the counter-rotating gyres in the upper and lower parts of the water column are so strongly locked dynamically that a crossing of the topographic obstacle is prevented.

Effective communication of climate signals from the Arctic and high northern latitudes in the Nordic Seas is however possible through sea ice induced salinity anomalies (or in general anomalies that are confined to near the surface in the Nordic Seas).

Köberle and Gerdes (2000) prescribe a sea ice anomaly in Fram Strait such that a fresh water anomaly is injected in the EGC. The amount of fresh water, 2000 km^3 distributed over 2.5 years, is comparable to what has been estimated for the GSA in the Labrador Sea. (New calculations with the coupled LRM indicate that the total fresh water anomaly due to the ice export event 1967 / 1968 was at least twice as much.) The surface salinity anomaly (Fig. 33) propagates from the Fram Strait area through Denmark Strait and into the Labrador Sea. During later stages of the simulation, the fresh water anomaly can be traced through the subpolar North Atlantic with propagation times that are realistic according to the GSA data. A considerable part of the salinity anomaly is diverted early on into the area north of Iceland and starts to move around the Nordic Seas. This anomaly has not passed the Iceland-Scotland-Ridge from the south. The effect on Labrador Sea convection can be seen in the Hovmöller diagram for mixed layer depth on a zonal section through the central Labrador Sea (Fig. 34). The regular seasonal cycle is modified by a shallowing of the mixed layer starting in year 12 of the simulation and reaching its greatest extent in year 15 (5 years after first introducing the sea ice anomaly in Fram Strait). Convection recovers after passing of the anomaly into the open Atlantic.

The NAO is the dominating forcing in the area of interest. It consists of many different elements, like the wind stress forcing, changes in surface heat fluxes due to changes in the strength of the wind, and the surface air temperature. Enhanced precipitation occurs over the Nordic Seas and Scandinavia during high NAO phases because low pressure systems take a more northerly route. Different NAO elements affect the sea ice that modifies the ocean - atmosphere fluxes and the fresh water input into the ocean. This complex forcing and its influence on sea ice and ocean are difficult to disentangle. In numerical experiments, we investigated the response of the ocean-sea ice system to individual forcing elements of the NAO. Gerdes and Köberle (2000) describe the development of fresh water anomalies that are introduced off Norway (simulating enhanced precipitation and run-off although the effect of enhanced Atlantic inflow and evaporation over an anomalously warm ocean may be more important) and in the Laptev Sea (simulating wind induced changes in sea ice formation rate

and/or changes in Siberian river run-off). The first anomaly moves into the Barents Sea where it is mixed vertically by winter convection. The fresh water leaves the Barents Sea through the St.Anna trough and takes part in the cyclonic circulation around the Eurasian Basin. After approximately 10 years the signal has reached the central Lomonosov Ridge with maximum amplitude at intermediate depths. Since this signal will leave the Arctic through Fram Strait this mechanism could be important for the properties of the intermediate water that is available for the overflow at Denmark Strait. The Laptev Sea anomaly remains surface trapped and spreads along the oceanic transpolar drift towards Fram Strait. The time scale is much shorter than for the intermediate water described above. The propagation is reminiscent of sea ice induced signals in the Arctic that were seen in the hindcast experiments (Fig. 19).

One of the most prominent events in the atmospheric forcing during the VEINS period was the sudden drop of the NAO index in 1995/96 that followed a prolonged period of high NAO index years. In the model we compare a continuous high NAO forcing reference experiment with two scenarios where (only) the wind stress switches to low NAO forcing for different periods (Fig. 35). In "switch" the forcing changes permanently to low NAO while it returns to high NAO forcing after one year in "peak" (Brauch et al., 1999). The experiments show a clear response to a sudden drop in NAO and the following recovery. There is a direct connection between the wind stress and the sea ice cover and a subsequent reaction of the SSS and SST fields. SSS in both experiments decreases in the Laptev and Kara seas as well as in large parts of the Eurasian Basin as a consequence of closer sea ice cover and increased ice thickness. This prevents the new formation of sea ice and the associate brine release that raises salinity in the reference experiment. South of Fram Strait we find higher salinities in the EGC as the melt water input is reduced with the Fram Strait ice export (Fig. 36). The response in the "peak" experiment is limited because the anomalous fluxes only act for a relative short time compared to the transport time scales from the Arctic into the Nordic Seas. Compared to the SST - NAO relationship in the full hindcast simulations we find similar SST anomalies in the Barents Sea and the region south of Svalbard (Fig. 8). A negative temperature anomaly in the hindcast off the

south-east coast of Greenland did not occur in the response experiments (Fig. 37). This anomaly seems to be due to changes in the thermohaline fluxes associated with changes in NAO forcing.

Summary and thoughts toward a conceptual model

- to be completed -

Figure captions

Fig.1 Domain of the high resolution model (HRM). The color coding shows the bottom topography used in the model. The bold lines indicate the position of the sections for which transports have been calculated (see Fig. 4).

Fig.2 Domain of the lower resolution model (LRM). The color coding shows the bottom topography used in the model.

Fig.3 Surface circulation in the HRM averaged over the integration period 1979-1998. Color coding indicates the speed of the current, arrows give the direction.

Fig.4 Transport time series: a) Iceland-Faeroe, b) Faeroe-Scotland, c) Svinøy, d) Barents Sea inflow, e) Fram Strait, f) Denmark Strait. We distinguish northward and southward fluxes. Northward (southward) volume fluxes are computed as positive (negative) velocity component times the area of a grid box. Northward (southward) heat fluxes are computed as temperature above $-2^{o}C$ times positive (negative) velocity component times grid box area times the specific heat for sea water. Salt fluxes are calculated relative to 34.9 using the same convention for the direction of the flux as for the heat fluxes.

Fig.5 a) Fraction of the variability of the stream function that can be accounted for by a linear relation with the NAO index, b) associated standard deviation

Fig.6 a) and b) Temperature anomalies [K] from the long-term mean at 100m depth in two successive winters in the early 1980s. c) and d) same as a), b) for the SST in two successive winters around 1990.

Fig.7 a) EOF #1 and b) #2 for SST anomalies from the HRM.

Fig.8 a) Fraction of the SST variability that can be accounted for by a linear response to the NAO, b) associated standard deviation

Fig.9 a) Fraction of the SSS variability that can be accounted for by a linear response to the NAO, b) associated standard deviation

Fig.10 a) Fraction of the variability in surface fresh water flux that can be accounted for by a linear response to the NAO, b) associated standard deviation

Fig.11 a) Fraction of the temperature variability on a quasi-zonal section across the

Nordic Seas that can be accounted for by a linear relationship with NAO, b) associated standard deviation

Fig.12 a) Standard deviation of the temperature variability at 200m depth that is described by a linear relation with NAO, b) same for 500 m depth

Fig.13 Standard deviation of the temperature variability at 500m depth that is described by a linear relation with NAO for the LRM

Fig.14 Fraction of the SST variability that can be accounted for by a linear relationship with the NAO at different time lags: a) -3 years lag (i.e. the SST signal precedes the NAO by 3 years), b) -2 years lag, c) -1 year lag, d) zero lag (identical with Fig. 8a), e) 1 year lag, f) 2 years lag, g) 3 years lag.

Fig.15 Fraction of the surface heat flux variability that can be accounted for by a linear relationship with the NAO at different time lags: a) zero lag, b) 1 year lag, c) 2 years lag, d) 3 years lag

Fig.16 Temperatures at 500m depth for 9/1990 – 3/1992. Only temperatures between 0 and 3^{o}C are shown.

Fig.17 Fraction of the temperature variability at 200 m depth that can be accounted for by a linear relationship with the NAO at different time lags: a) zero lag, b) one year lag, c) two years lag, d) three years lag

Fig.18 Surface salinity anomaly (LRM) from ten year means centered in 19xx and 19yy, respectively, a) 19zz (after 1967/68 ice export event), b) 19ss (after 1994/95 ice export event)

Fig.19 Fraction of the SSS variability fraction that can be accounted for by a linear relationship with the Fram Strait ice transport time series (Fig.6 from Kauker et al. 1999a)

Fig.20 EOFs #1 and #2 for the heat transport (see text for a definition) in the Iceland-Scotland area

Fig.21 a) Correlation of PC #1 with large scale heat transport anomalies, and b) the total heat transport for different strengths of the Iceland-Scotland heat flux EOF #1. In b) the pattern from a) is multiplied with a factor between -2 and 2, roughly reflecting the amplitude of the PC, and added to the mean transport

(shown for factor 0).

Fig.22 same as Fig. 21 for EOF #2

Fig.23 Standard deviation of the streamfunction variability that is described by a linear relation with the PCs of the Iceland-Scotland heat transport modes a) EOF #1, b) EOF #2

Fig.24 Standard deviation of the SLP variability that is described by a linear relation with the PCs of the Iceland-Scotland heat transport modes a) EOF #1, b) EOF #2.

Fig.25 EOFs #1 and #2 for the heat transport in the Denmark Strait area

Fig.26 as Fig. 20 for the Denmark Strait heat transport modes

Fig.27 EOFs #1 and #2 for the heat transport in the Fram Strait area. These results are taken from the HRM hindcast

Fig.28 as Fig. 21 for the Fram Strait area

Fig.29 a) Fraction of the variability of the SLP variability that can be accounted for by a linear relation with PC #2 of the Fram Strait are heat transport EOFs, b) associated standard deviation

Fig.30 Hovmöller diagram for the meridional velocity component at 100 m depth on a quasi-zonal section through the Nordic Seas a) daily varying wind over the whole domain, b) daily varying wind only north of 80^{o}N while the wind varies monthly over the rest of the domain

Fig.31 Anomalous streamfunction as a response to deep convection in the Labrador Sea

Fig.32 Anomalous streamfunction as a response to deep convection in the Greenland Sea

Fig.33 Surface salinity anomaly four years after first introducing a sea ice anomaly in Fram Strait (see text)

Fig.34 Hovmöller diagram for mixed layer depth on a section through the Labrador Sea in the Fram Strait sea ice anomaly experiment. A fresh water anomaly arrives at the section in year 13 on the Greenland (upper) side and leads to a reduction in convection depth.

Fig.35 Experimental design for the switch in NAO wind (Fig.2 from Brauch et al., 1999)

Fig.36 Difference in surface salinity in the winter of year 10/11 between the "switch" experiment and the reference run (Fig.3 from Brauch et al., 1999)

Fig.37 Difference in SST in the winter of year 10/11 between the "switch" experiment and the reference run (Fig.7 from Brauch et al., 1999).

References

Brauch, J, R Gerdes, M Karcher, F Kauker, and C Köberle, 1999: Response experiments with NAO related forcing, , ICES CM 1999/L:28, 6pp.

Dickson, R.R., J. Meincke, S.-A. Malmberg, and A.J. Lee, 1988: The great salinity anomaly in the northern North Atlantic, 1968-1982, Prog. Oceanogr., 20, 103-151

Gerdes R, 1995: Convection and deep water spreading. Proceedings of the Toulon workshop on "Topographic effects in the ocean".

Gerdes, R, 2000: Modelling the variability of exchanges between the Arctic Ocean and the Nordic Seas, in L.E.Lewis (ed.), The Arctic Ocean freshwater budget, NATO ARW, Kluever, Dordrecht (in press)

Gerdes, R and C Köberle, 1995: On the influence of DSOW in a numerical model of the North Atlantic general circulation, J.Phys.Oceanogr. **25**, 2624-2642

Gerdes, R, and C Köberle, 2000: Numerical simulation of salinity anomaly propagation in the Nordic Seas and the Arctic Ocean (Polar Research, in press)

Gerdes R, and C Köberle, 2000: Arctic sea ice volume variability from a hindcast simulation. Proceedings of the ACSYS Conference, Koblenz, Germany (in press).

Gerdes R, C Köberle, F Kauker, 1999: Possible influence of sea ice on decadal atmospheric variability in the North Atlantic (in preparation)

Gerdes, R, M Karcher, C Köberle, B Fritzsch, and J Brauch, 1999: Propagation of Atlantic Water into the Nordic Seas and the Arctic Ocean in high-resolution coupled sea ice-ocean simulations (in preparation)

Gerdes, R and U Schauer, 1997: Large-scale circulation and water mass distribution in the Arctic Ocean from model results and observations, J.Geophys.Res., **102** (C4), 8467-8483

Kalnay et al., 1996: The NCEP/NCAR 40-year reanalysis project, Bull.Am.Met.Soc., 77, 437-495

Karcher, M., J. Brauch, B. Fritzsch, R. Gerdes, F.Kauker, C.Köberle, and M. Prange, 1999: Variability in the Nordic Seas exchange – model results 1979-1993, ICES CM 1999/L:18, 7pp.

Kauker, F., 1998: Regionalization of climate model results for the North Sea. PhD thesis University of Hamburg, 109 pp.

Kauker, F., R. Gerdes, and C. Köberle, 1999a: Propagation of temperature and salinity anomalies in the Nordic Seas derved from a multi-decadal OGCM simulation, ICES ASC 1999 – CM 1999/L:12, 8 pp.

Kauker F, R Gerdes, and C Köberle, 1999b: Decadal predictability of North East Atlantic sea surface temperature as derived from a multi-decadal OGCM simulation (submitted to Geophysical Research Letters)

Köberle C, and R Gerdes, 1999: Modelling of sea ice induced salinity anomalies in the North Atlantic (in preparation)

Köberle C, and R Gerdes, 2000: Mechanisms determining Fram Strait ice export variability (in preparation)

Köberle, C., R. Gerdes, and F.Kauker, 1999: Mechanisms determining Fram Strait ice

export variability, ICES ASC 1999 – CM 1999/L:25, 7 pp.

Lazier, J.R.N., 1980: Oceanographic conditions at Ocean Weather Ship BRAVO; 1964-1974, Atmos.-Ocean., 18, 227-238

Rhein, M., 1991: Ventilation rates of the Greenland and Norwegian Seas derived from distributions of the chlorofluoromethanes F11 and F12, Deep-Sea Res., 38, 485-503

Steele, M., and T.Boyd, 1998: Retreat of the cold halocline layer in the Arctic Ocean, J.Geophys.Res., 103(C5), 10419-10435

Sutten, R.T., and M.R. Allen, 1997: Decadal predictability of North Atlantic sea surface temperature and climate, Nature, 388, 563-567

Zhang J., D.A. Rothrock, and M. Steele, 1998: Warming of the Arctic Ocean by a strengthened Atlantic inflow: Model results, Geophysical Res. Letters

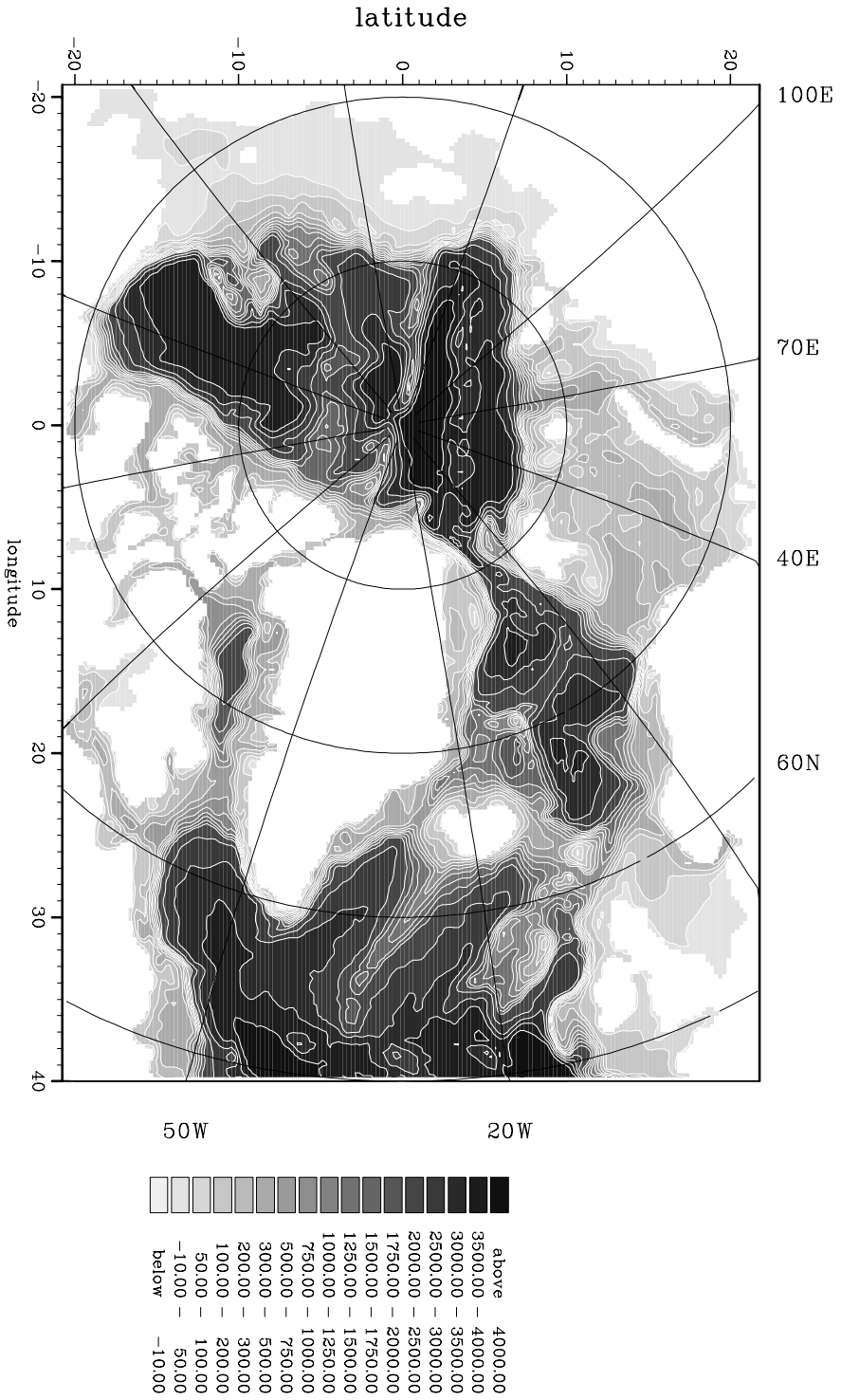

Fig.1 Domain of the high resolution model (HRM). The color coding shows the bottom topography used in the model. The bold lines indicate the position of the sections for which transports have been calculated (see Fig. 4).

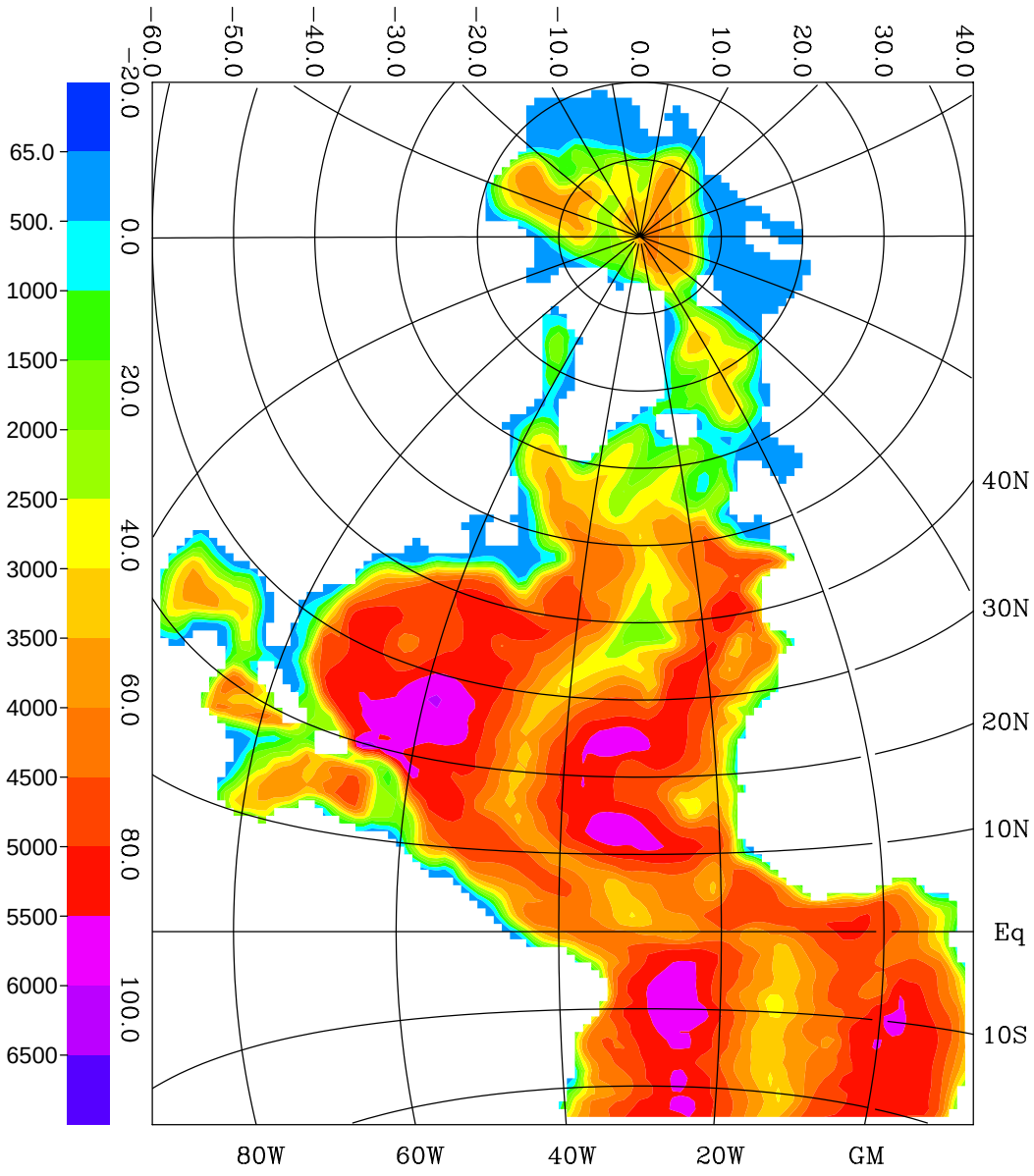

Fig.2 Domain of the lower resolution model (LRM). The color coding shows the bottom topography used in the model.

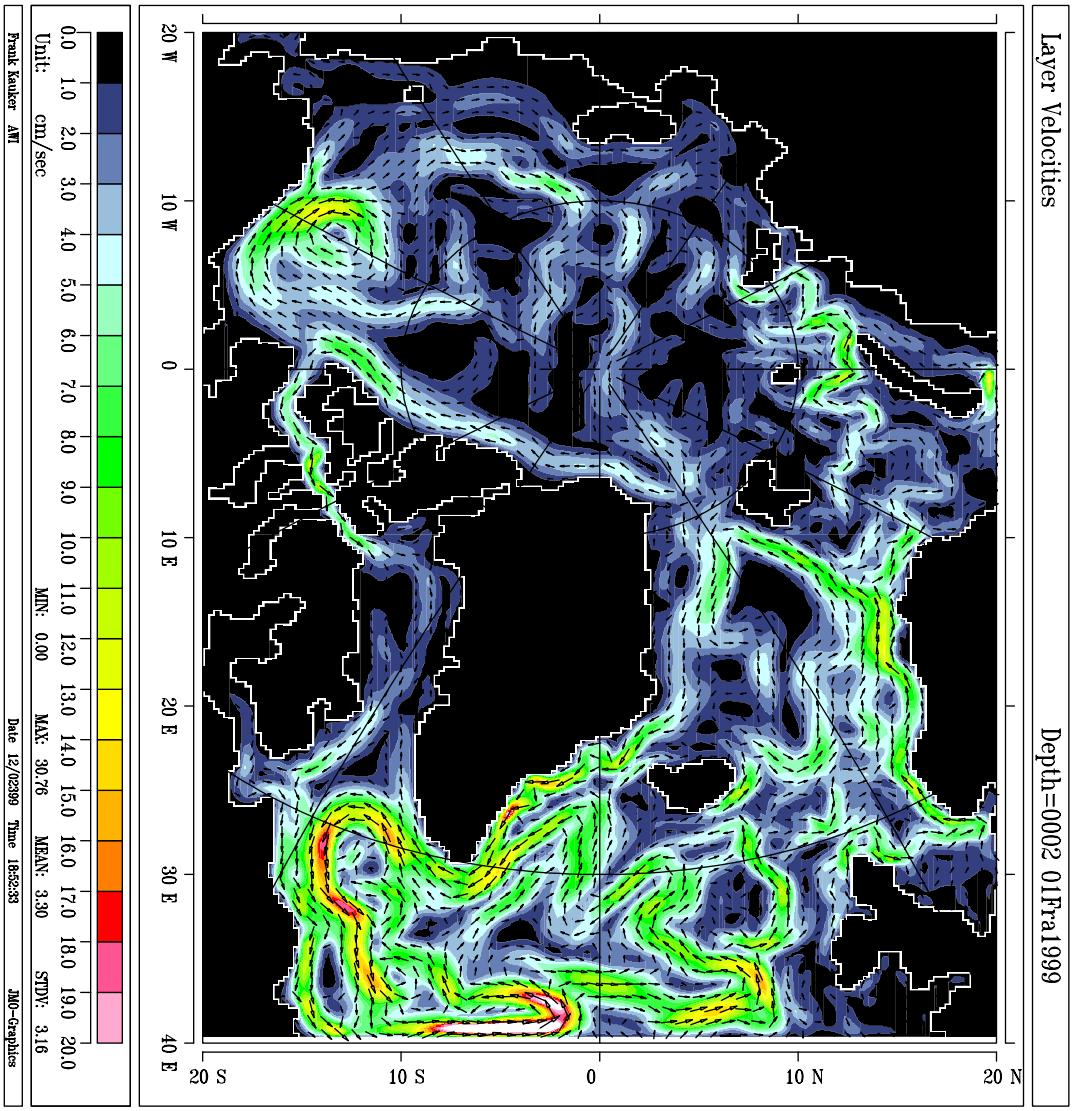

Fig.3 Surface circulation in the HRM averaged over the integration period 1979-1998. Color coding indicates the speed of the current, arrows give the direction.

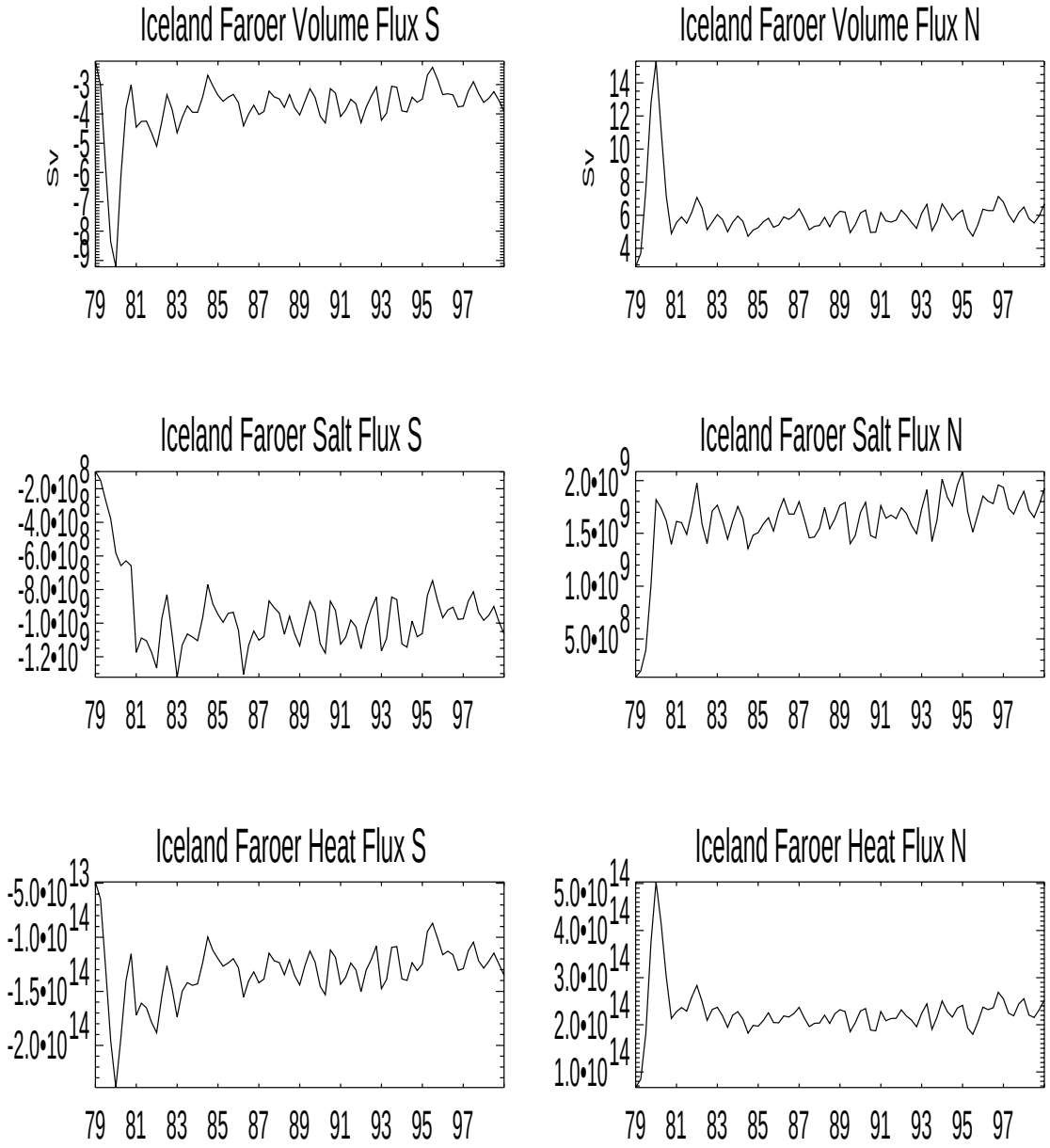

Fig. 4a

Fig.4 Transport time series: a) Iceland-Faeroe, b) Faeroe-Scotland, c) Svinøy, d) Barents Sea inflow, e) Fram Strait, f) Denmark Strait. We distinguish northward and southward fluxes. Northward (southward) volume fluxes are computed as positive (negative) velocity component times the area of a grid box. Northward (southward) heat fluxes are computed as temperature above –2^{o}C times positive (negative) velocity component times grid box area. Salt fluxes are calculated relative to 34.9 using the same convention for the direction of the flux as for the heat fluxes.

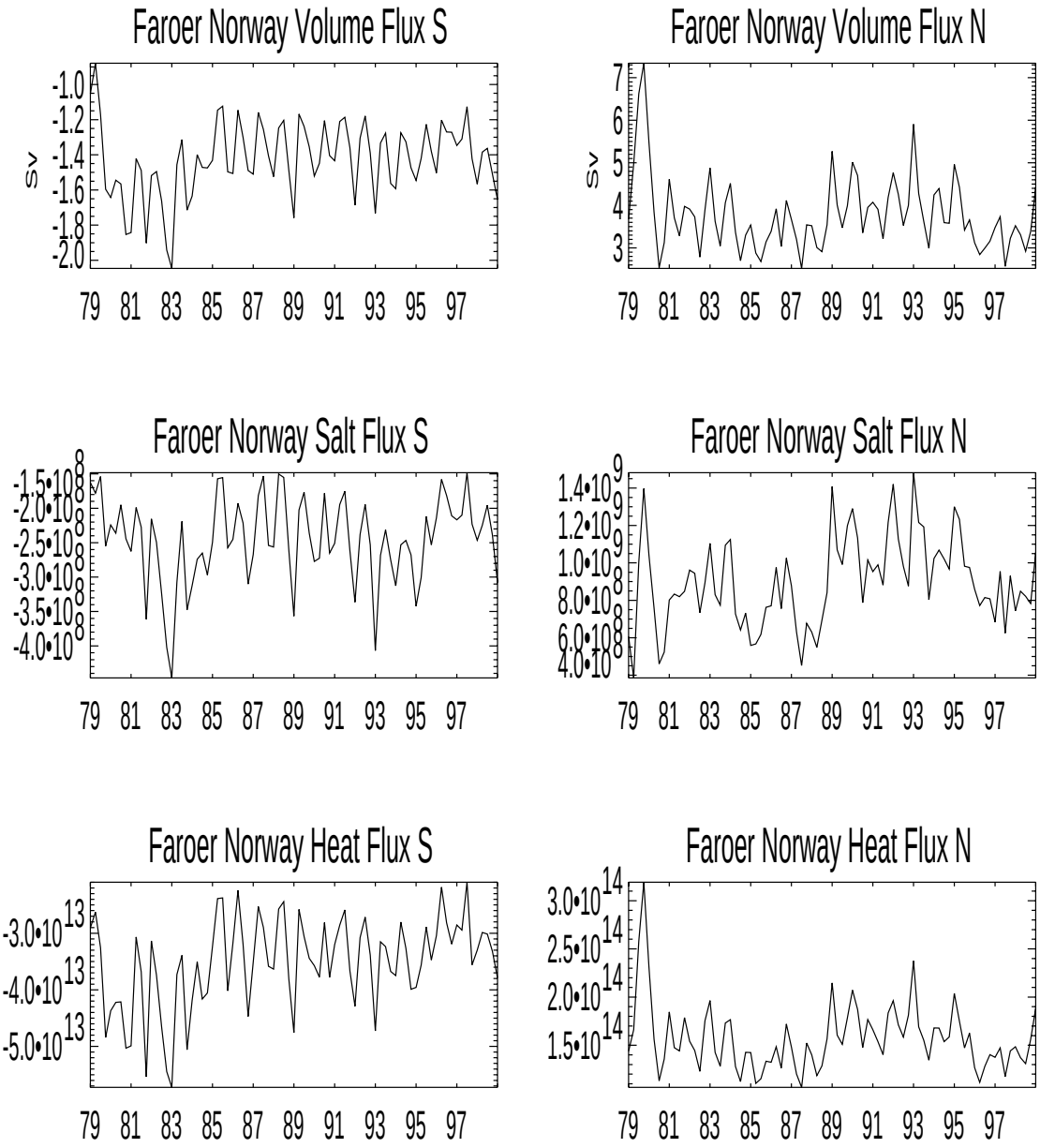
Faroer Norway Volume Flux S
Sv
-1.0
-1.2
-1.4
-1.6
-1.8
-2.0
79 81 83 85 87 89 91 93 95 97
Faroer Norway Volume Flux N
Sv
7
6
5
4
3
79 81 83 85 87 89 91 93 95 97
Faroer Norway Salt Flux S
-1.5•10^8
-2.0•10^8
-2.5•10^8
-3.0•10^8
-3.5•10^8
-4.0•10^8
79 81 83 85 87 89 91 93 95 97
Faroer Norway Salt Flux N
1.4•10^9
1.2•10^9
1.0•10^8
8.0•10^8
6.0•10^8
4.0•10^8
79 81 83 85 87 89 91 93 95 97
Faroer Norway Heat Flux S
-3.0•10^13
-4.0•10^13
-5.0•10^13
79 81 83 85 87 89 91 93 95 97
Faroer Norway Heat Flux N
3.0•10^14
2.5•10^14
2.0•10^14
1.5•10^14
79 81 83 85 87 89 91 93 95 97

Fig.4b

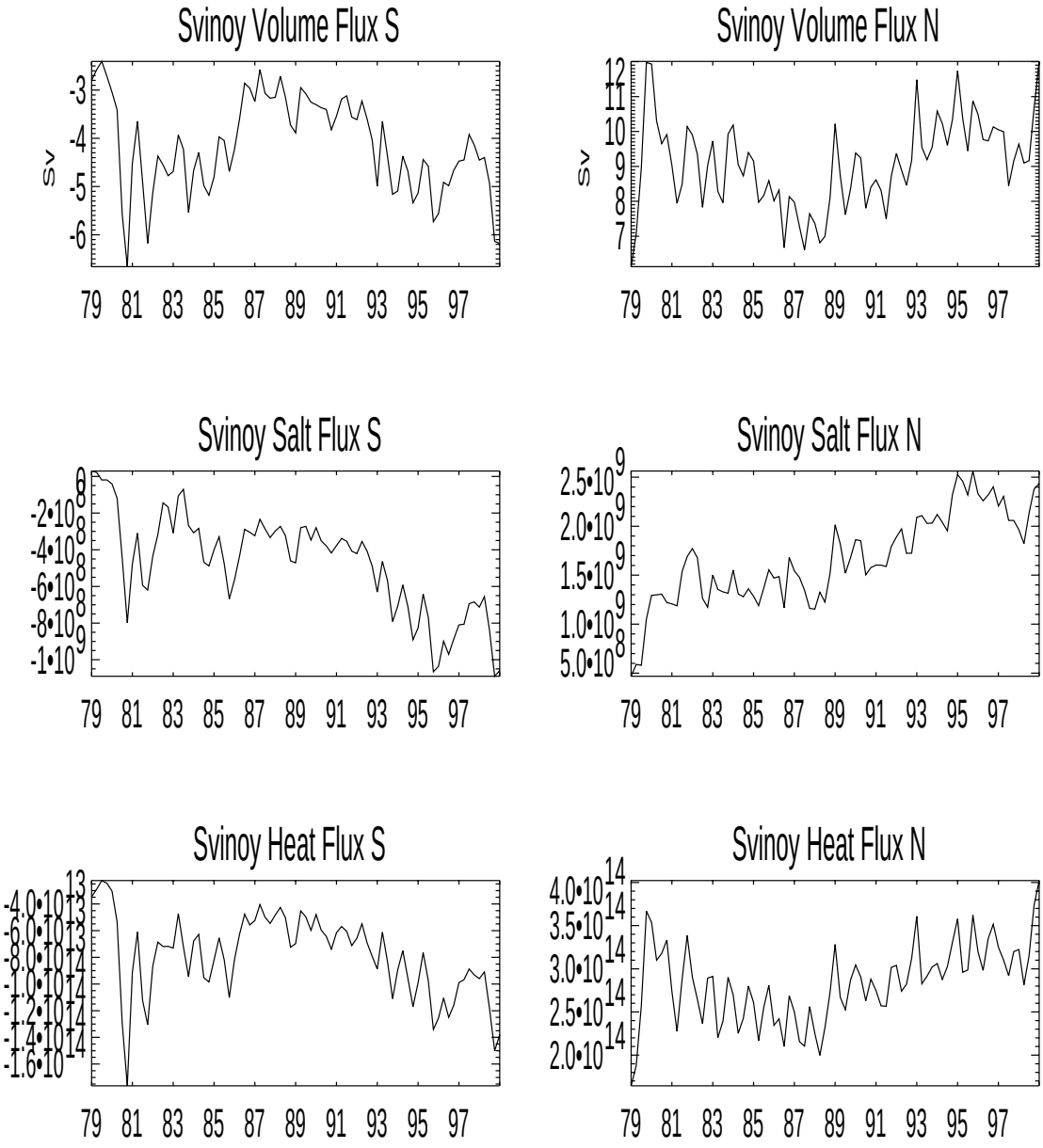
Svinoy Volume Flux S
sv
-3
-4
-5
-6
79 81 83 85 87 89 91 93 95 97
Svinoy Volume Flux N
sv
12
11
10
9
8
7
79 81 83 85 87 89 91 93 95 97
Svinoy Salt Flux S
0
-2•10^8
-4•10^8
-6•10^8
-8•10^8
-1•10^9
79 81 83 85 87 89 91 93 95 97
Svinoy Salt Flux N
2.5•10^9
2.0•10^9
1.5•10^9
1.0•10^9
5.0•10^8
79 81 83 85 87 89 91 93 95 97
Svinoy Heat Flux S
-4.0•10^13
-6.0•10^13
-8.0•10^13
-1.0•10^14
-1.2•10^14
-1.4•10^14
-1.6•10^14
79 81 83 85 87 89 91 93 95 97
Svinoy Heat Flux N
4.0•10^14
3.5•10^14
3.0•10^14
2.5•10^14
2.0•10^14
79 81 83 85 87 89 91 93 95 97

Fig. 4c

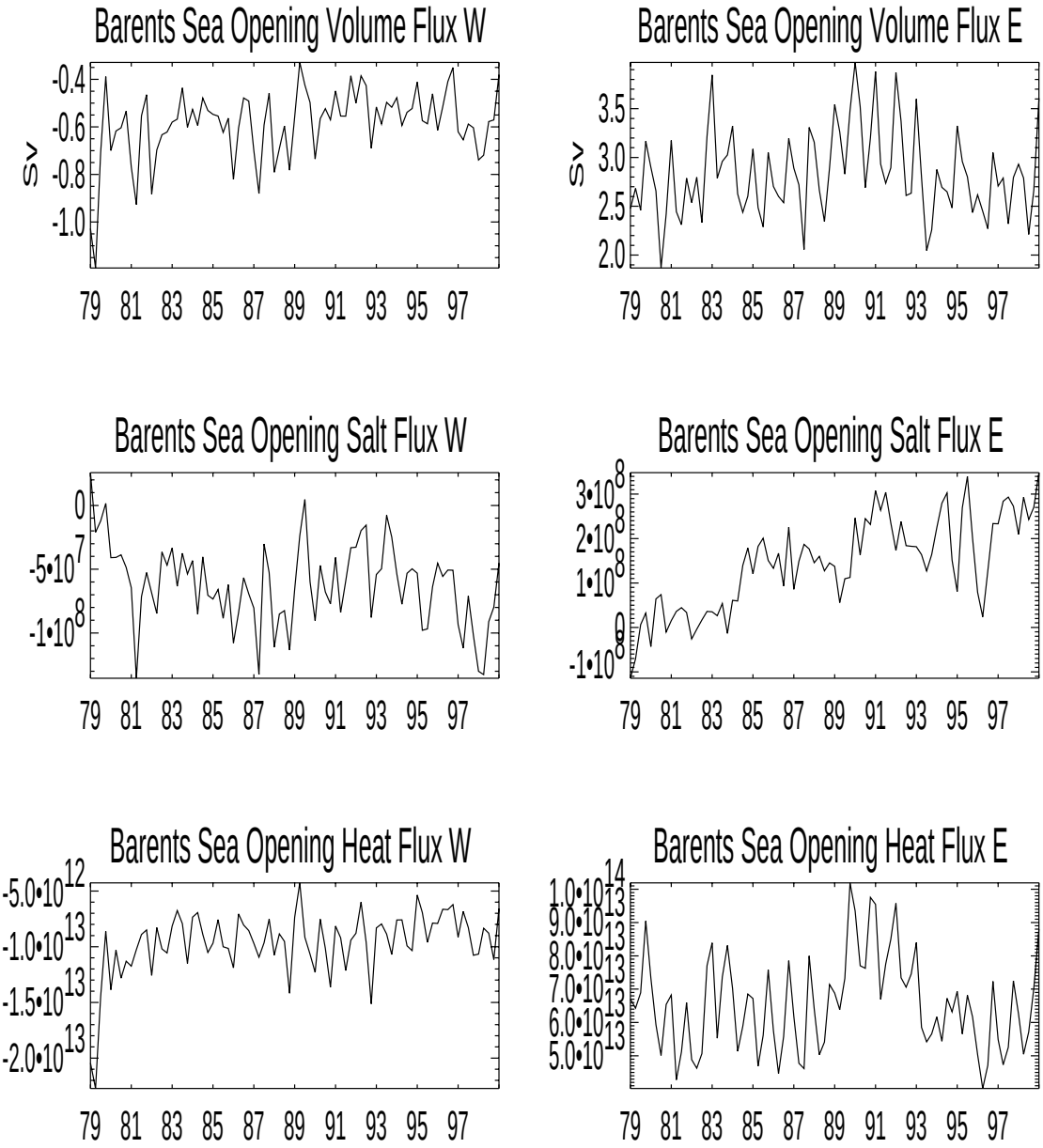
Barents Sea Opening Volume Flux W
Sv
-0.4
-0.6
-0.8
-1.0
79 81 83 85 87 89 91 93 95 97
Barents Sea Opening Volume Flux E
Sv
3.5
3.0
2.5
2.0
79 81 83 85 87 89 91 93 95 97
Barents Sea Opening Salt Flux W
0
-5•10^7
-1•10^8
79 81 83 85 87 89 91 93 95 97
Barents Sea Opening Salt Flux E
3•10^8
2•10^8
1•10^8
0
-1•10^8
79 81 83 85 87 89 91 93 95 97
Barents Sea Opening Heat Flux W
-5.0•10^12
-1.0•10^13
-1.5•10^13
-2.0•10^13
79 81 83 85 87 89 91 93 95 97
Barents Sea Opening Heat Flux E
1.0•10^14
9.0•10^13
8.0•10^13
7.0•10^13
6.0•10^13
5.0•10^13
79 81 83 85 87 89 91 93 95 97

Fig. 4d

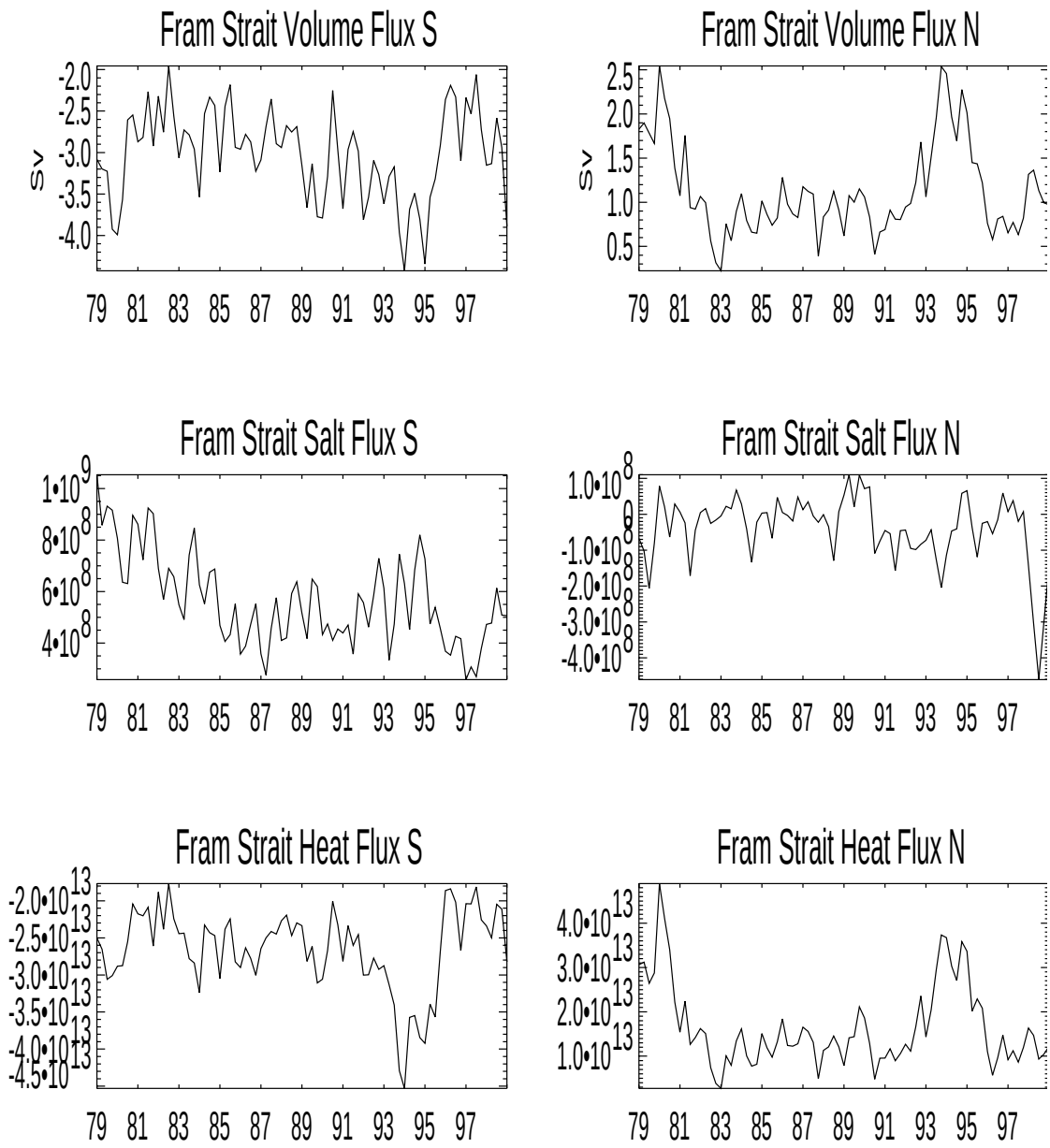
Fram Strait Volume Flux S
Sv
-2.0
-2.5
-3.0
-3.5
-4.0
79 81 83 85 87 89 91 93 95 97
Fram Strait Volume Flux N
Sv
2.5
2.0
1.5
1.0
0.5
79 81 83 85 87 89 91 93 95 97
Fram Strait Salt Flux S
1•10^9
8•10^8
6•10^8
4•10^8
79 81 83 85 87 89 91 93 95 97
Fram Strait Salt Flux N
1.0•10^8
-1.0•10^8
-2.0•10^8
-3.0•10^8
-4.0•10^8
79 81 83 85 87 89 91 93 95 97
Fram Strait Heat Flux S
-2.0•10^13
-2.5•10^13
-3.0•10^13
-3.5•10^13
-4.0•10^13
-4.5•10^13
79 81 83 85 87 89 91 93 95 97
Fram Strait Heat Flux N
4.0•10^13
3.0•10^13
2.0•10^13
1.0•10^13
79 81 83 85 87 89 91 93 95 97

Fig. 4e

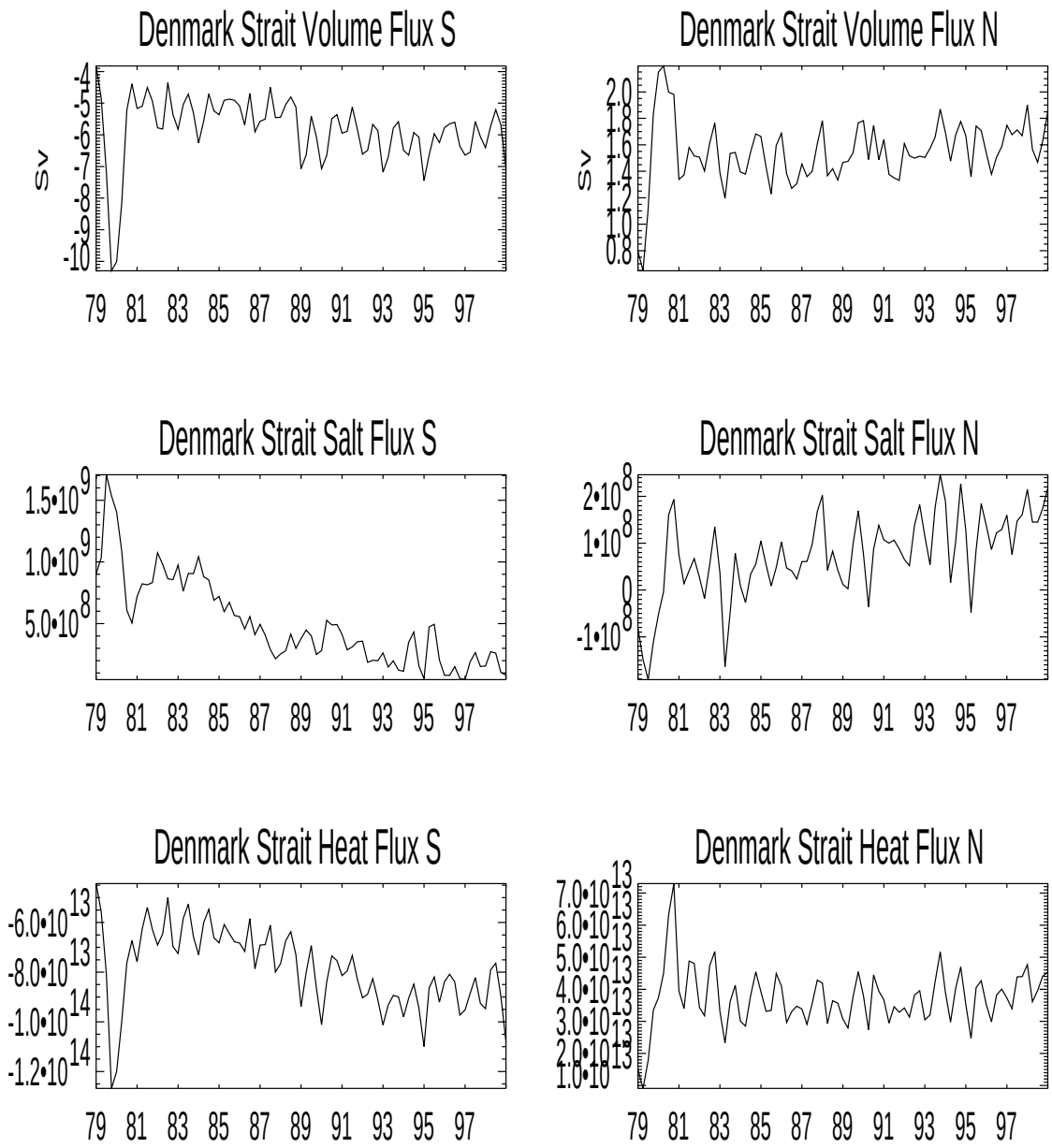
Denmark Strait Volume Flux S
Sv
-4
-6
-8
-10
79 81 83 85 87 89 91 93 95 97
Denmark Strait Volume Flux N
Sv
2.0
1.8
1.6
1.4
1.2
1.0
0.8
79 81 83 85 87 89 91 93 95 97
Denmark Strait Salt Flux S
1.5•10^9
1.0•10^9
5.0•10^8
79 81 83 85 87 89 91 93 95 97
Denmark Strait Salt Flux N
2•10^8
1•10^8
0
-1•10^8
79 81 83 85 87 89 91 93 95 97
Denmark Strait Heat Flux S
-6.0•10^13
-8.0•10^13
-1.0•10^14
-1.2•10^14
79 81 83 85 87 89 91 93 95 97
Denmark Strait Heat Flux N
7.0•10^13
6.0•10^13
5.0•10^13
4.0•10^13
3.0•10^13
2.0•10^13
1.0•10^13
79 81 83 85 87 89 91 93 95 97

Fig. 4f

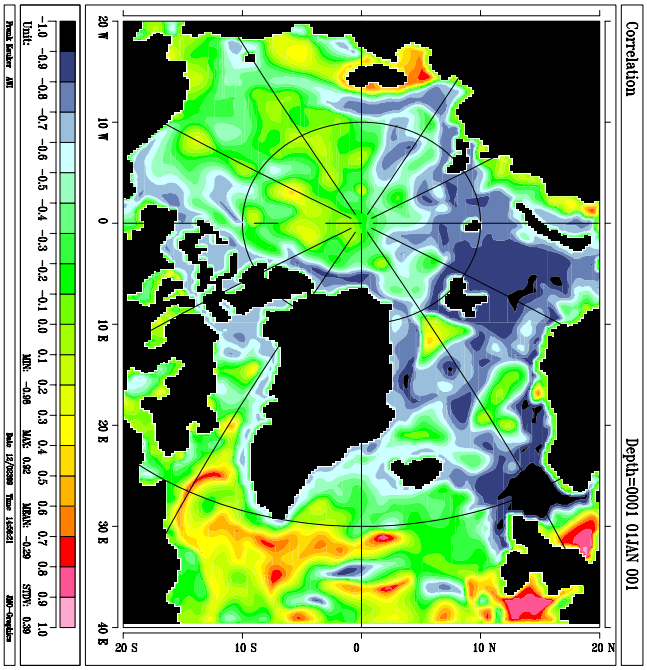

a)

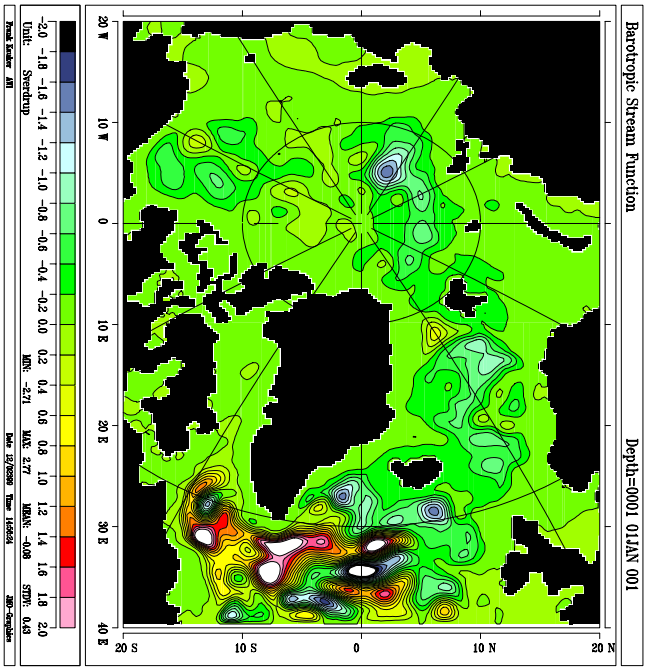

b)

Fig.5 a) Fraction of the variability of the stream function that can be accounted for by a linear relation with the NAO index, b) associated standard deviation

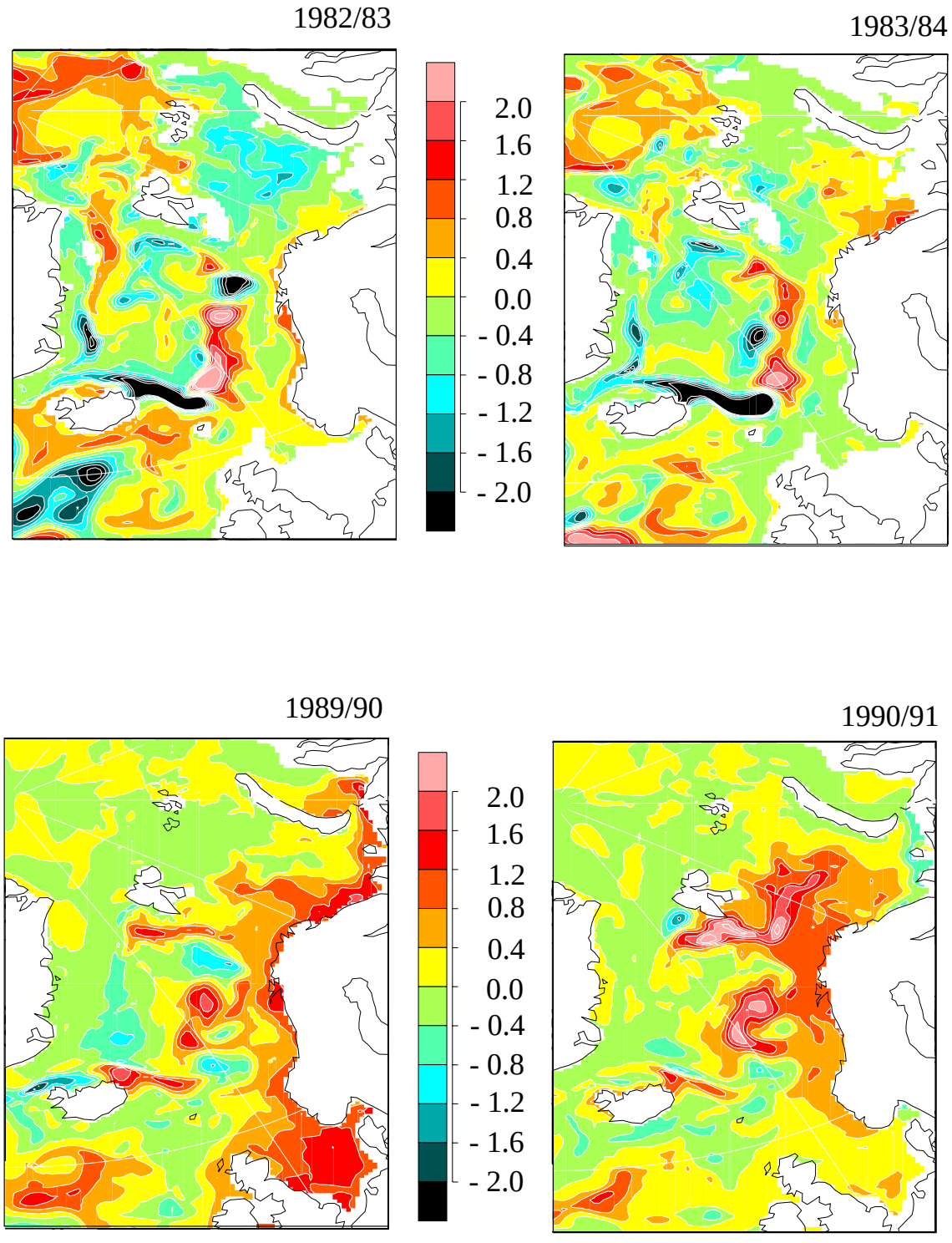

Fig.6 a) and b) Temperature anomalies [K] from the long-term mean at 100m depth in two successive winters in the early 1980s. c) and d) same as a), b) for the SST in two successive winters around 1990.

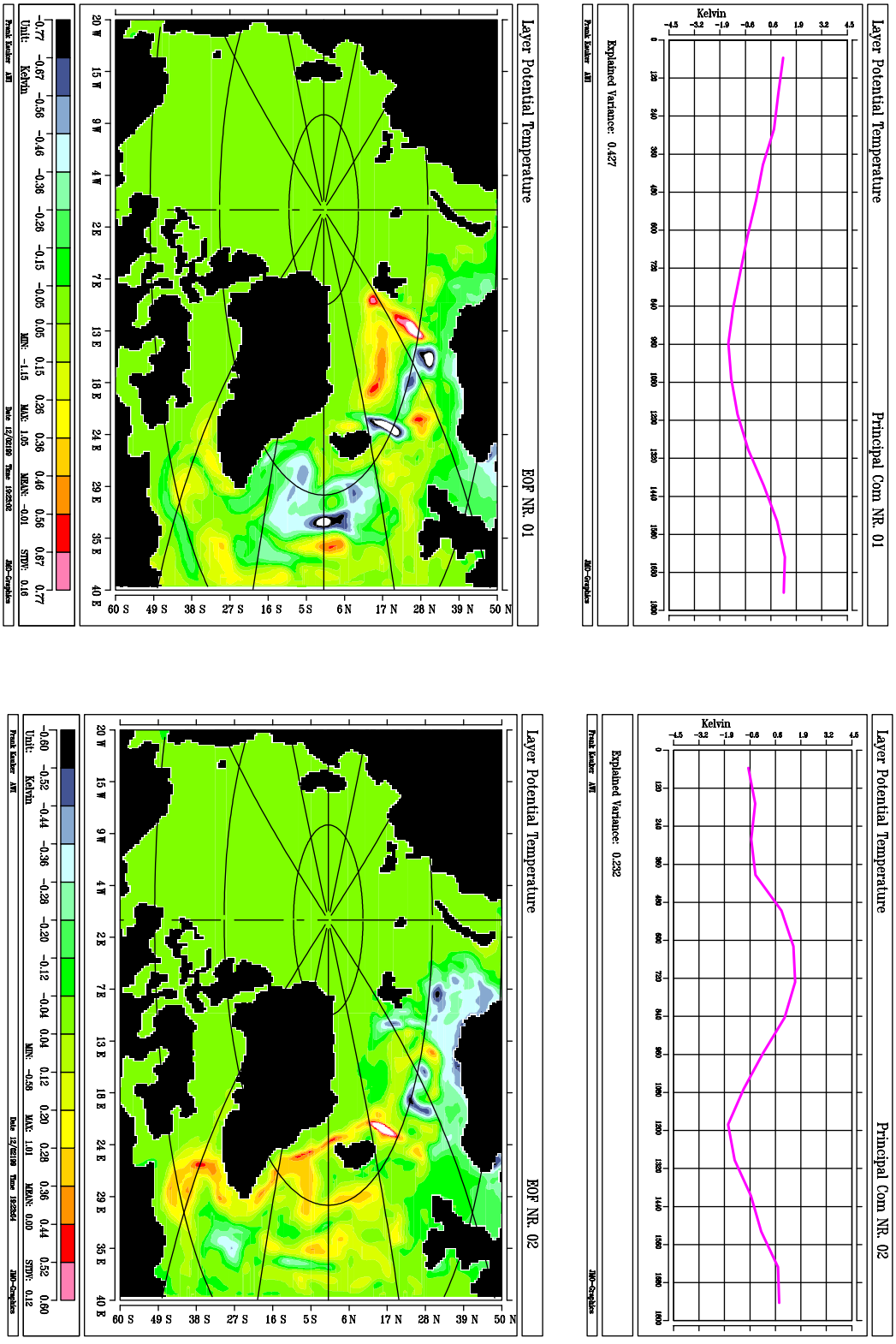

Fig.7 a) EOF #1 and b) #2 for SST anomalies from the HRM.

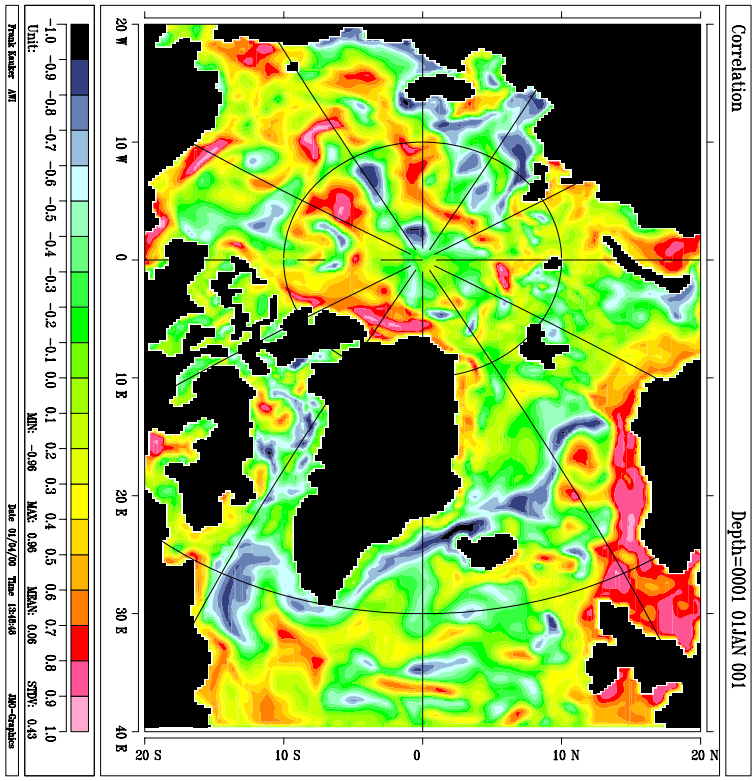

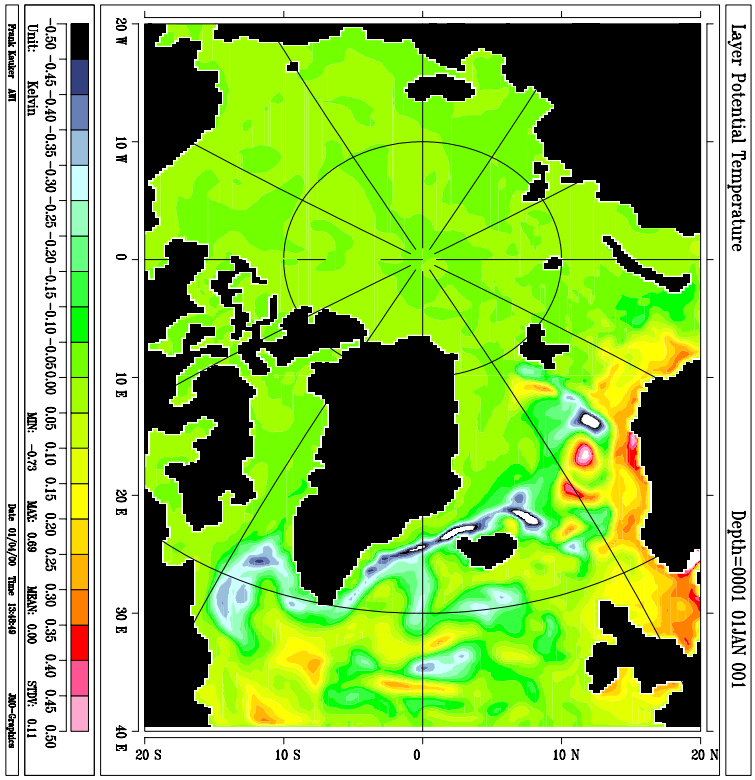

Fig.8 a) Fraction of the SST variability that can be accounted for by a linear response to the NAO, b) associated standard deviation

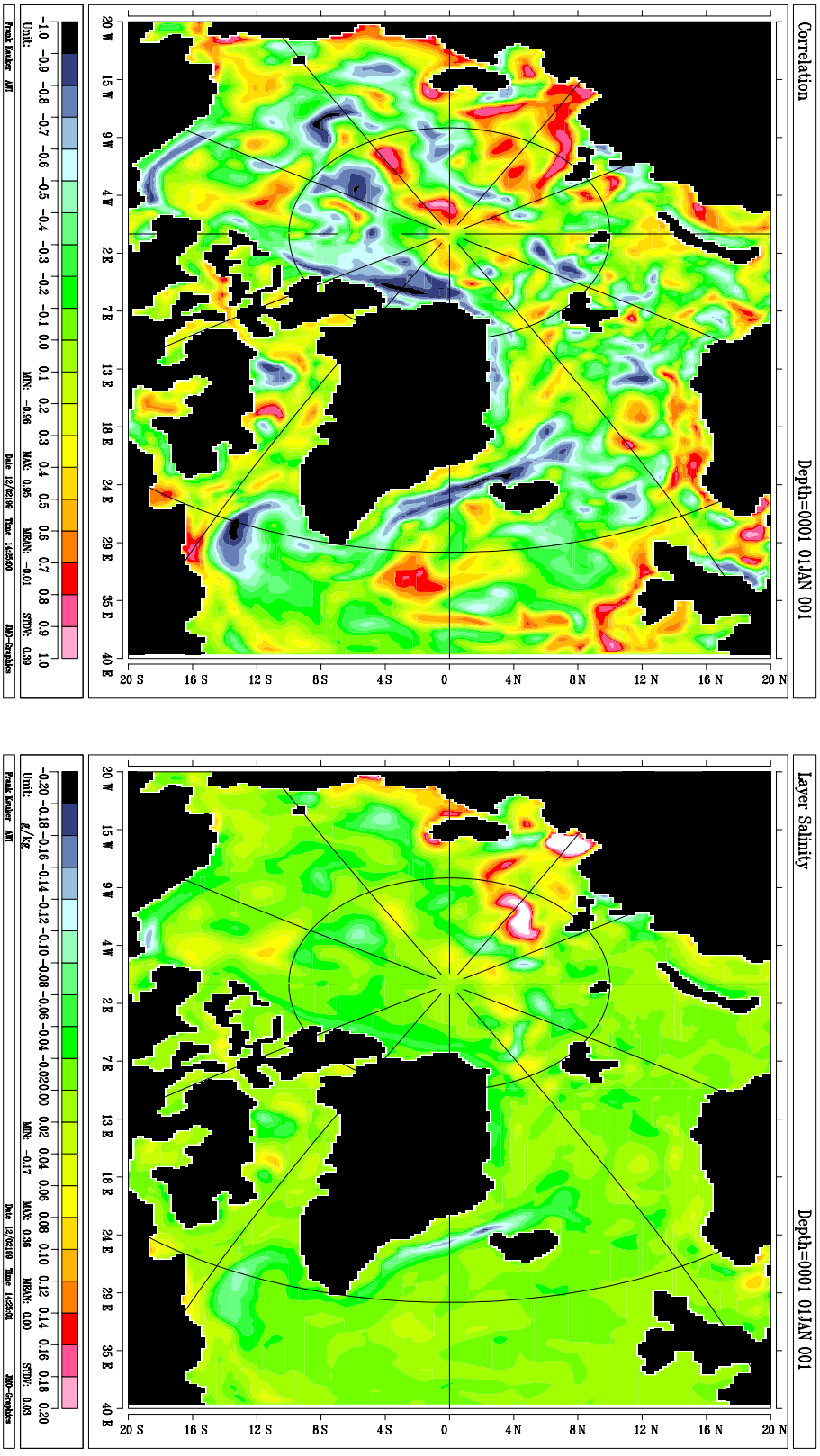

Fig.9 a) Fraction of the SSS variability that can be accounted for by a linear response to the NAO, b) associated standard deviation

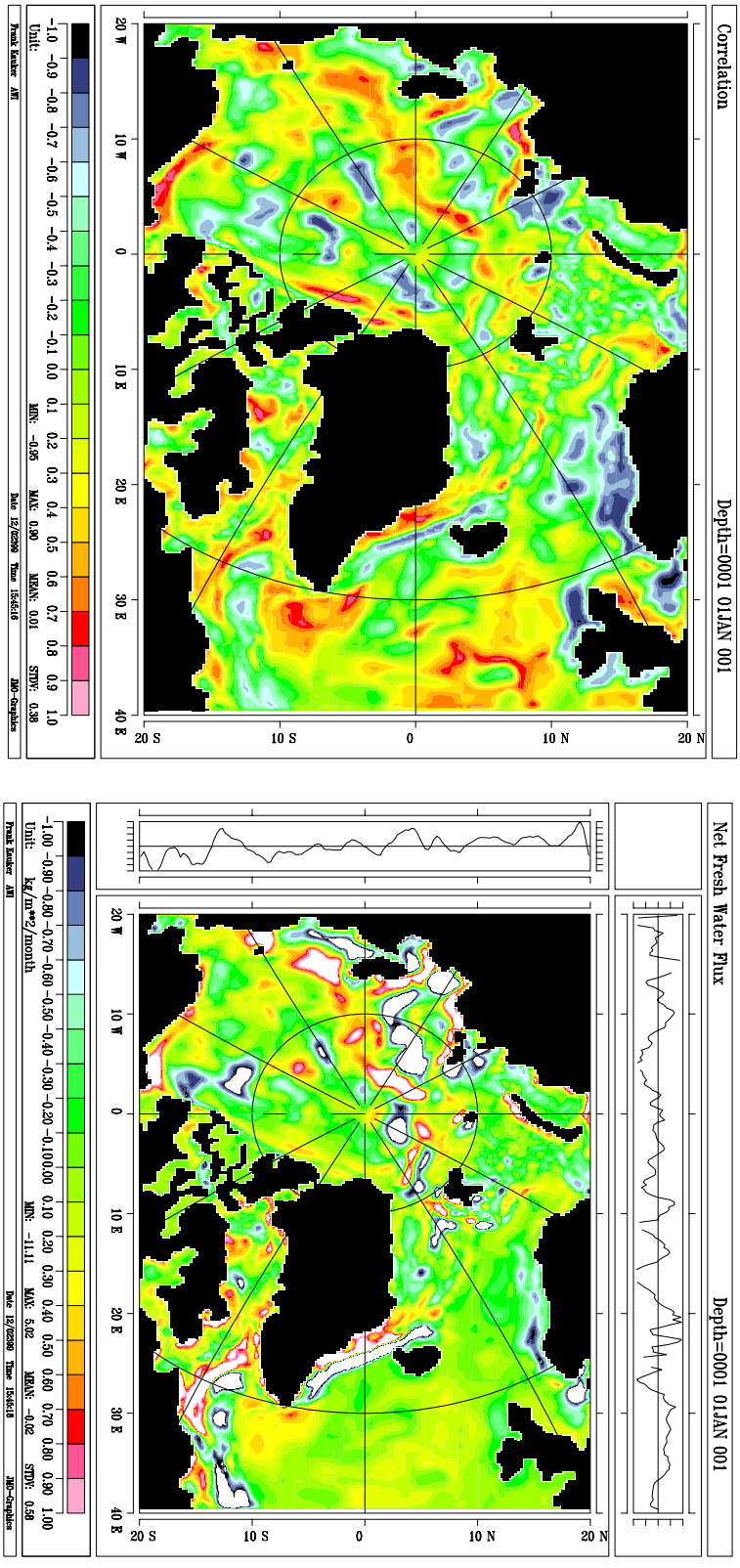

Fig.10 a) Fraction of the variability in surface fresh water flux that can be accounted for by a linear response to the NAO, b) associated standard deviation

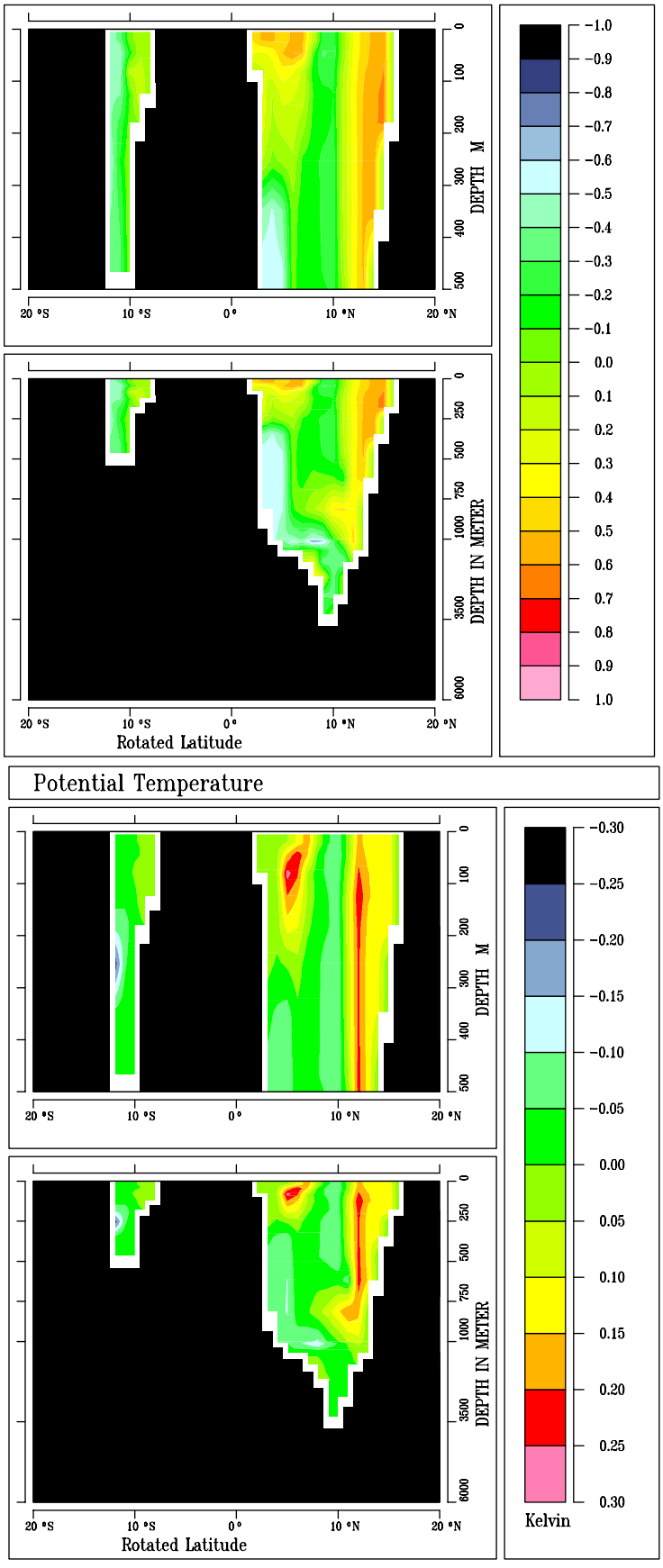

Fig.11 a) Fraction of the temperature variability on a quasi-zonal section across the Nordic Seas that can be accounted for by a linear relationship with NAO, b) associated standard deviation

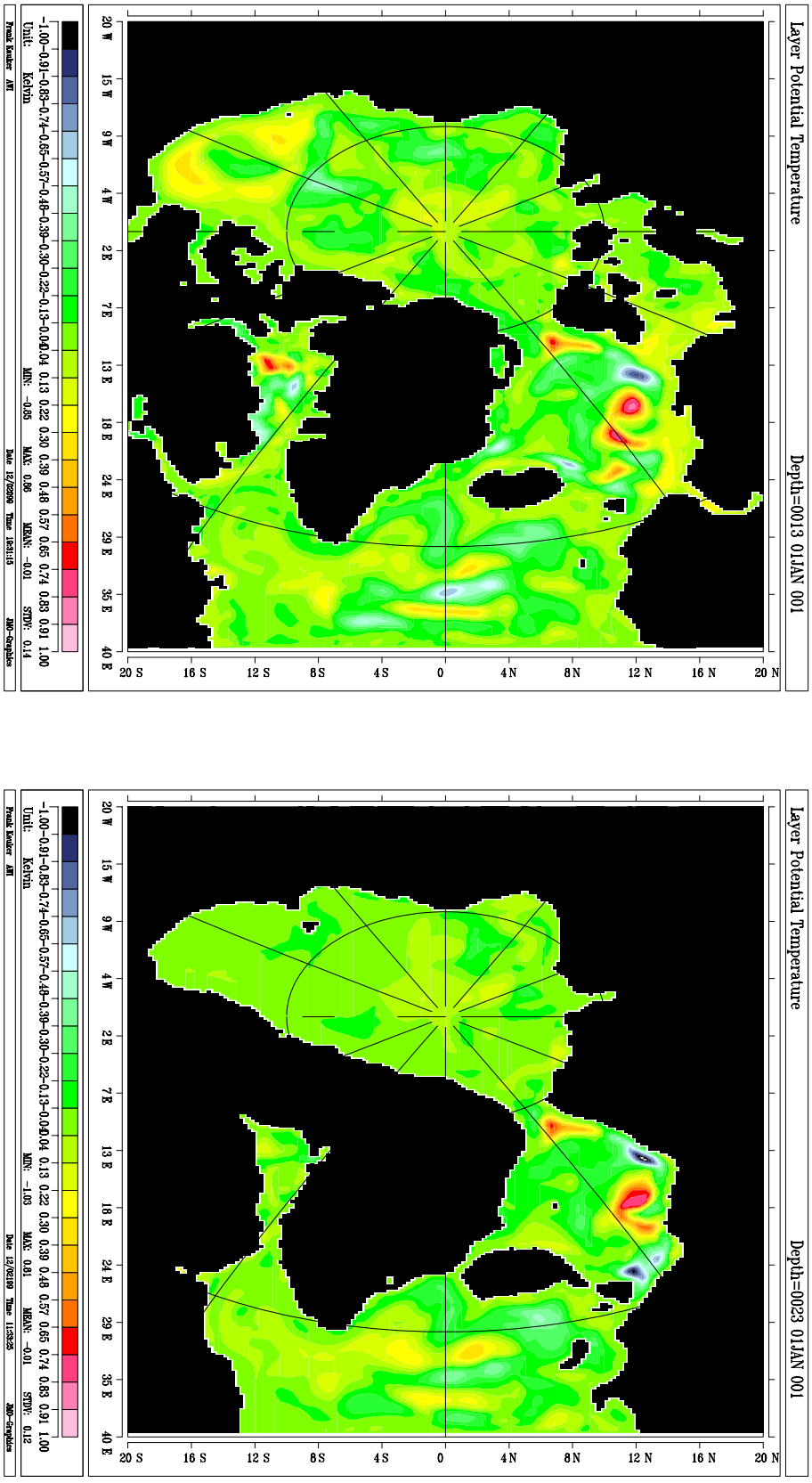

Fig.12 a) Standard deviation of the temperature variability at 200m depth that is described by a linear relation with NAO, b) same for 500 m depth

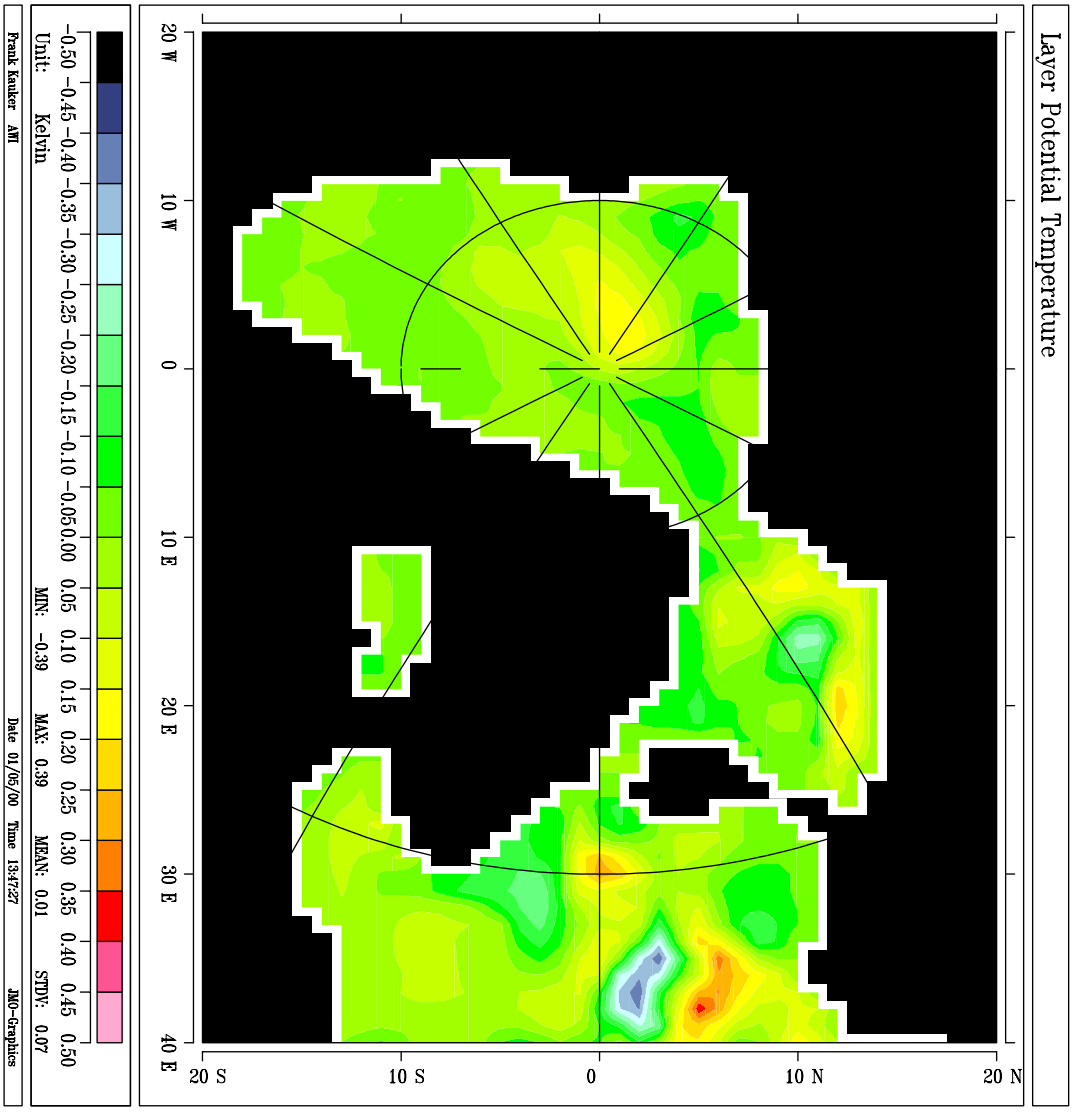

Fig.13 Standard deviation of the temperature variability at 500m depth that is described by a linear relation with NAO for the LRM

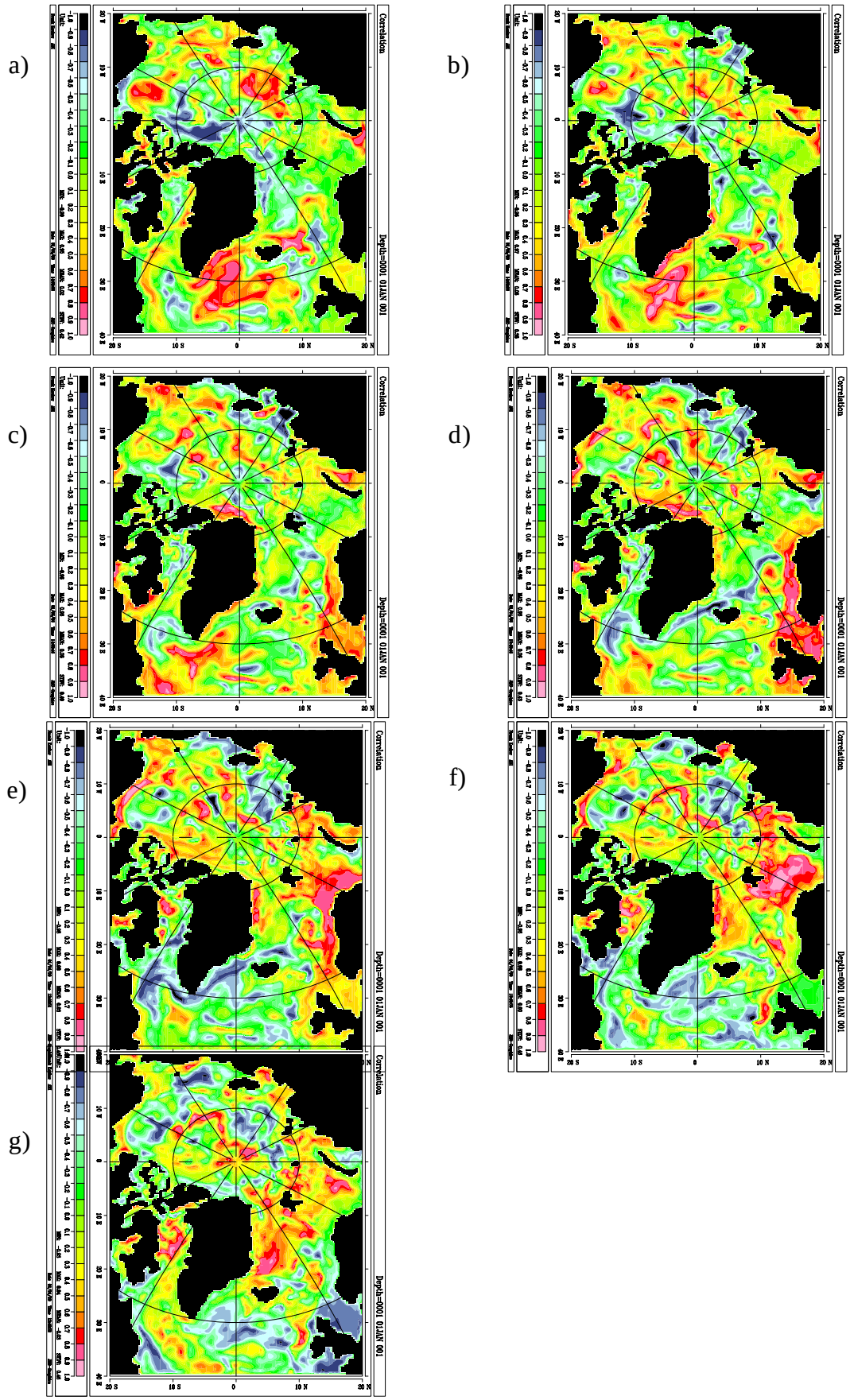

Fig.14 Fraction of the SST variability that can be accounted for by a linear relationship with the NAO at different time lags: a) -3 years lag (i.e. the SST signal precedes the NAO by 3 years), b) -2 years lag, c) -1 year lag, d) zero lag (identical with Fig. 8a), e) 1 year lag, f) 2 years lag, g) 3 years lag.

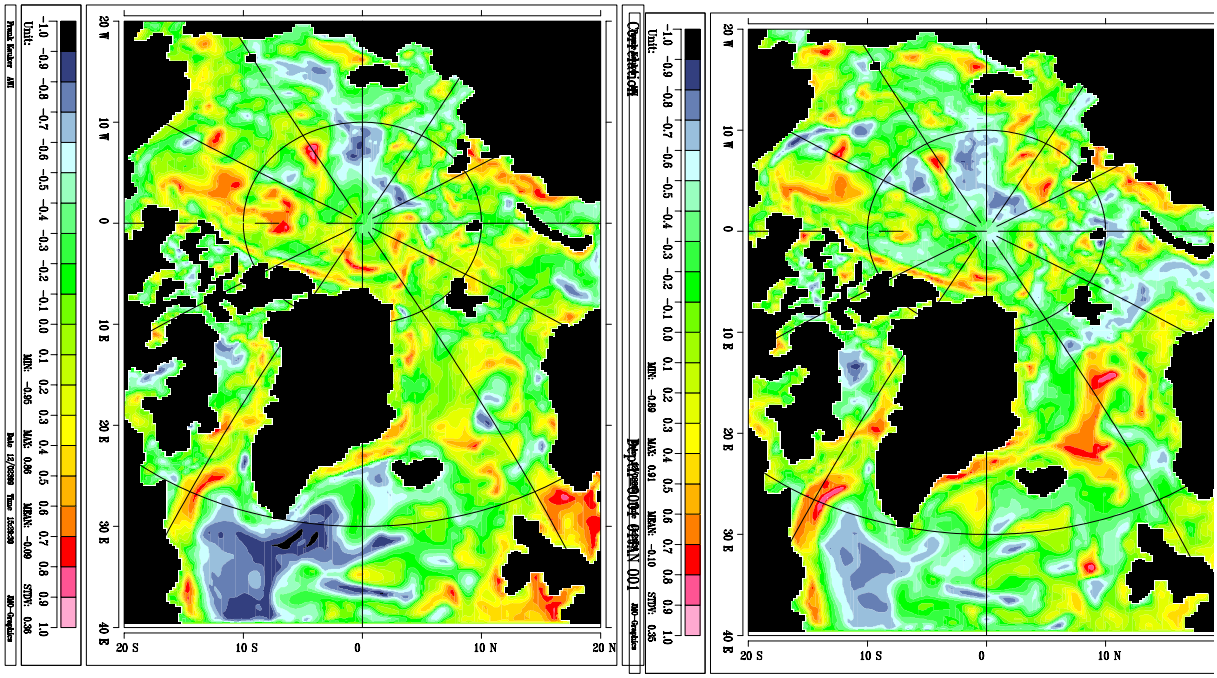

a) b)

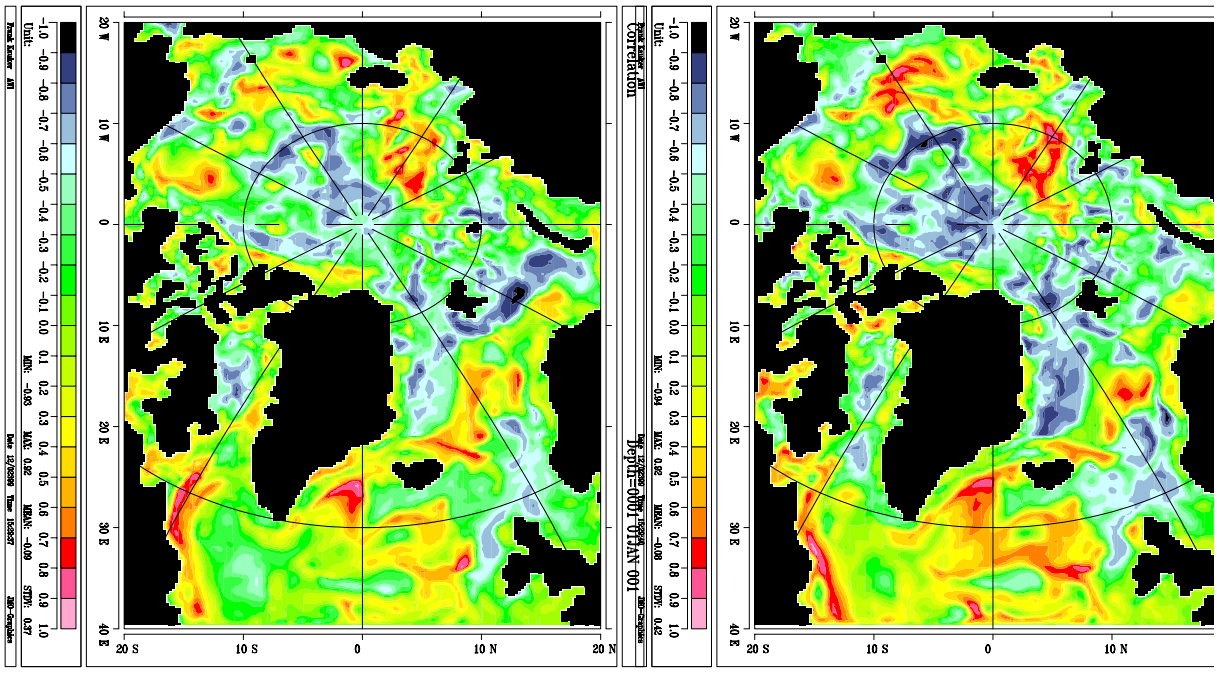

c) d)

Fig.15 Fraction of the surface heat flux variability that can be accounted for by a linear relationship with the NAO at different time lags: a) zero lag, b) 1 year lag, c) 2 years lag, d) 3 years lag

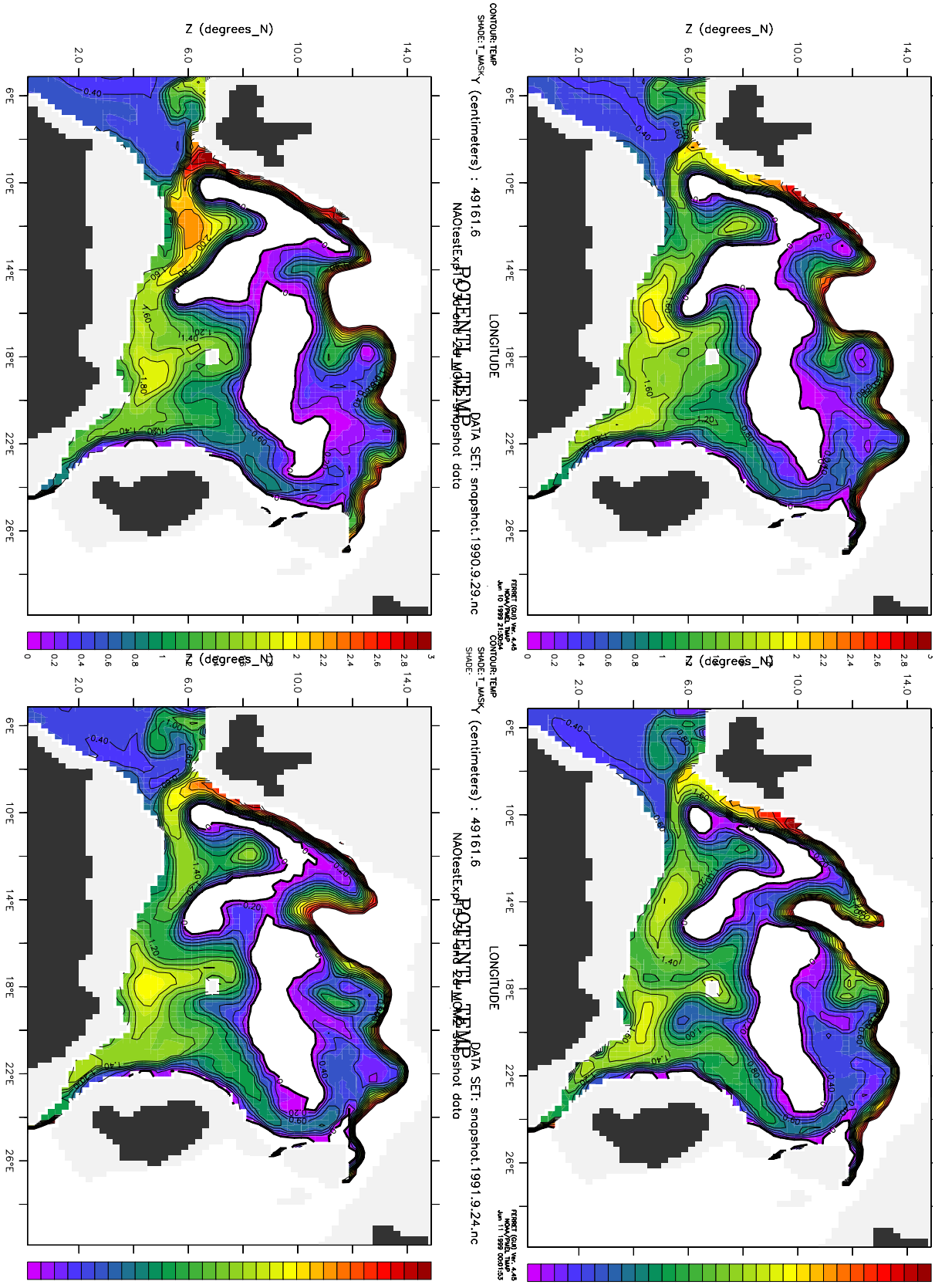

Fig.16 Temperatures at 500m depth for 9 / 1990 – 3 / 1992. Only temperatures between 0 and 3^{o}C are shown.

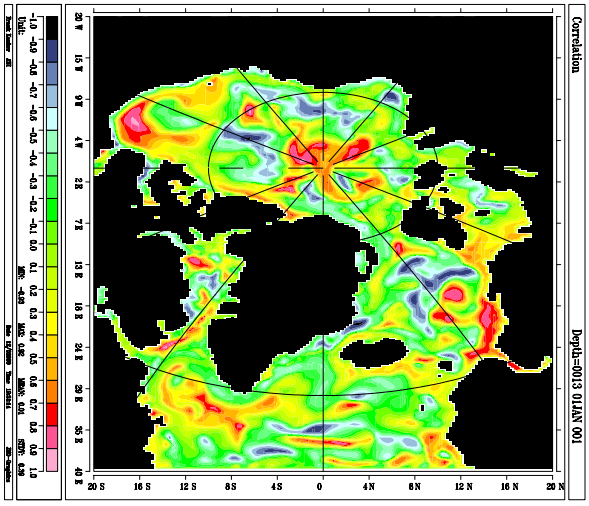

a)

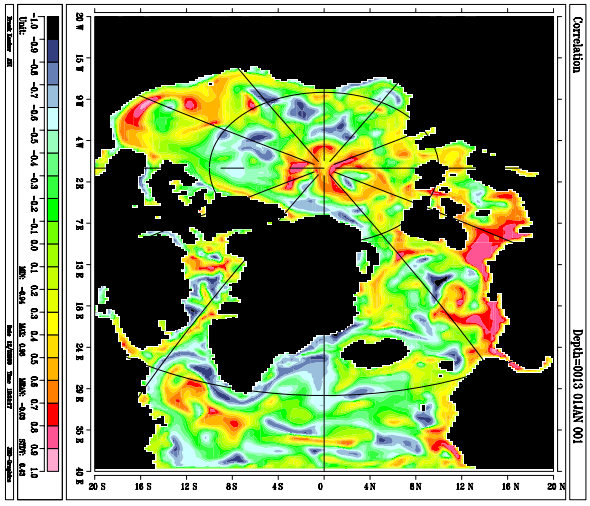

b)

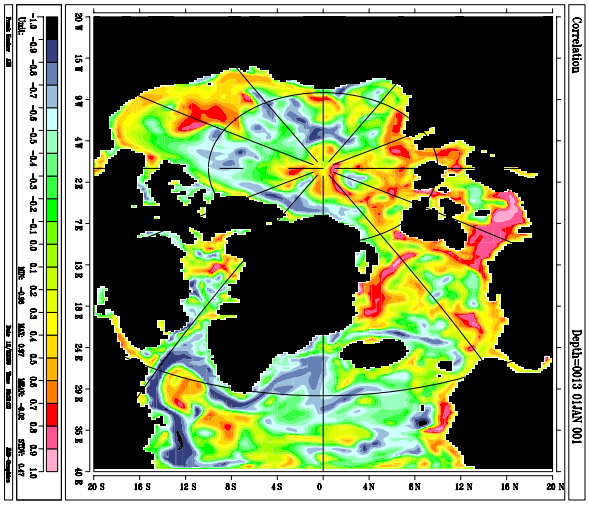

c)

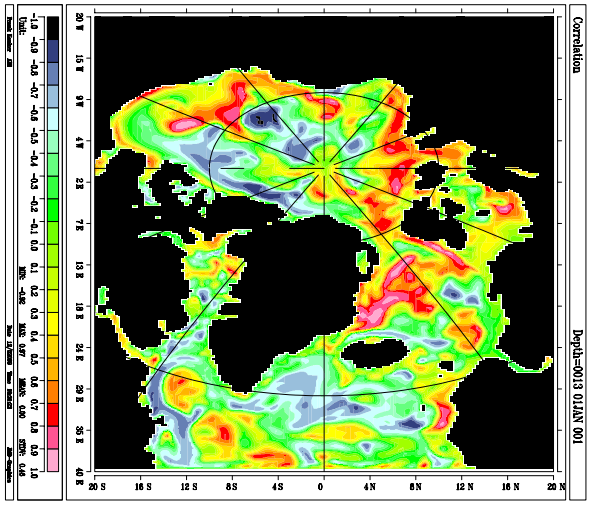

d)

Fig.17 Fraction of the temperature variability at 200 m depth that can be accounted for by a linear relationship with the NAO at different time lags: a) zero lag, b) one year lag, c) two years lag, d) three years lag

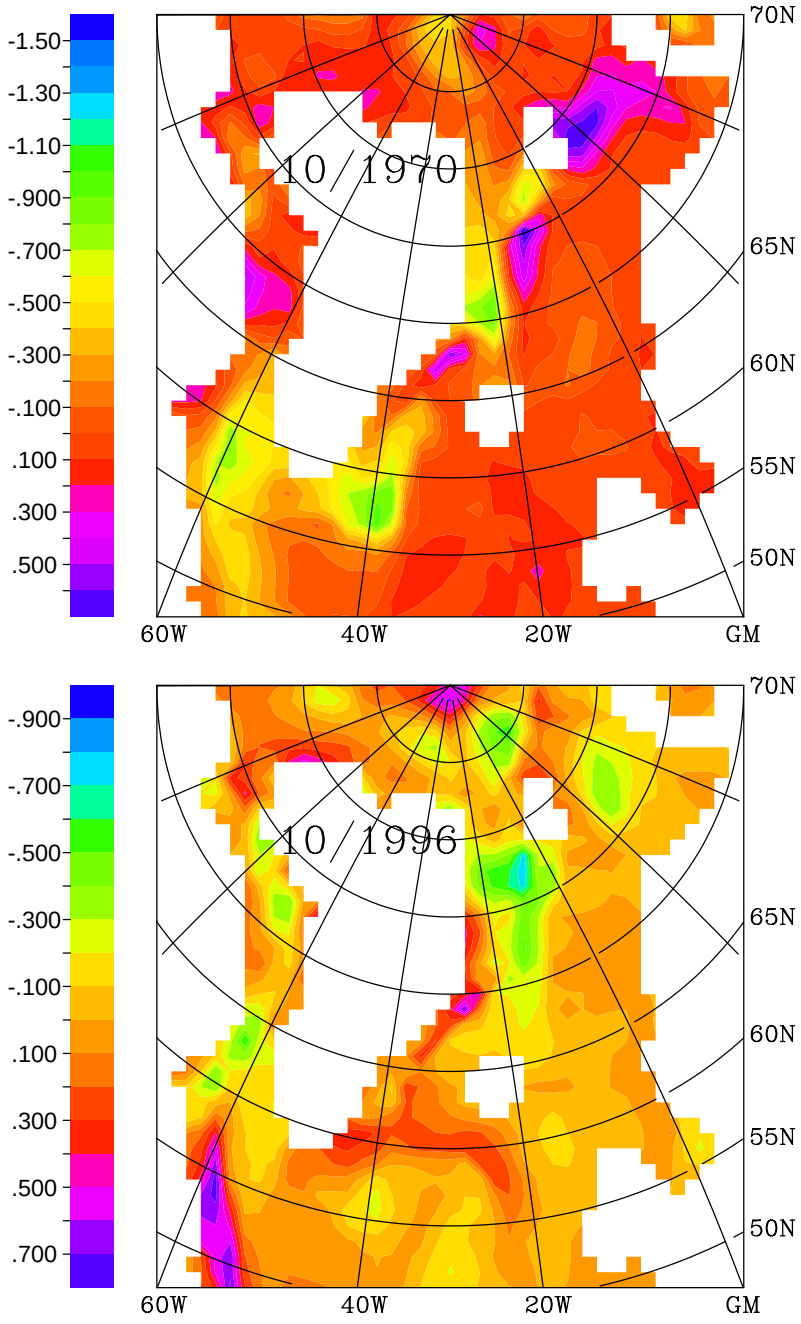

Fig.18 Surface salinity anomaly (LRM) from ten year means centered in 1967 and 1993, respectively, a) 1970 (after 1967/68 ice export event), b) 1996 (after 1994/95 ice export event)

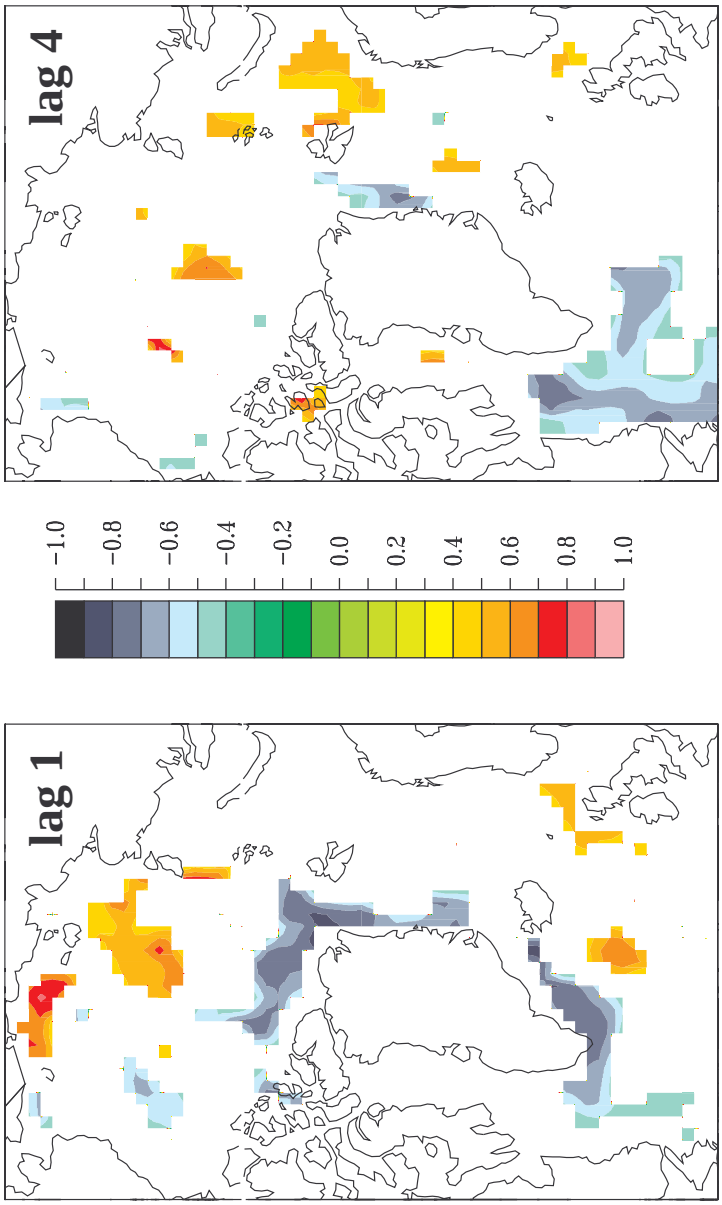

Fig.19 Fraction of the SSS variability fraction that can be accounted for by a linear relationship with the Fram Strait ice transport time series (Fig.6 from Kauker et al. 1999a)

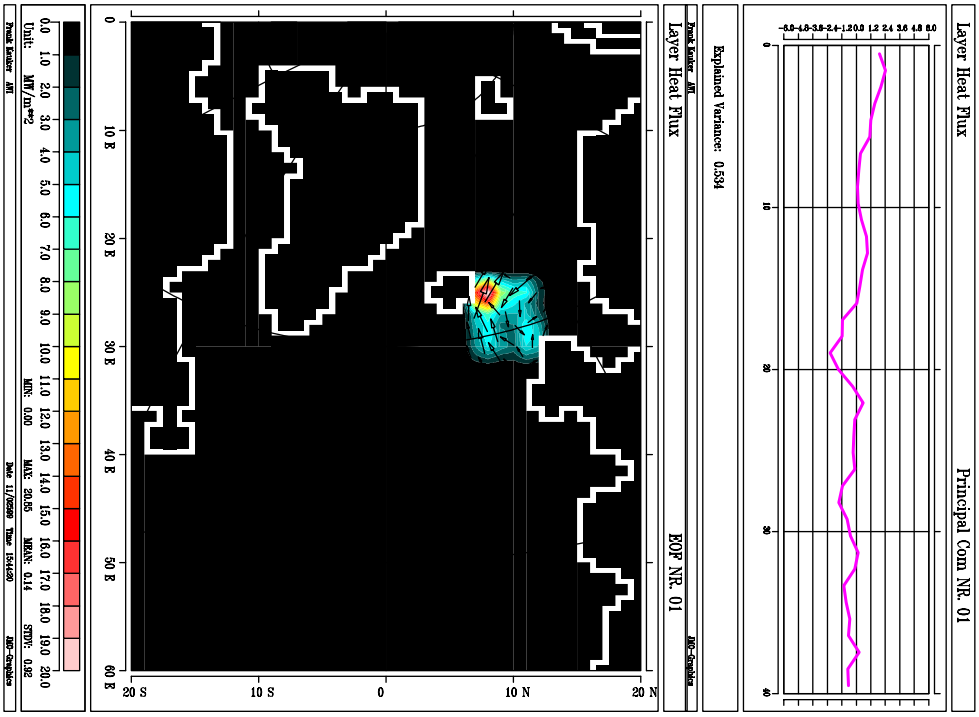

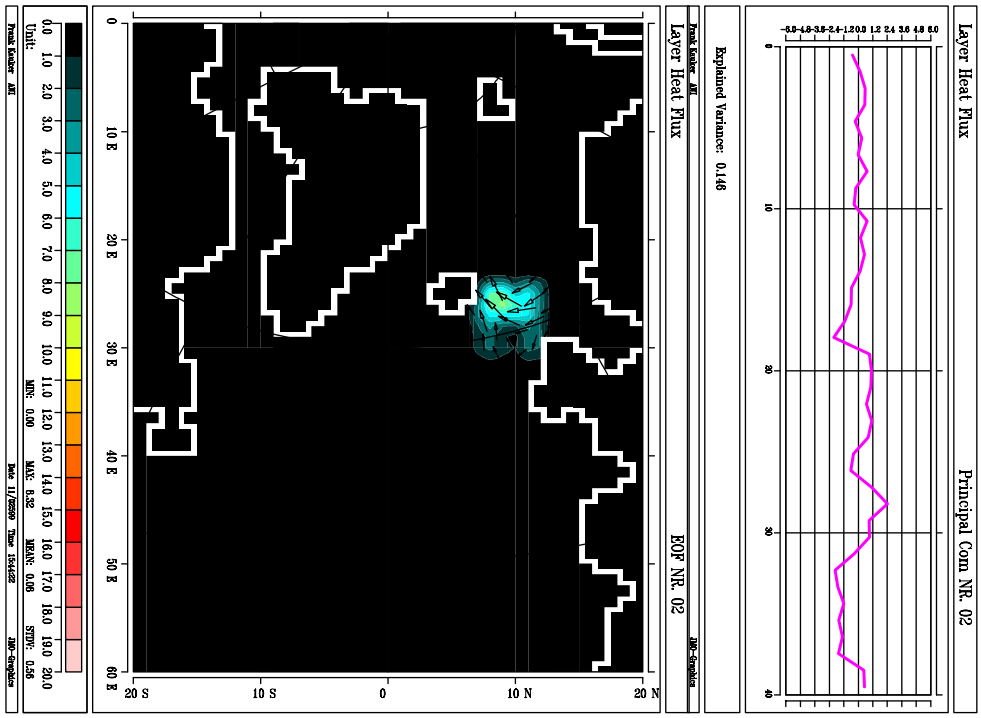

g.20 EOFs #1 and #2 for the heat transport (see text for a definition) in the Iceland-Scotland area

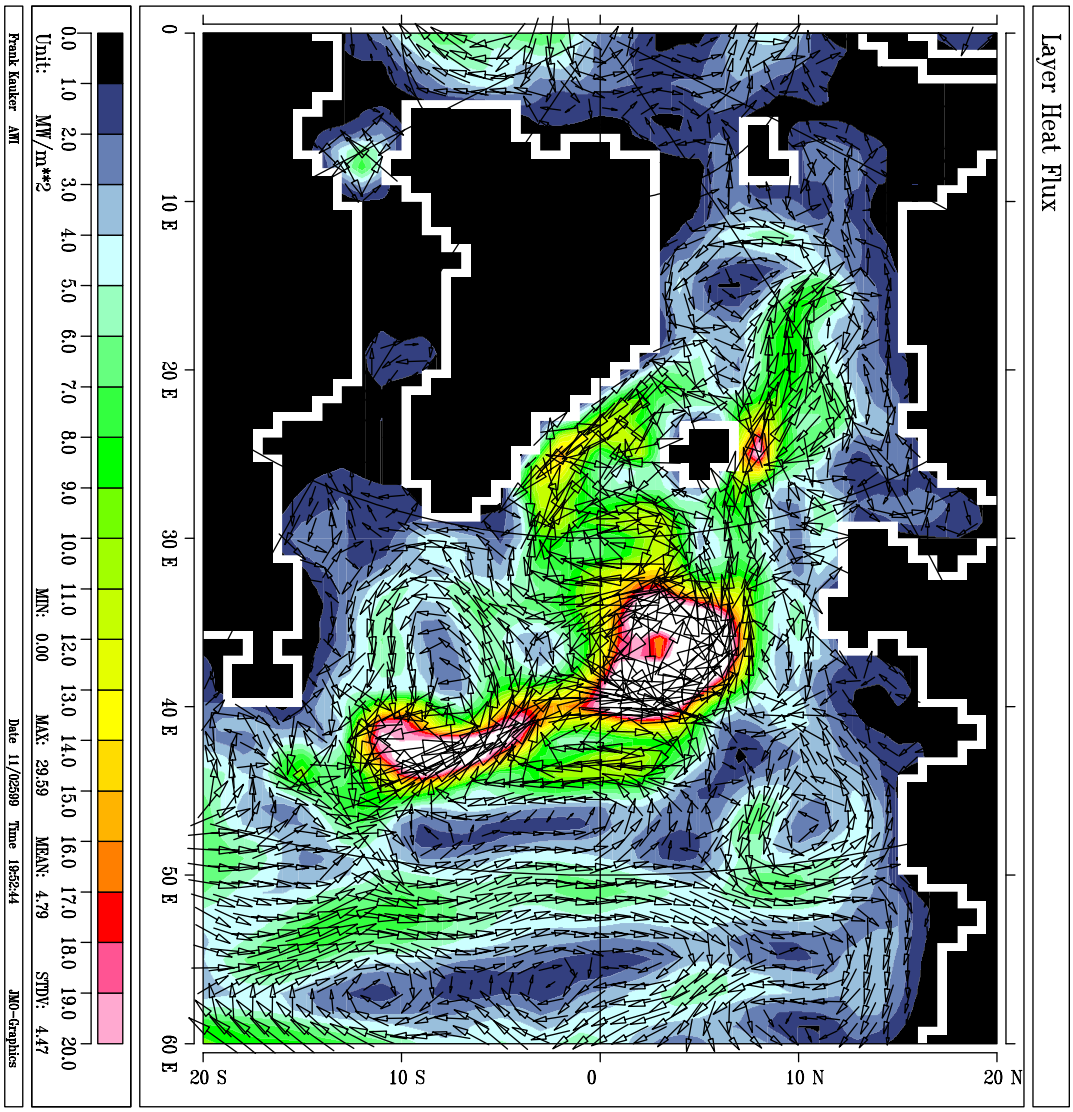

Fig.21 a) Correlation of PC #1 with large scale heat transport anomalies, and b) the total heat transport for different strengths of the Iceland-Scotland heat flux mode #1. In b) the pattern from a) is multiplied with a factor between -2 and 2, roughly reflecting the amplitude of the PC, and added to the mean transport (shown for factor 0).

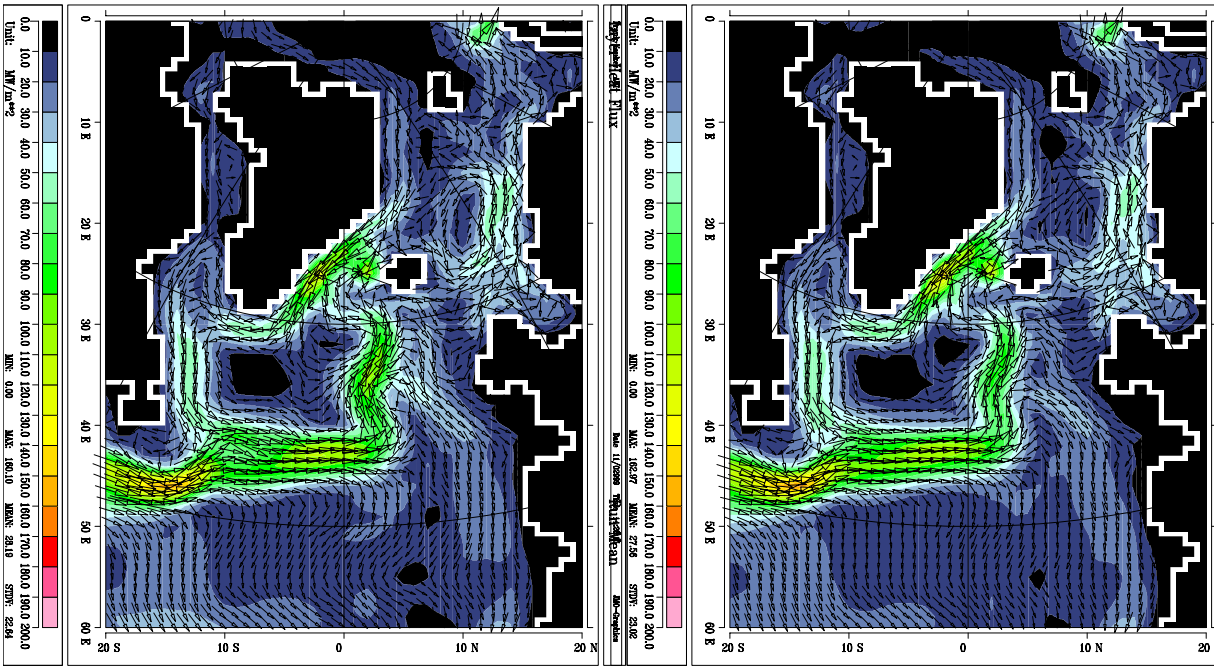

-2 -1

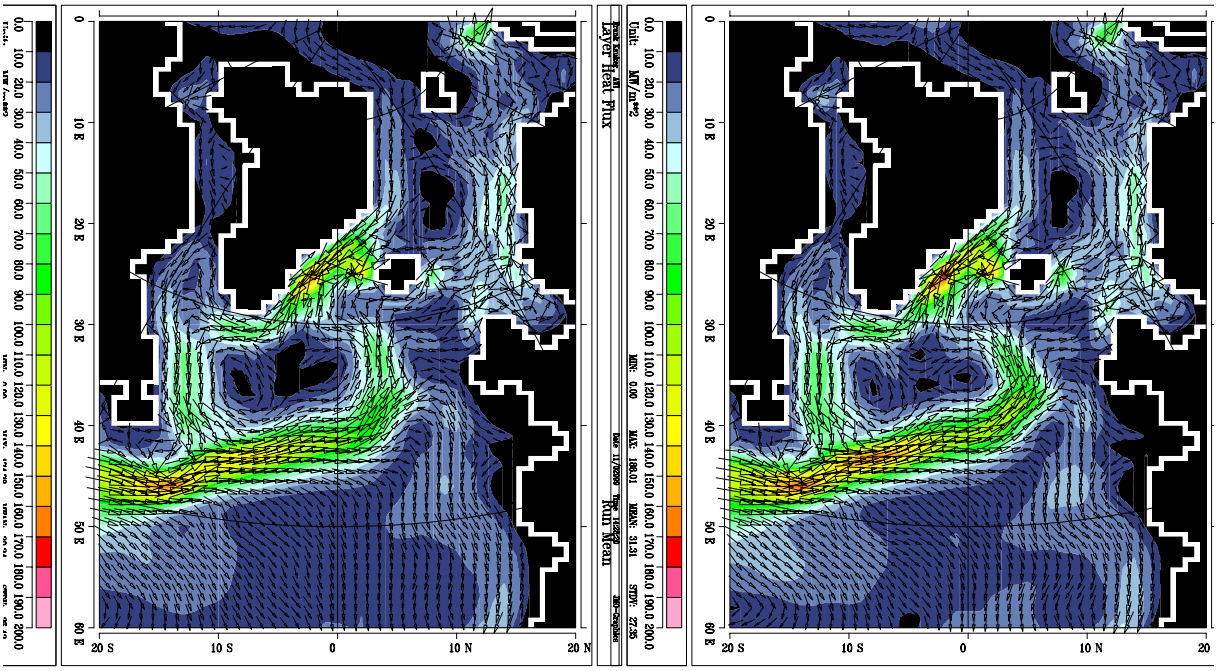

+1 +2

Fig. 21 b

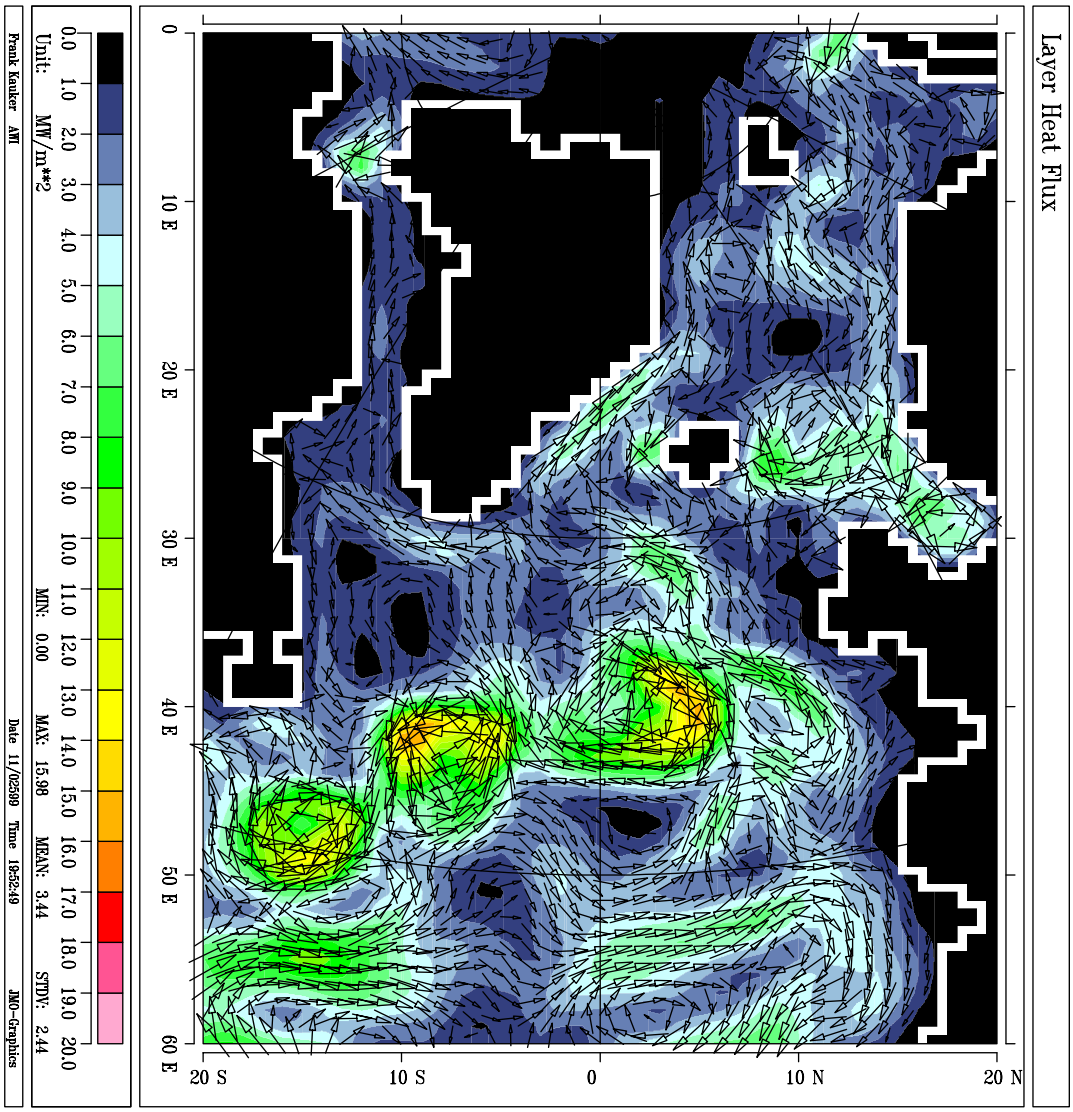

Fig.22 a) Correlation of PC #2 with large scale heat transport anomalies, and b) the total heat transport for different strengths of the Iceland-Scotland heat flux mode #2. In b) the pattern from a) is multiplied with a factor between -2 and 2, roughly reflecting the amplitude of the PC, and added to the mean transport (shown for factor 0).

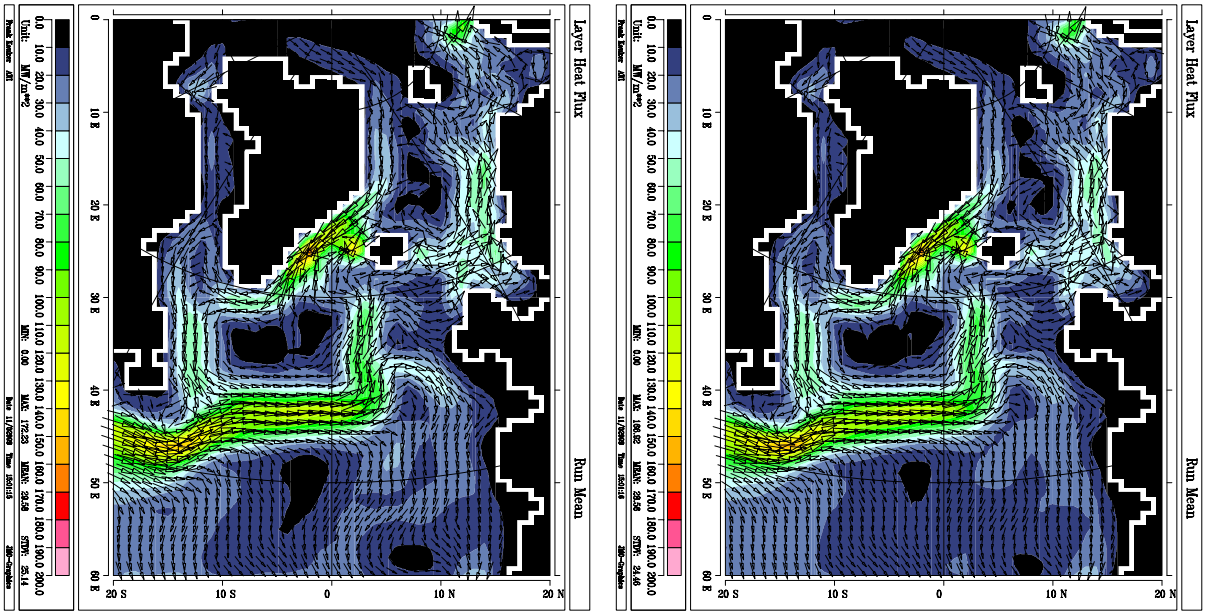

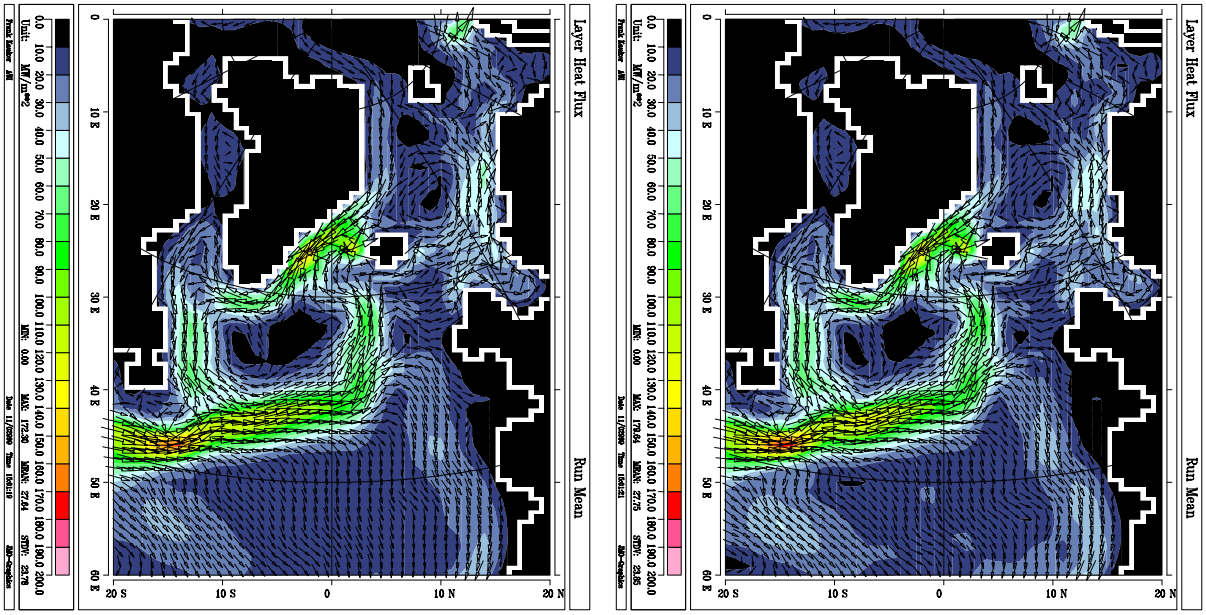

Fig. 22b

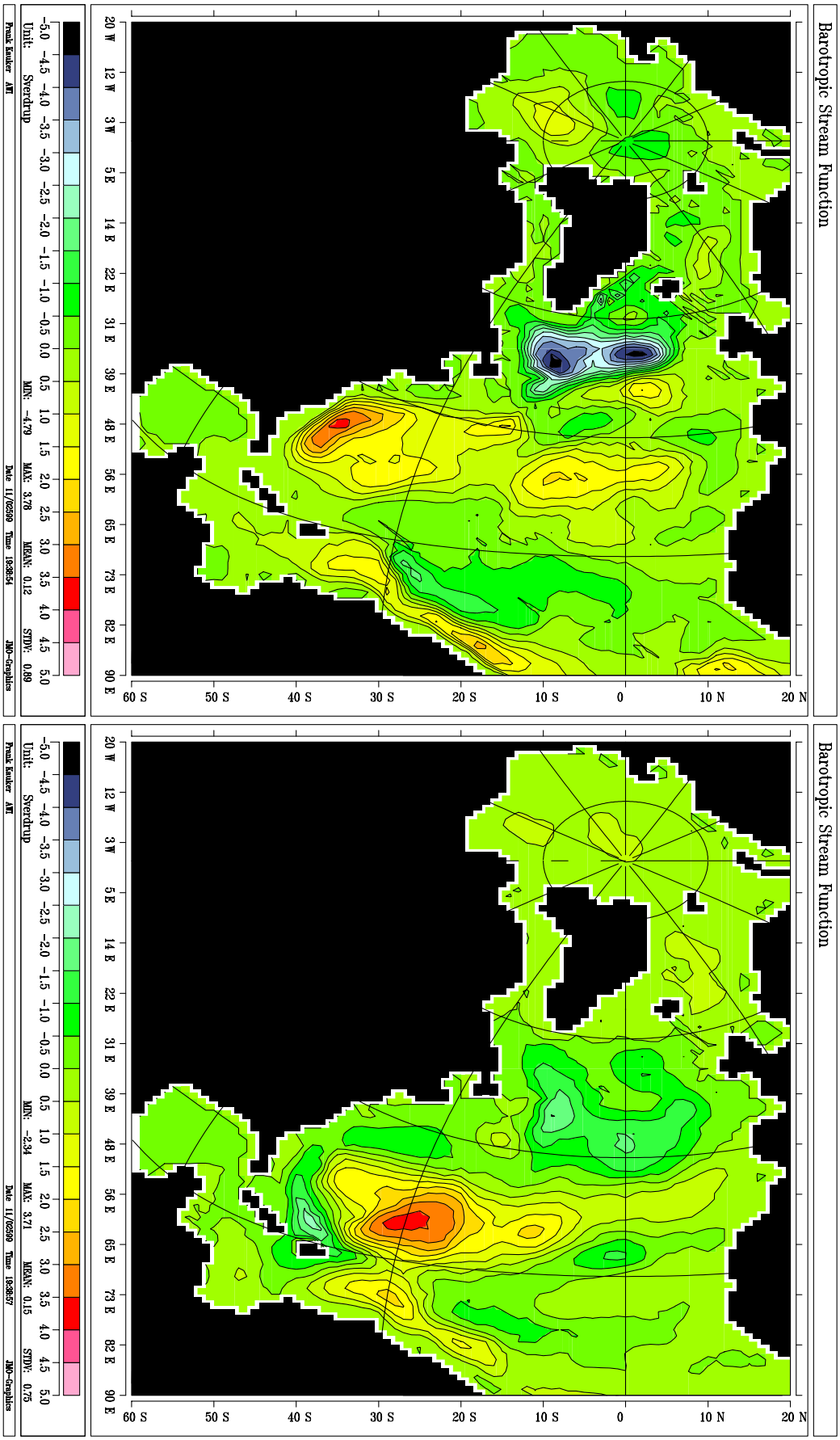

Fig.23 Standard deviation of the streamfunction variability that is described by a linear relation with the PCs of the Iceland-Scotland heat transport modes a) mode #1, b) mode #2

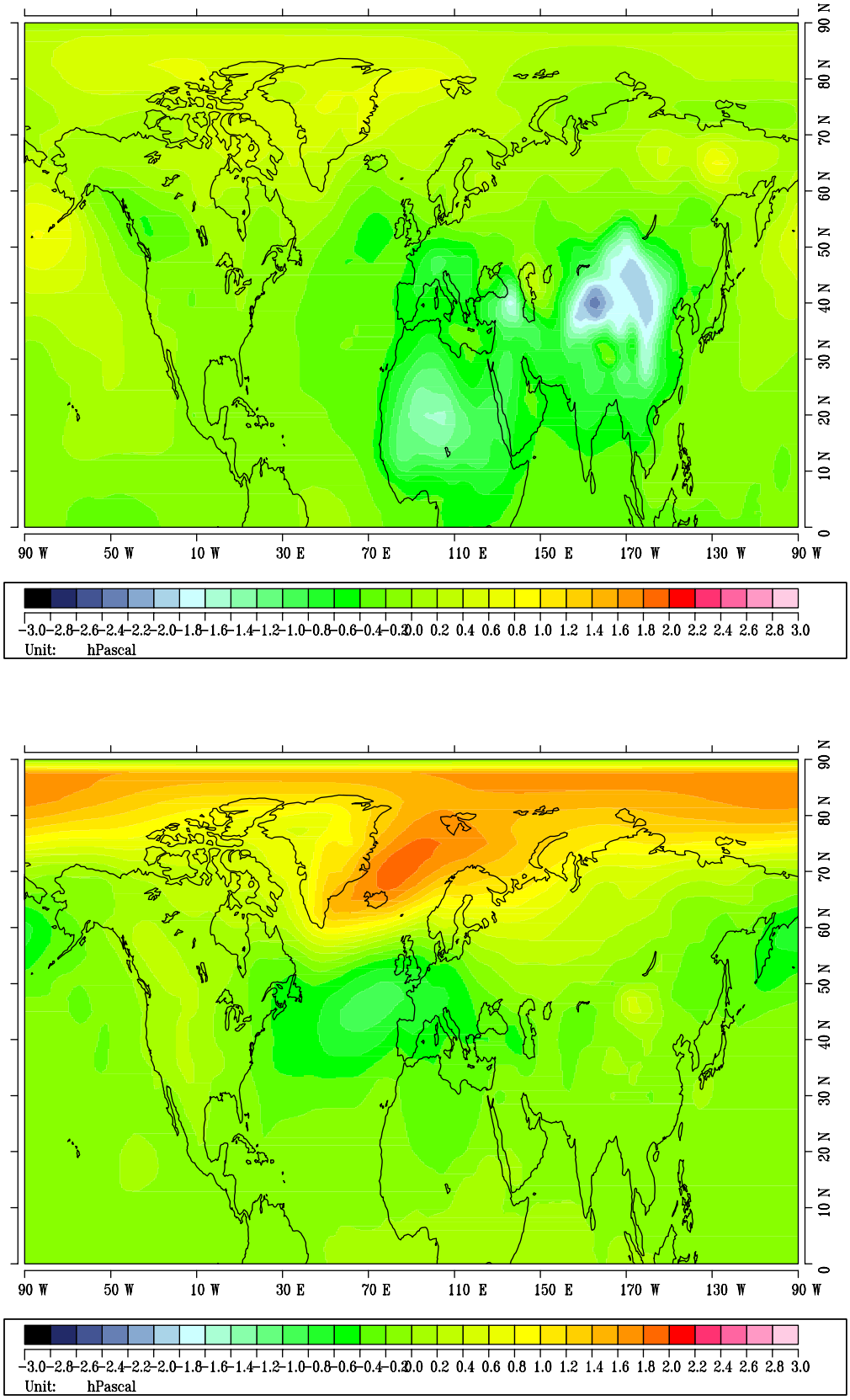

Fig.24 Standard deviation of the SLP variability that is described by a linear relation with the PCs of the Iceland-Scotland heat transport modes a) EOF #1, b) EOF #2.

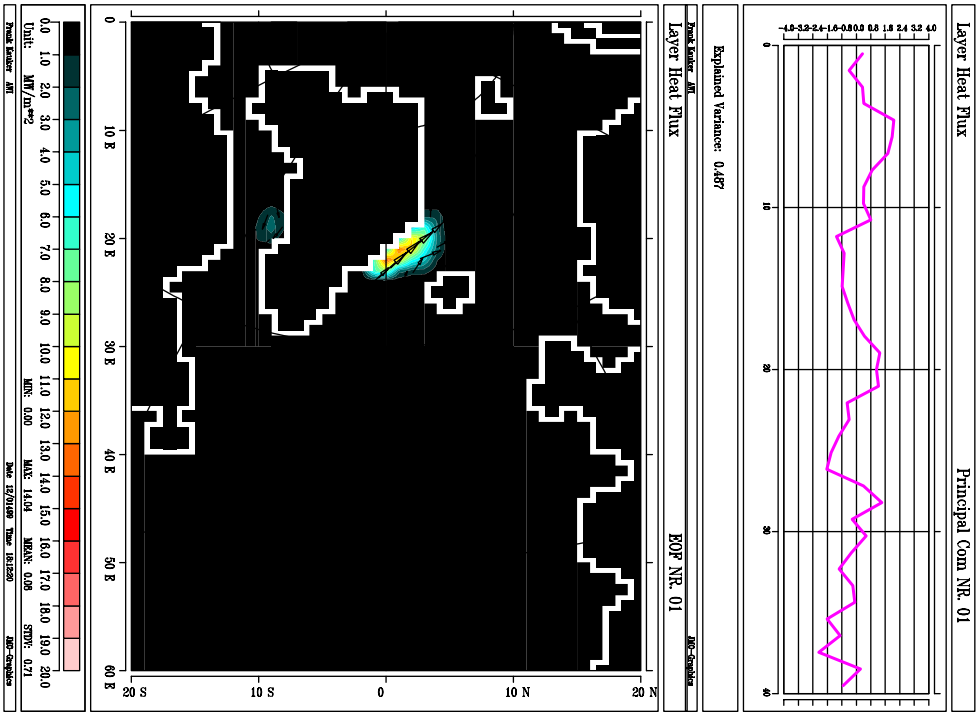

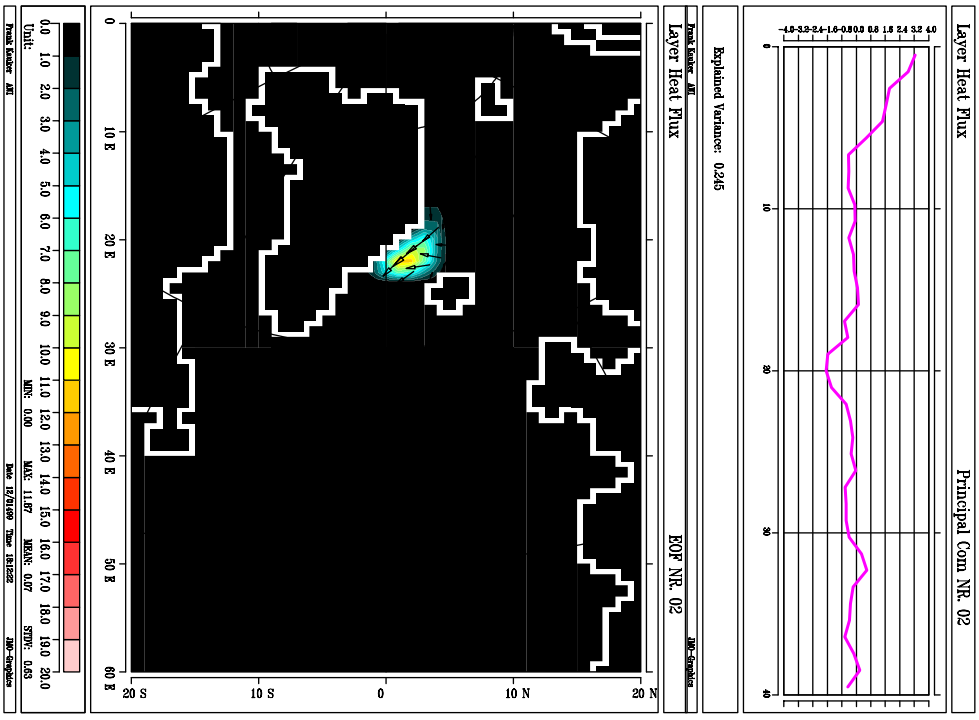

Fig.25 EOFs #1 and #2 for the heat transport in the Denmark Strait area

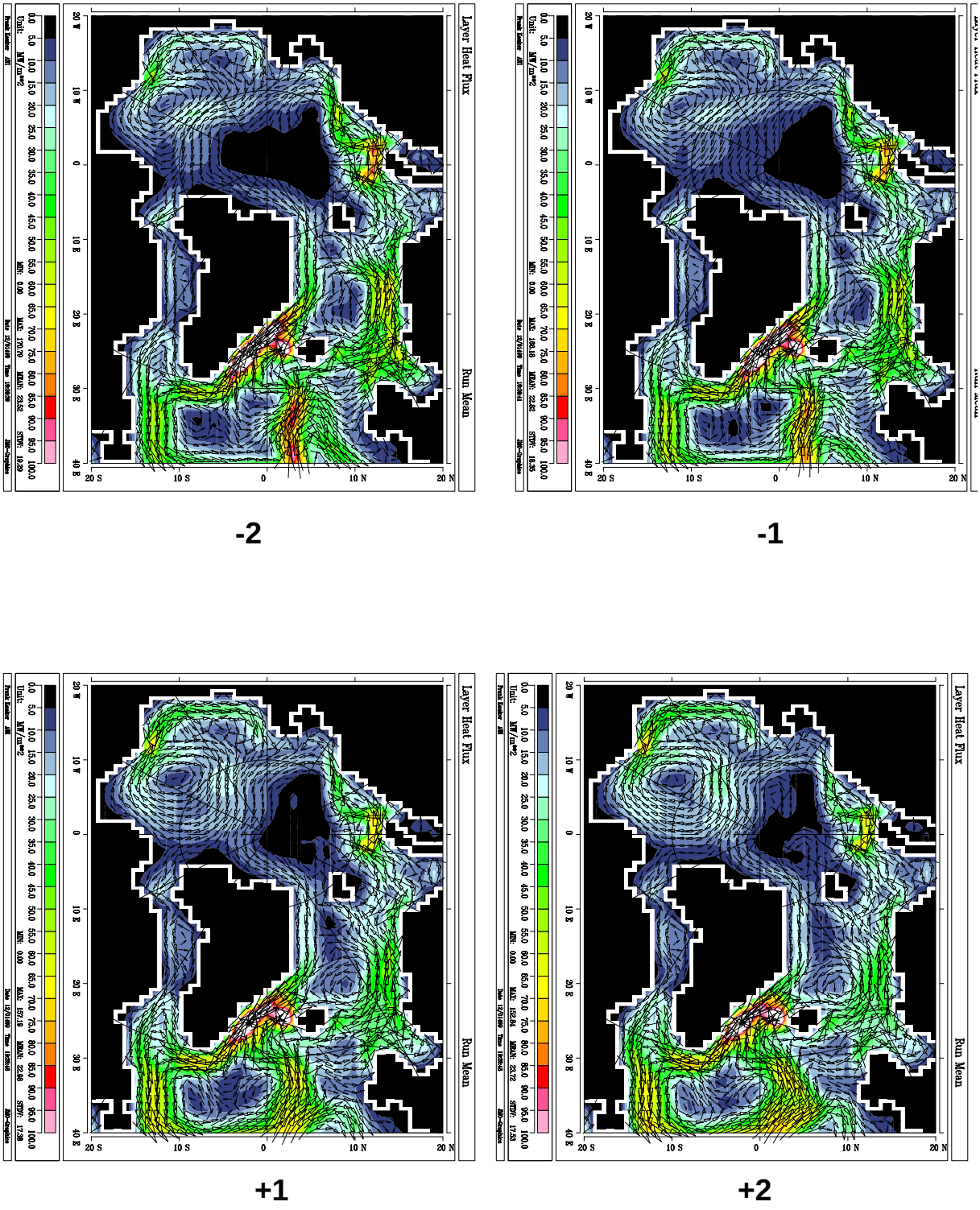

Fig.26 a) Correlation of PC #1 with large scale heat transport anomalies, and b) the total heat transport for different strengths of the Denmark Strait heat flux mode #1. In b) the pattern from a) is multiplied with a factor between -2 and 2, roughly reflecting the amplitude of the PC, and added to the mean transport (shown for factor 0).

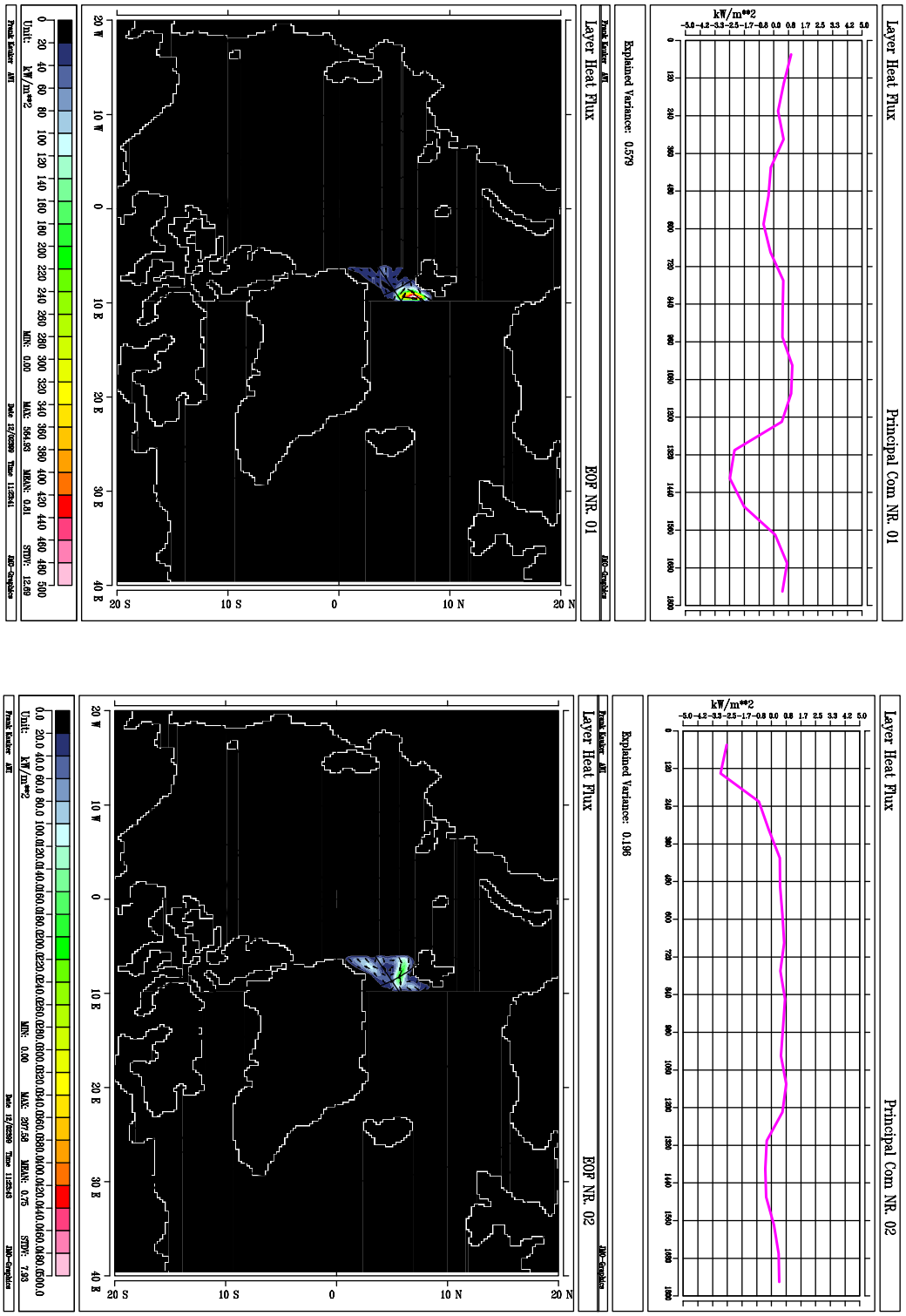

Fig.27 EOFs #1 and #2 for the heat transport in the Fram Strait area. These results are taken from the HRM hindcast

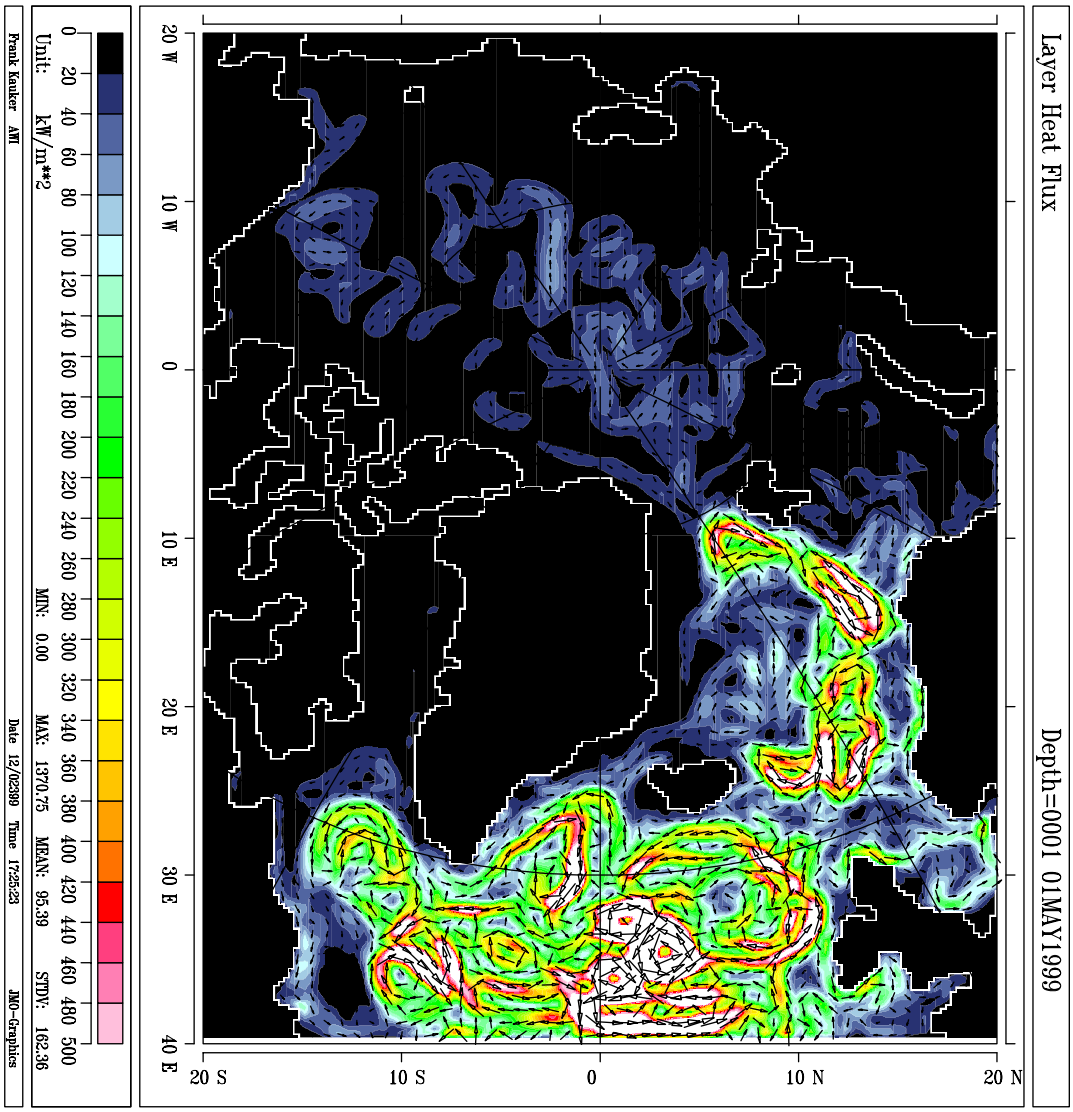

Fig.28 a) Correlation of PC #1 with large scale heat transport anomalies, and b) the total heat transport for different strengths of the Fram Strait heat flux mode #1. In b) the pattern from a) is multiplied with a factor between -2 and 2, roughly reflecting the amplitude of the PC, and added to the mean transport (shown for factor 0).

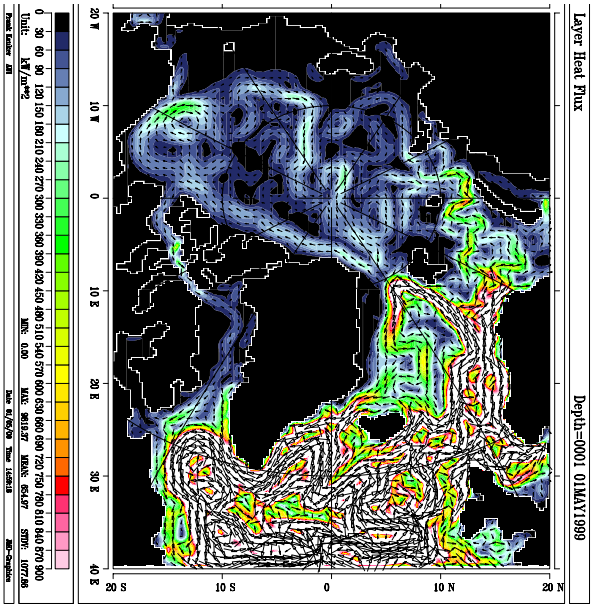
Layer Heat Flux
Depth=0001 01MAY1999
20 S
10 S
0
10 N
20 N
0 E
10 E
20 E
30 E
40 E

-2

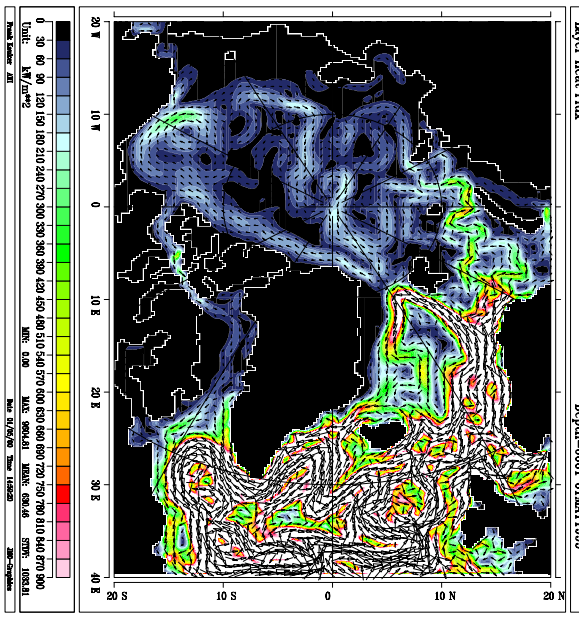
20 S
10 S
0
10 N
20 N
0 E
10 E
20 E
30 E
40 E

-1

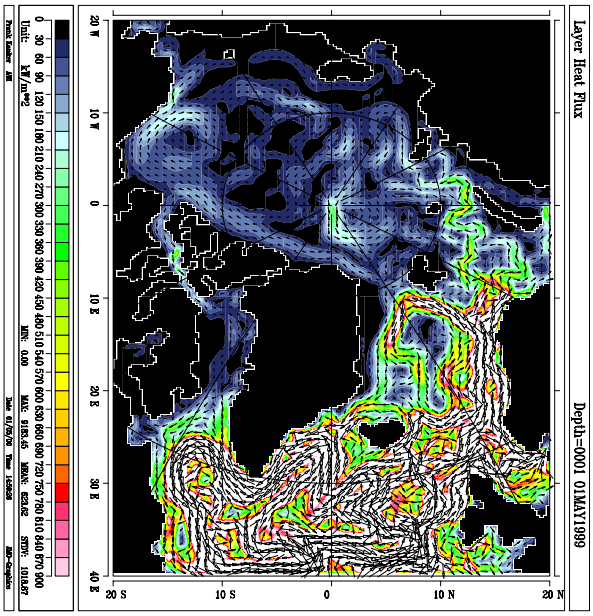
Layer Heat Flux
Depth=0001 01MAY1999
20 S
10 S
0
10 N
20 N
0 E
10 E
20 E
30 E
40 E

+1

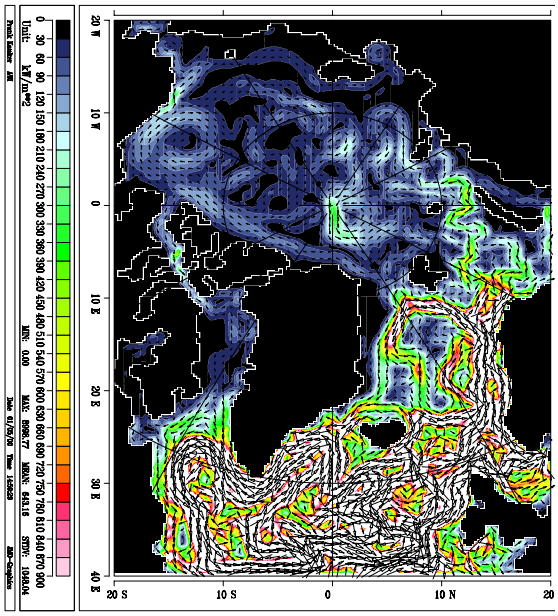
20 S
10 S
0
10 N
0 E
10 E
20 E
30 E
40 E

+2

Fig. 28b

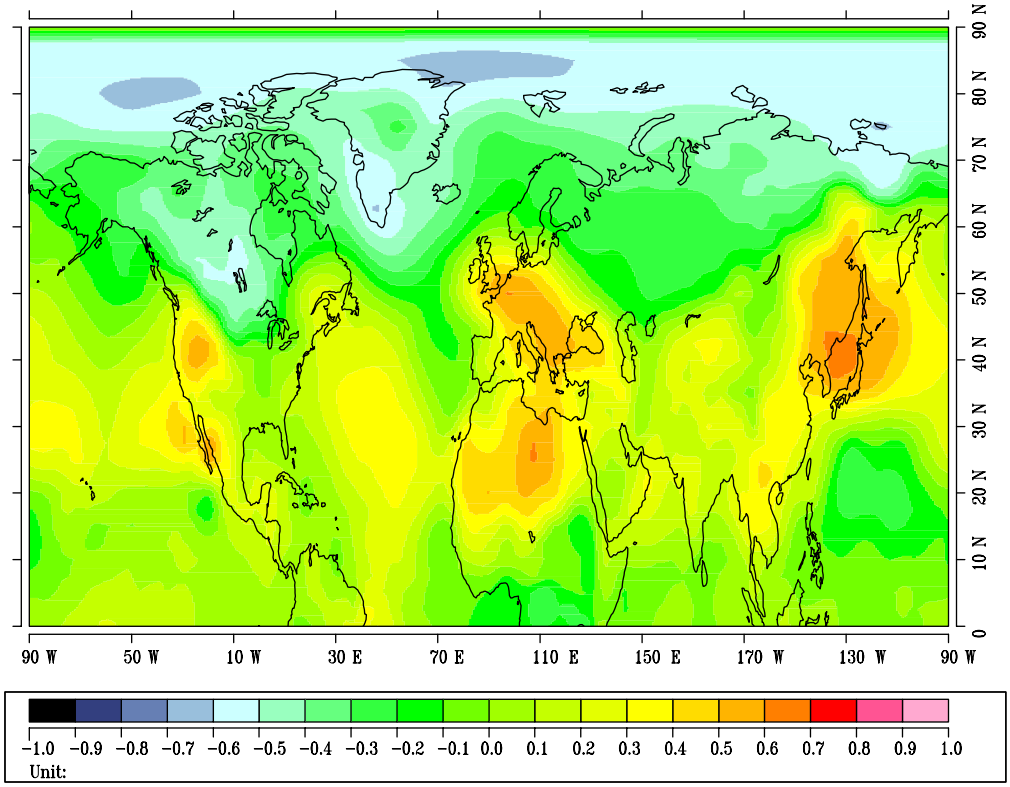

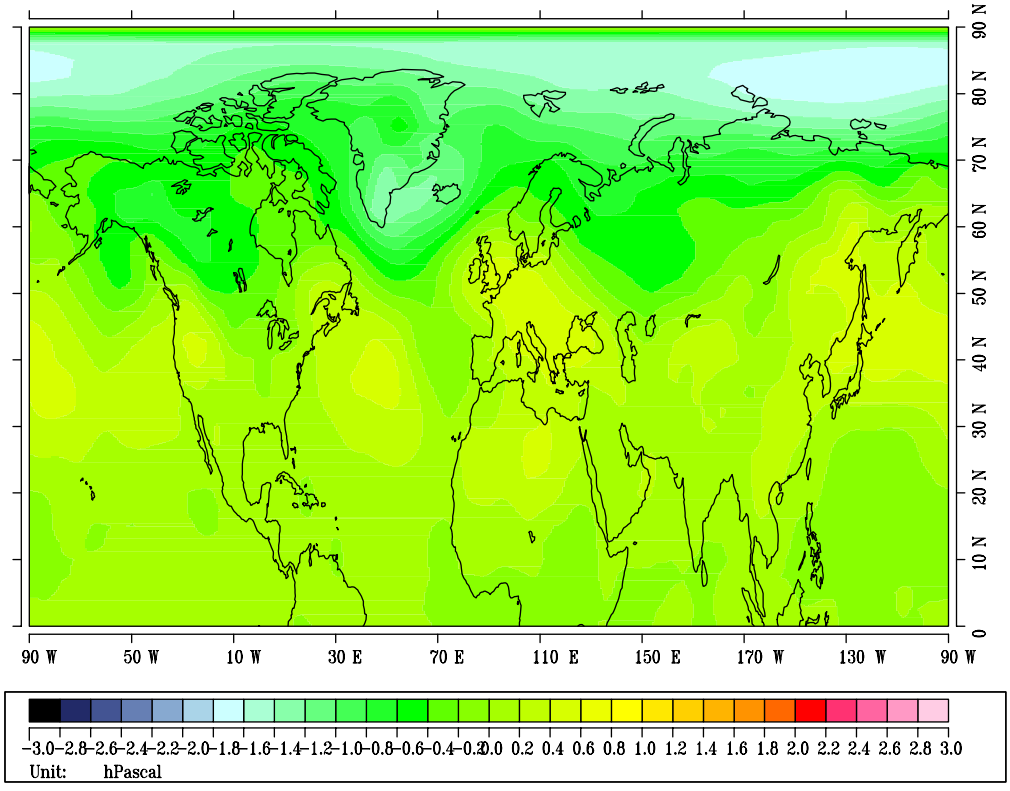

Fig.29 a) Fraction of the variability of the SLP variability that can be accounted for by a linear relation with PC #2 of the Fram Strait are heat transport modes, b) associated standard deviation

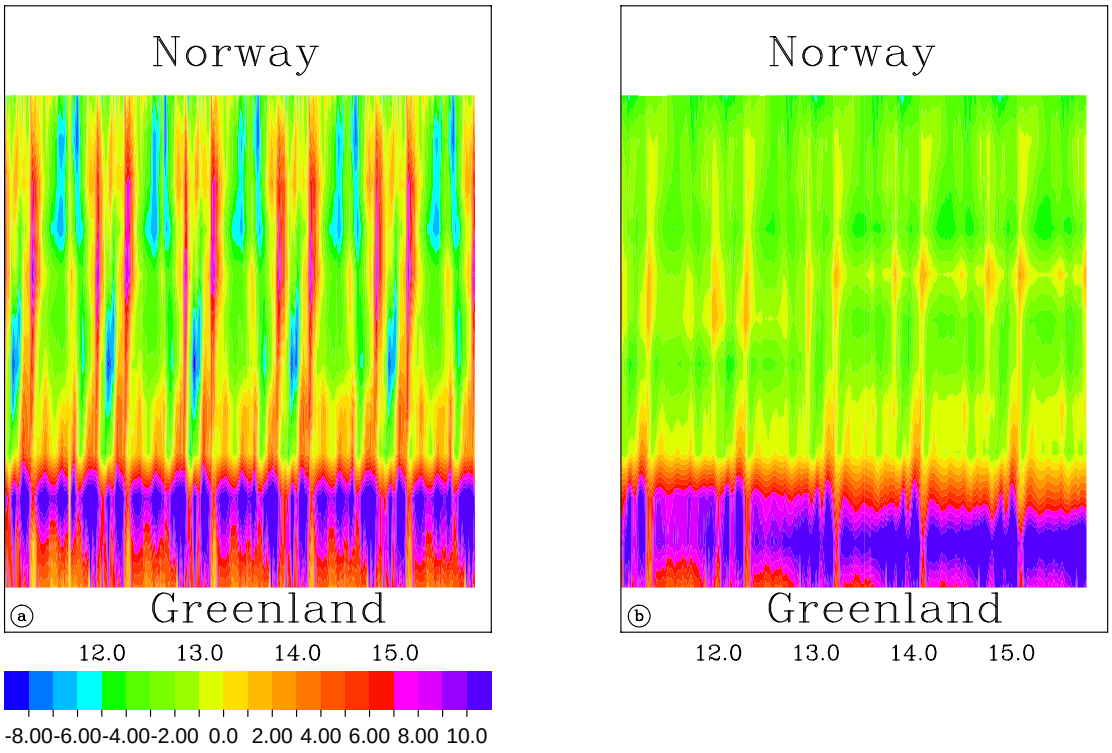

Fig.30 Hovmöller diagram for the meridional velocity component at 100 m depth on a quasi-zonal section through the Nordic Seas a) daily varying wind over the whole domain, b) daily varying wind only north of 80^{o}N while the wind varies monthly over the rest of the domain

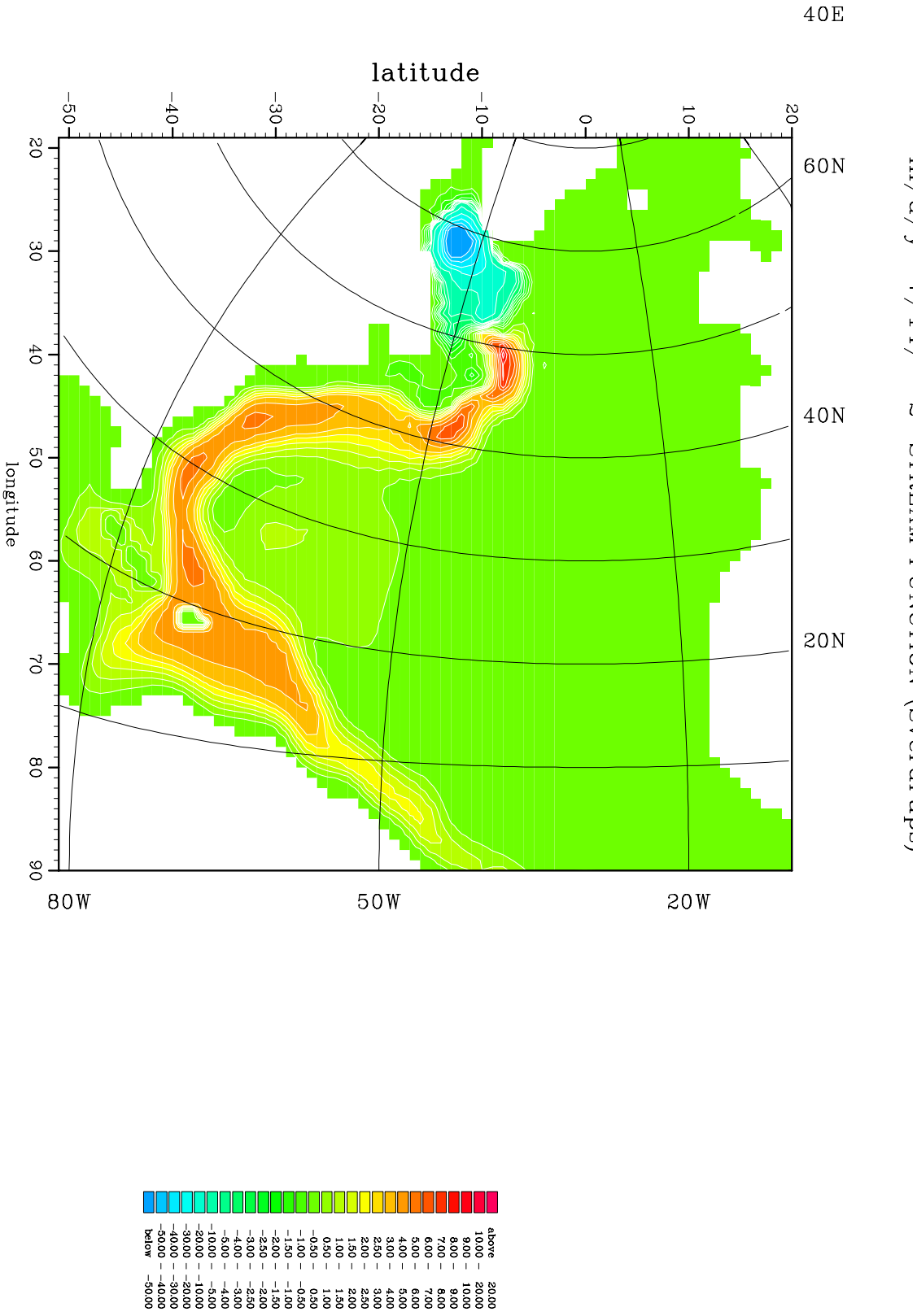

Fig.31 Anomalous streamfunction as a response to deep convection in the Labrador Sea

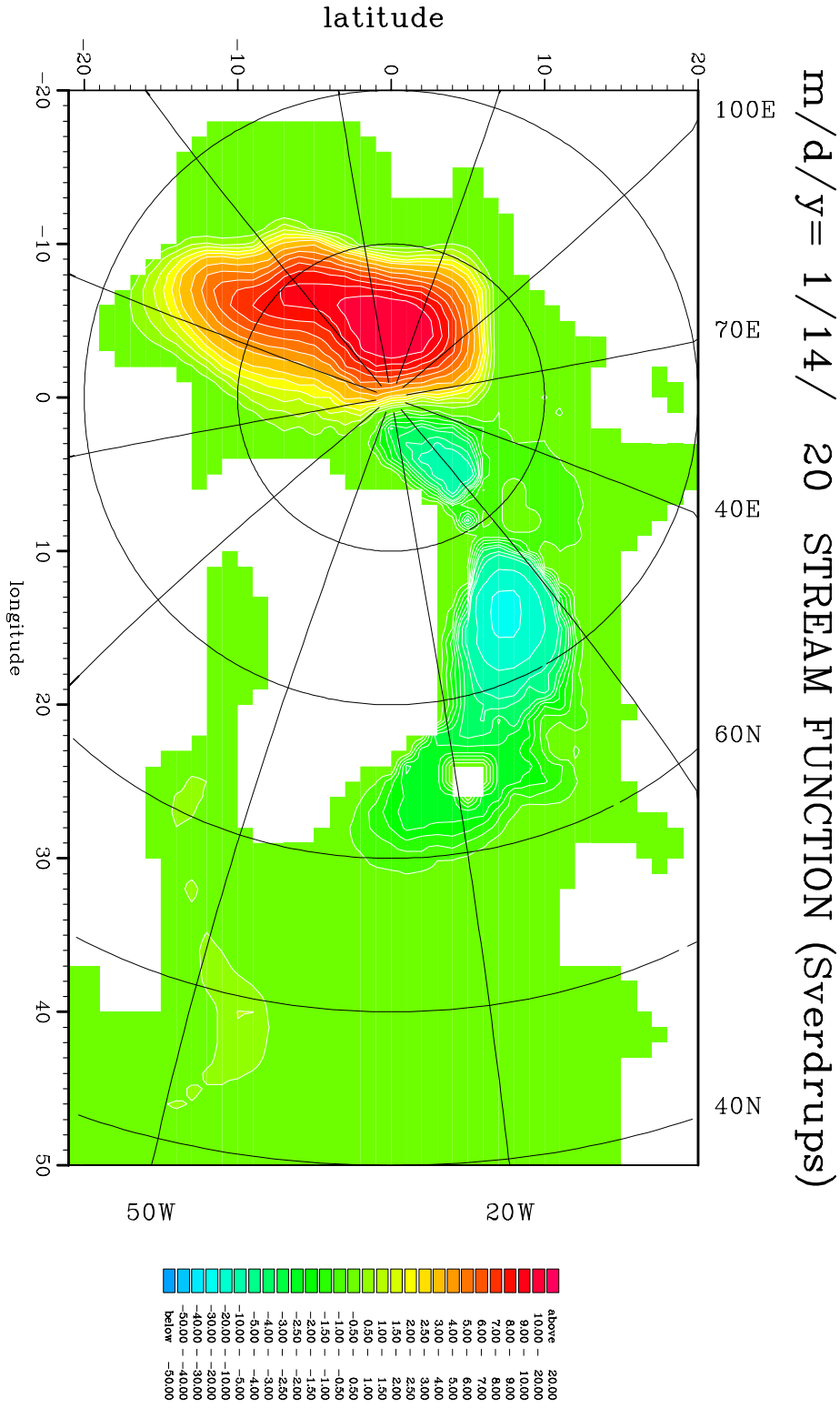

Fig.32 Anomalous streamfunction as a response to deep convection in the Greenland Sea

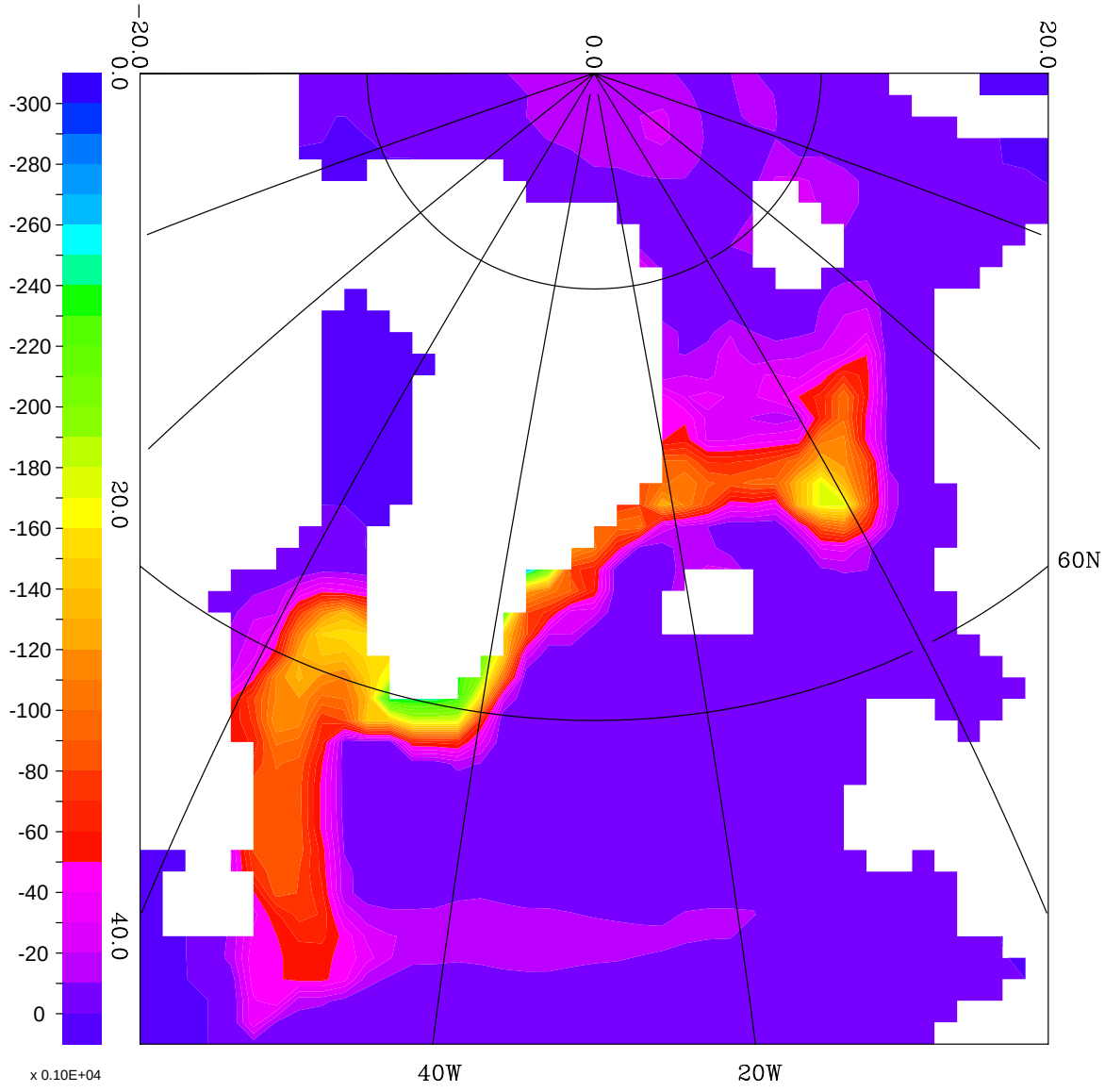

Fig.33 Surface salinity anomaly four years after first introducing a sea ice anomaly in Fram Strait (see text)

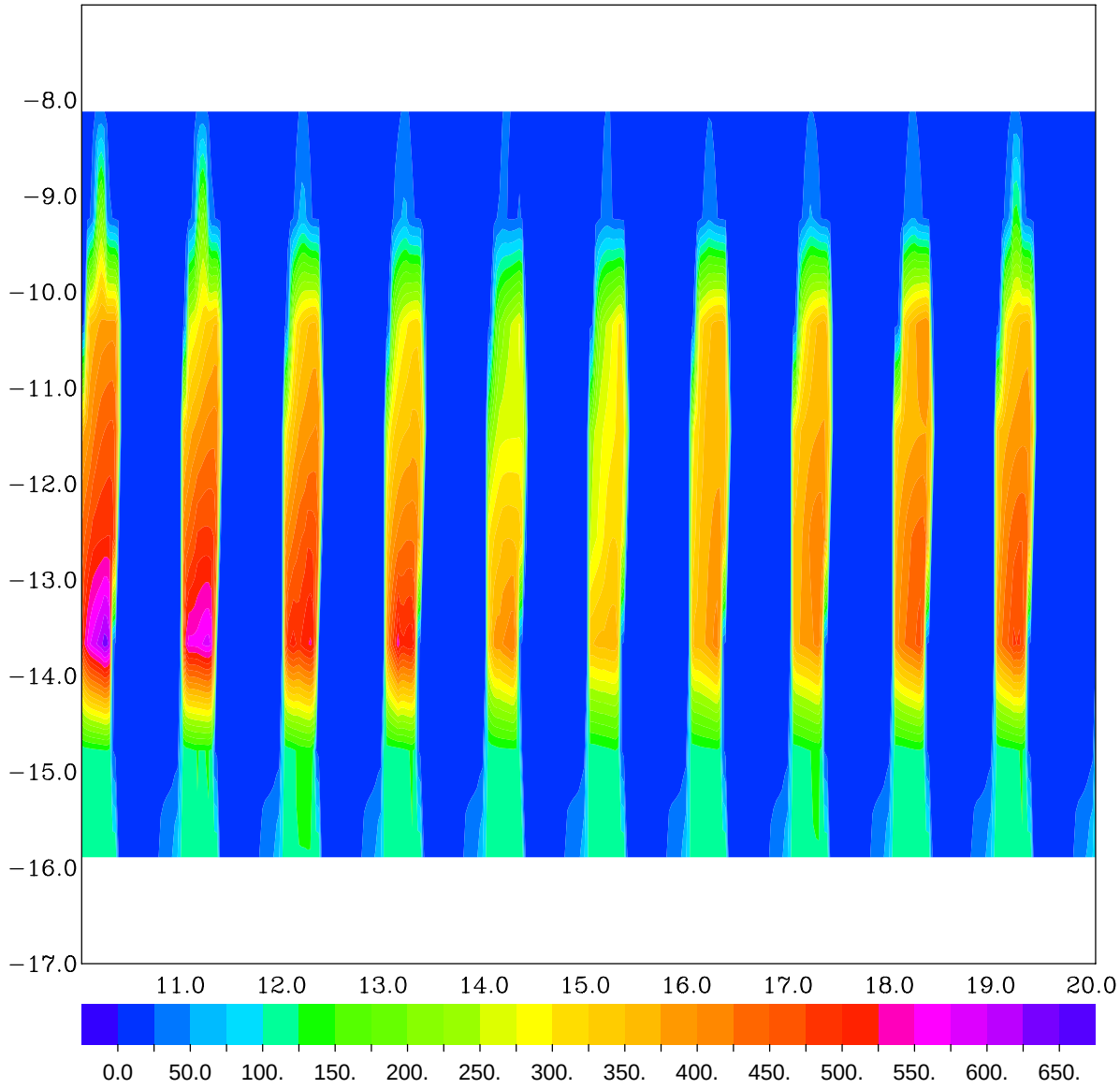

Fig.34 Hovmöller diagram for mixed layer depth on a section through the Labrador Sea in the Fram Strait sea ice anomaly experiment. A fresh water anomaly arrives at the section in year 13 on the Greenland (upper) side and leads to a reduction in convection depth.

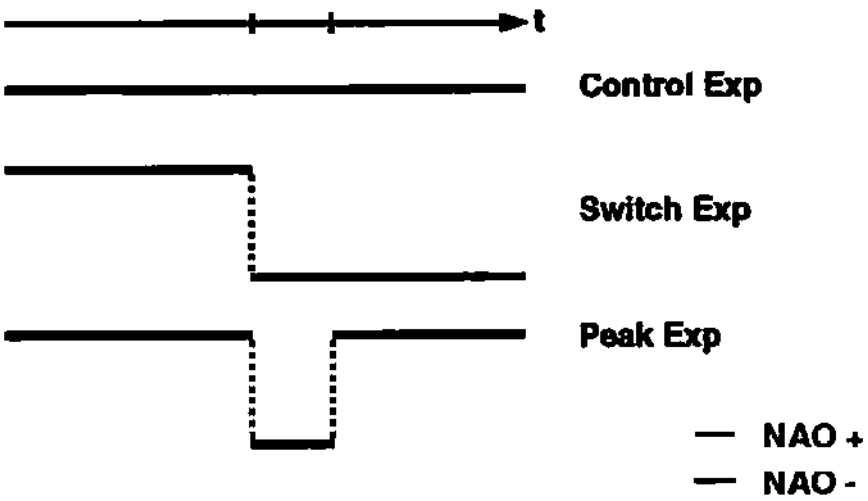

Fig.35 Experimental design for the switch in NAO wind (Fig.2 from Brauch et al., 1999)

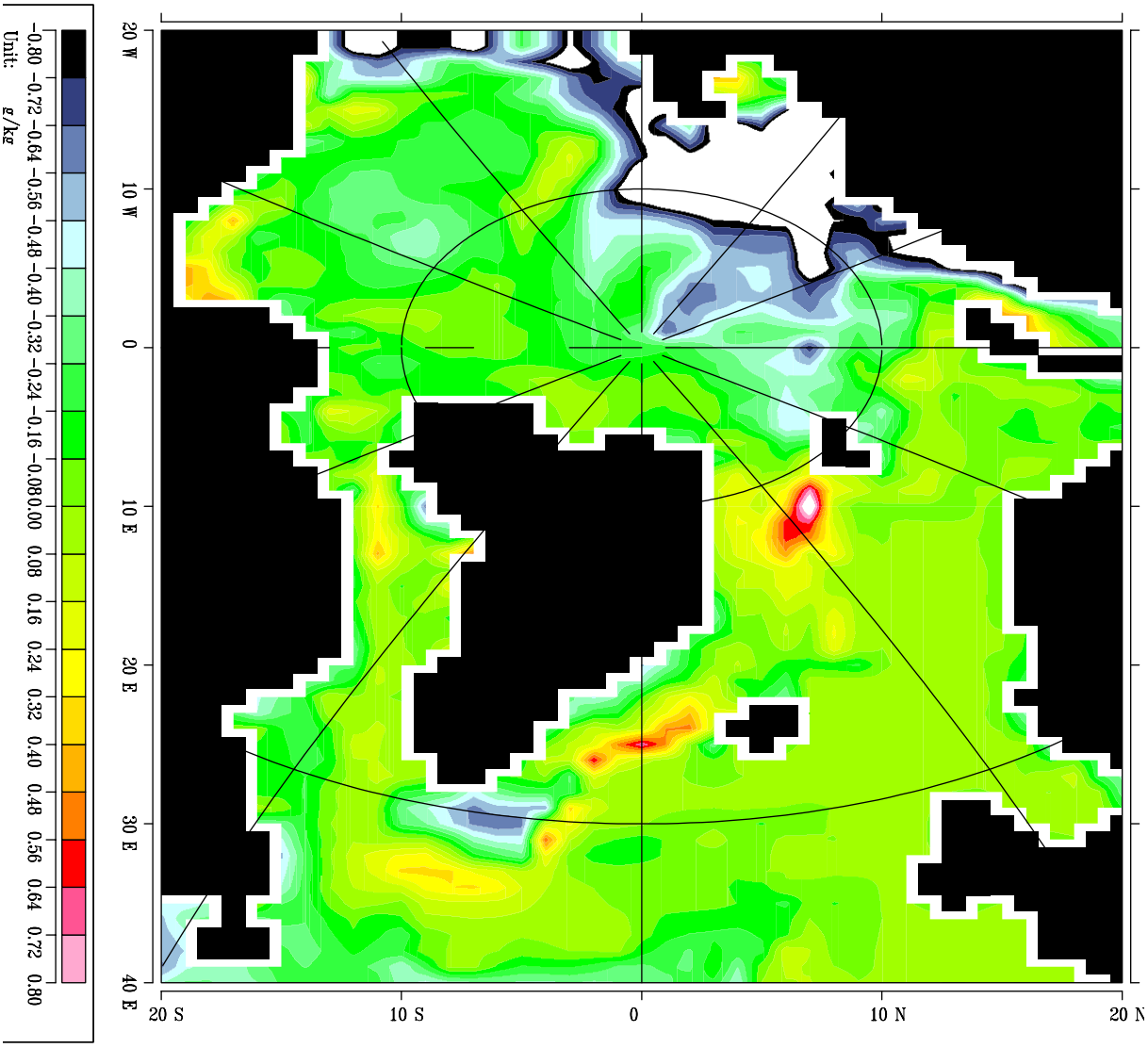

Fig.36 Difference in surface salinity in the winter of year 10/11 between the "switch" experiment and the reference run (Fig.3 from Brauch et al., 1999)

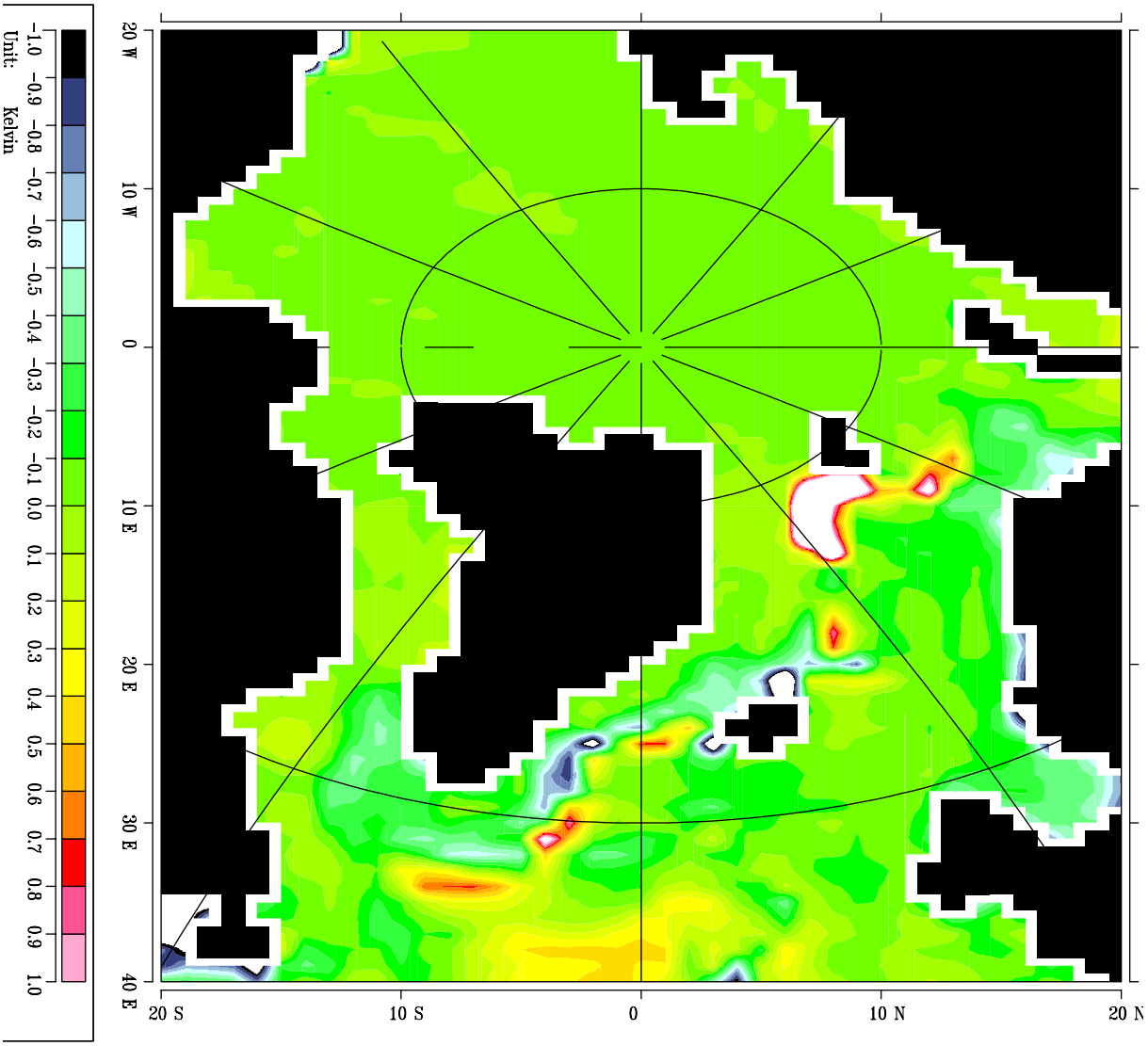

Fig.37 Difference in SST in the winter of year 10 / 11 between the "switch" experiment and the reference run (Fig.7 from Brauch et al., 1999).